Doctoral Dissertations   Student Scholarship

Spring 2012

Cavity ring down: Construction, validation and experiments measuring the optical extinction of pure clays and their mixtures with salts and carboxylic acids under a range of atmospherically relevant conditions

Alexis Rae Attwood
University of New Hampshire, Durham

Follow this and additional works at: https://scholars.unh.edu/dissertation

CAVITY RING DOWN: CONSTRUCTION, VALIDATION AND EXPERIMENTS
MEASURING THE OPTICAL EXTINCTION OF PURE CLAYS AND THEIR
MIXTURES WITH SALTS AND CARBOXYLIC ACIDS UNDER A RANGE OF
ATMOSPHERICALLY RELAVENT CONDITIONS

BY

ALEXIS RAE ATTWOOD
Bachelor of Arts, Assumption College, 2005

DISSERTATION

Submitted to the University of New Hampshire

in Partial Fulfillment of ·

the Requirements for the Degree of

Doctor of Philosophy

in

Chemistry

May, 2012

UMI Number: 3525055

UMI

Dissertation Publishing

ProQuest®

This dissertation has been examined and approved.
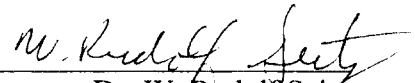
_____
Dissertation Advisor, Dr. Margaret E. Greenslade
Assistant Professor, Department of Chemistry
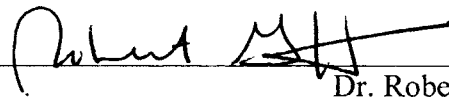
_____
Dr. Howard R. Mayne,
Professor, Department of Chemistry

_____
Dr. Carolyn Jordan,
Research Scientist, Climate Change Research Center

_____
Dr. W. Rudolf Seitz
Professor, Department of Chemistry

_____
Dr. Robert Griffin,
Associate Professor, Department of Civil and Environmental Engineering
Rice University

_____4/9/2012_____
Date

DEDICATION

This thesis is dedicated to my grandfather who encouraged me to be a great thinker and more importantly, a great person.

ACKNOWLEDGEMENTS

TABLE OF CONTENTS

LIST OF TABLES

LIST OF FIGURES

ABSTRACT

CAVITY RING DOWN: CONSTRUCTION, VALIDATION AND EXPERIMENTS

MEASURING THE OPTICAL EXTINCTION OF PURE CLAYS AND THEIR

MIXTURES WITH SALTS AND CARBOXYLIC ACIDS UNDER A RANGE OF

ATMOSPHERICALLY RELEVANT CONDITIONS

by

Alexis Rae Attwood

University of New Hampshire, May 2012

Aerosols interact directly with solar radiation by scattering and absorbing incident light to affect the Earth's climate system. Models indicate that aerosols cool the Earth counterbalancing greenhouse gases, but contribute the largest uncertainty to anthropogenic effects on climate. To address these uncertainties, a cavity ring down spectrometer (CRD) was built and performance tests were conducted to validate its capabilities for measuring optical properties of laboratory generated, atmospherically relevant aerosols over a range of conditions. The CRD provides an absolute and unbiased *in situ* measurement of total extinction and can reduce uncertainties associated with aerosols having unusual chemical and physical properties.

Mineral dust particles are a large fraction of the total aerosol mass and thus contribute extensively to the climate balance. Assessing this impact is complicated by the irregular shape and sheet-like structures of these species making them difficult to model using standard Mie theory, thus direct experimental results are desirable. Further,

variability in measurements of optical properties can result from water uptake and changes in chemical composition due to interactions with the immediate environment. Three different clay proxies for mineral dust and relevant mixtures were selected for study. First, pure kaolinite, montmorillonite and illite were characterized as a function of relative humidity (RH) revealing differences when compared to Mie theory generated from literature values for size or mass change. Second, internal mixtures of largely insoluble montmorillonite with sodium chloride or ammonium sulfate were studied and a lowering of the optically observed deliquescence RH was observed in comparison to the pure salts. Further, experimental results were compared with Mie theory generated from volume weighted mixing rules to reveal deviations near deliquescence. Lastly, optical properties of montmorillonite internally mixed with atmospherically relevant dicarboxylic acids were used to simulate atmospheric processing and compared to freshly emitted, pure montmorillonite aerosols under dry and humid environments. In all cases, the optical properties measured by cavity ring down have been used to obtain a better estimate of the magnitude of the climate forcing caused by mineral dust aerosols under a range of conditions.

CHAPTER 1

ATMOSPHERIC AEROSOLS

Aerosol Background

Climate change has been shown to adversely affect many of the Earth's physical

and biological systems and as a result, human health in diverse ways. These effects

include sea level rise, the melting of arctic sea ice and glaciers, increased extreme

drought conditions and the disruption of sensitive ecosystems.[1] Such changes can lead to

increased allergic disorders due to an increase in the duration and intensity of the pollen

season, increased occurrences of waterborne illness such as cholera due to an increase in

water temperature, increased mortality due to thermal stress in areas of high temperature

rise, injuries due to flooding and reduced crop production caused by droughts.[2]

Greenhouse gases and aerosols are two of the largest contributors to anthropogenic (man-

made) climate change based on the magnitude of their radiative forcing (Wm^{-2}).[1]

Radiative forcing is a measure of the difference in outgoing radiation with and without

greenhouse gases or aerosols present. For example, a negative forcing by aerosols at the

top of the atmosphere corresponds to the outgoing radiation being greater with aerosols

than without, leading to a net cooling whereas a positive forcing indicates an increase in

energy at the top of the atmosphere as a result of perturbation.

Figure 1.1 shows the principal components contributing to the radiative forcing of

climate.[1] Greenhouse gases, like methane and carbon dioxide, absorb infrared radiation

1

		LOSU
CO_2		High
CH_4		High
N_2O		High
Halocarbons		High
Total Aerosol { Direct Effect		Med-low
Cloud Albedo Effect		Low
Total		

Radiative Forcing (W m⁻²)
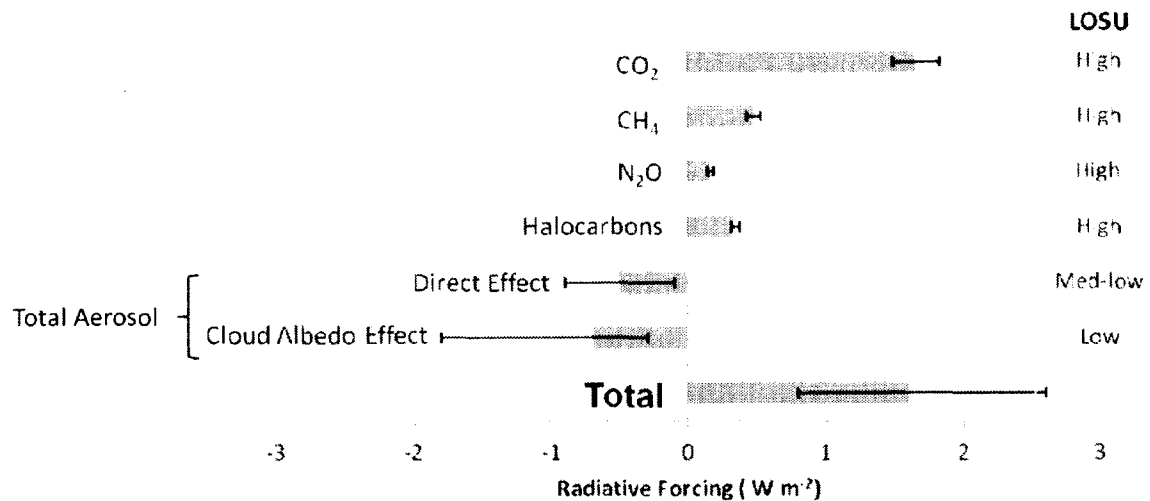
Figure 1.1: A summary of the anthropogenic radiative forcing estimates for atmospheric constituents and their level of scientific understanding (LOSU) adapted from the IPCC. Error bars represent the 90% confidence range. Results shown are derived from published values and their ranges.[1]

and lead to positive forcing, or warming of the atmosphere. The effects of these gases are well characterized due to their atmospheric stability and long lifetimes allowing them to be well mixed throughout the atmosphere. They have been extensively modeled for many years and the Intergovernmental Panel on Climate Change (IPCC) reports the level of scientific understanding (LOSU) for the effects of greenhouse gases on the Earth's climate system as high. Aerosols, on the other hand, lead to a net negative forcing and have a LOSU between low and medium-low. The radiative effects for aerosols are poorly understood in comparison to greenhouse gases due to their short atmospheric lifetimes and their spatial and temporal variability. In addition, there is a lack of spectroscopic data for aerosols due to their variability, while the spectral signature of greenhouse gases is well known. As seen in Figure 1.1, aerosols contribute the largest uncertainty in the calculation of anthropogenic effects on climate.[1]

Atmospheric aerosols are solid or liquid particles suspended in air and contribute to a large range of phenomena including dust, fog, haze, smoke and soot.[3] The interaction of solar radiation with aerosols affects the Earth's climate system by direct scattering and absorption of incident light. The degree to which aerosols interact with incoming solar radiation depends on a combination of aerosol properties such as loading, chemical composition, size distribution and shape, and variability in these properties makes quantification of radiative forcing magnitude on a global scale difficult. Aerosols can scatter the radiation back towards space, cooling the Earth's atmosphere, or absorb solar radiation leading to heating of the atmosphere while reducing the amount of light penetrating to the Earth's surface. In addition, long-wavelength thermal infrared radiation emitted by the Earth's surface can be absorbed by aerosol species, also leading to positive radiative forcing.[4] This additional absorption near the surface means that determining the top of the atmosphere forcing by aerosols is not sufficient for climate change and this additional radiative heating must be included in predictions. In sum, the direct effect of aerosols on the radiation budget is predicted to counterbalance some of the warming caused by greenhouse gases. Indirectly, particles can also affect the climate through the cloud albedo effect by acting as cloud condensation nuclei (CCN). This changes the number concentration of droplets in clouds as well as their size distribution altering precipitation rates. Additionally, CCN will alter the lifetime and reflectivity of a cloud.[5] These indirect effects contribute the largest uncertainty in the total aerosol contribution to radiative forcing as shown in Figure 1.1.

Greenhouses gases and aerosols also have an effect on a positive water feedback loop in the Earth's atmosphere. It is relatively well understood with respect to greenhouse

gases but the complicated effect of aerosols remains to be established. An increase in temperature will increase the water-holding capacity of the atmosphere, increasing the amount of water vapor and causing further warming due to the absorption capability of water.[1] The additional atmospheric water will also impact aerosols with two opposing effects. In one case, absorbing aerosols take up water and their absorption is enhanced causing increased heating of the atmosphere.[6] Under the same conditions, more light will be reflected by scattering from aerosols due to an increase in size, thus enhancing their cooling effect. The relative magnitude of these two effects is not well characterized.

Aerosol Sizes, Sources and Removal Mechanisms

Aerosols typically range in size from a few nanometers (nm) to several micrometers (μm) covering a size range over several orders of magnitude. The lower limit in their size is constrained by measurement techniques that can typically only measure particles larger than a few nanometers. They are generally classified as "fine" or "coarse" particles with the latter signifying particles greater than 2.5 μm. In addition to size, aerosols are further classified as being natural or anthropogenic (man made). This distinction between these size and type classifications is important because the physical and chemical characteristics, sources, formation and removal mechanisms are different, based on classification as shown in Table 1.1 and discussed below.[3]

The smallest particles provide the largest number concentration of particles in the atmosphere, whereas larger particles contribute most particulate mass concentration, even at a lower total number concentration. In addition to having the largest number concentration, fine particles also account for the greatest particle surface area concentrations and stay in the atmosphere longer than coarse particles.[3] Fine particles can

be further separated into three sub-classifications: nucleation mode particles with diameters up to 10 nm, Aitken mode with diameters spanning 10 nm to 100 nm and accumulation mode with diameters extending from 100 nm to 2.5 μm. Nucleation and Aitken mode particles are formed

Table 1.1: Sources, sizes and emission estimates for the major aerosol classes.[3]

Source	Size Mode	Estimated Flux (Tg yr^{-1})
Natural		
Primary		
Mineral Dust	Fine	308
	Coarse	2672
Seasalt	Coarse	10100
Volcanic Ash	Coarse	30
Biological Debris	Coarse	50
Secondary		
Sulfates from DMS	Fine	12.4
Sulfates from Volcanic SO_2	Fine	20
Organic aerosol from biogenic VOC	Fine	11.2
Anthropogenic		
Primary		
Industrial dust	Fine/Coarse	100
Black Carbon	Fine	12
Organic aerosol	Fine	81
Secondary		
Sulfates from SO_2	Fine	48.6
Nitrates from NO_x	Fine	21.3

through condensation of vapors in combustion processes and nucleation of gaseous species in the atmosphere. These particles coagulate with themselves or attach to larger particles to form particles with diameters in the accumulation mode as their principal removal mechanism.[3]

Accumulation mode particles are largely formed through coagulation of finer mode particles and condensation of vapors onto existing particles to increase their size. The name is fitting because removal mechanisms are not as efficient in this size range and therefore large amounts of particles start to accumulate at these sizes. They are

mainly removed via wet deposition but tend to stay in the atmosphere on the order of a week or more. During their lifetime, accumulation mode particles can be transported far away from their source, changing their physical and chemical makeup through atmospheric processing.[3]

Coarse particles are greater than 2.5 μm in diameter and are mainly mechanically generated particles like seasalt and dust. These large particles make up the majority of aerosol mass in the atmosphere. Efficient removal from the atmosphere occurs via dry deposition or rapid settling.[3]

It is important to note that although particle size is referred to by a diameter, implying a spherical particle, some aerosols are irregular and can be quite variable in shape making such a description inaccurate. The particle shape can determine surface area for reactions and have implications for optical properties. Some common irregular particle shapes are fractal, amorphous, crystalline, rod, disk and aggregate. Irregular shaped particles are classified using an "equivalent" diameter that depends on physical, not geometric properties.[5] There are several types of equivalent diameters all of which represent the diameter of a sphere that would have the same value of a particular physical property as that of the irregular particle.[7] For example, our instrumentation selects particle size based on the particles electrical mobility diameter (D_m) and therefore throughout this manuscript diameters will be reported as such. The relationship between D_m and its volume equivalent diameter, D_{ve} is obtained from the electrical mobility (Z_p). Z_p is a measure of the particle's ability to move in an electric field and is related to particle size by:[7]

$$Z_p = \frac{neC(D)}{3\pi\eta D_m} = \frac{neC(D)}{3\pi\eta\chi D_{ve}} \qquad [1.1]$$

6

where n is the number of elementary charges carried by the particle, e is electron charge, C(D) is the Cunningham slip correction which corrects for the non-continuum gas behavior for small particles, η is the absolute gas viscosity and χ is the dynamic shape factor for the particle.

In addition to size, aerosols can be classified based on their formation mechanisms. Primary aerosols are emitted directly into the atmosphere while a secondary classification indicates formation in the atmosphere through a gas to particle conversion process. These types of conversion processes occur as a result of oxidation, usually by O_3 or OH and NO_3 radicals, of a precursor gas to yield products of lower volatility that can partition into the particle phase.[8] Once condensed into particulate form, aerosols can change their physical and chemical characteristics through an equilibrium of condensation and evaporation, coagulation with other particles or chemical reaction.

Natural primary sources of particulate matter contribute a large flux as shown in Table 1.1 and include seasalt, mineral dust, volcanic ash and biological debris.[3] Anthropogenic, primary sources only account for a small percentage of particulate mass and arise mainly from industrial dust, black carbon from combustion processes and organic aerosol from domestic and agricultural fires.[3]

Natural secondary sources include sulfate aerosols released from dimethyl sulfate (DMS) produced in oceans and sulfates produced from volcanic activity. In addition, biogenic volatile organic compounds (VOC) like isoprene and pinene are released from vegetation and then can condense into secondary organic aerosols (SOA) as a result of atmospheric oxidation followed by gas to particle conversion of the lower volatility gas phase reaction products.[9] Anthropogenic secondary particulate matter is especially

prevalent in urban areas and includes products of burning of hydrocarbons, sulfates from SO$_2$ and nitrates from NO$_x$ (NO + NO$_2$).[5]

Interaction with Radiation

Aerosols have the ability to absorb and scatter incoming solar radiation. Absorption converts photons into electronic or thermal energy thus warming the atmosphere for a positive radiative forcing. Scattering changes the direction of the photons propagation, returning some to space for a cooling effect and a net negative radiative forcing. Collectively, the sum of scattering and absorption are referred to as extinction, which describes the total attenuation of light by particles in the atmosphere.

The amount of light a particular particle will scatter and absorb is dependent on various physical parameters including the particle size, morphology, wavelength of light and refractive index. The refractive index (m) is reported in the form:

$$m(\lambda) = n + ik \qquad\qquad [1.2]$$

where the real part (n) describes the scattering nature of the particle, the imaginary part (k), describes the particles ability to absorb light and i is an imaginary unit. Both scattering and absorption portions are wavelength dependent as denoted by the m(λ).

The scattering, absorption and extinction coefficients for a collection of particles in a volume (α_{scat}, α_{abs} and α_{ext}, respectively) describe the total light attenuated per unit distance and are reported in units of length^{-1}. The single particle scattering, absorption and extinction cross sections (σ_{scat}, σ_{abs} and σ_{ext}, respectively) have units of area particle^{-1} and are constants that describe the amount of light attenuated by an individual particle. This is parallel to molecular absorption cross sections. These two values (α and σ) are

8

related because integrating the extinction cross section over the aerosol size distribution in a volume yields the extinction coefficient.

The relative amount of scattering (cooling) versus absorption (warming) is described by the single scattering albedo parameter, ω, which is calculated using the scattering and extinction cross sections:

$$\omega = \frac{\sigma_{scat}}{\sigma_{scat} + \sigma_{abs}} = \frac{\sigma_{scat}}{\sigma_{ext}}. \qquad [1.3]$$

This parameter is crucial in determining whether an aerosol population will have a cooling or warming effect on the local atmosphere. As the absorption increases, the single scattering albedo will decrease from 1 (purely scattering) to a critical value of 0.85-0.91 indicating a change in the aerosol effect from cooling to warming with the exact point of this change depending on the underlying surface albedo.[10, 11] While all aerosol particles scatter light, absorption mainly occurs in species such as black carbon, brown carbon and mineral dust. When a photon is absorbed by a particle it is re-radiated as thermal energy in all directions, heating the air around it, similar to the effect from greenhouse gases.

Mixing States

The extent of radiative forcing by aerosols is largely dependent on their chemical composition. Aerosols most often exist as a complex mixture of multiple chemically defined components and are typically classified as being externally or internally mixed. Externally mixed aerosols are a collection of individual particles of homogenous composition with no physical or chemical interaction between the species. Internally mixed particles are composed of two or more species interacting with each other in a single particle.[12] Both are depicted in Figure 1.2.

internally mixed   externally mixed
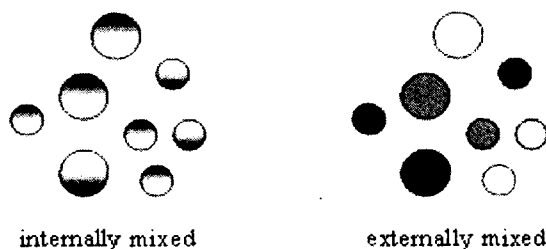
Figure 1.2: Cartoon depicting the mixing state of aerosols.

The diversity of an aerosol population at a given location is due to local sources

and long range transport creating complex aerosol mixtures whose composition is hard to

classify due to limitations in measurement techniques. The lack of detailed spectroscopic

data to identify the components of a complex mixture makes accurately predicting the

effect of aerosols on climate change difficult.

The chemical composition of a mixed aerosol determines the refractive index, its

hygroscopicity and can influence particle shape and size distribution, all of which will

contribute to its optical properties. Aerosols can contain a wide variety of both inorganic

and organic matter. Inorganic matter such as seasalt, sulfate and nitrate along with non-

absorbing organic matter directly affect the atmosphere by scattering radiation.

Absorbing compounds such as elemental carbon (also called black carbon or soot),

mineral dust and absorbing organics such as brown carbon, can both scatter and absorb

radiation. Mineral dust and fresh elemental carbon aerosols are particularly interesting

since they are insoluble in water and therefore act in different ways when mixed with

more soluble compounds. Upon mixing these aerosols can form a core shell structure that

is optically more complex than the mixtures shown in Figure 1.2.[13] Here, an insoluble

core made up of elemental carbon or mineral dust can be coated with another substance

making a shell around the particle. Likewise, a particle can exist as soluble material with

a number of insoluble inclusions throughout. Both of these scenarios have different

implications for the optical properties of the mixed particle. For example, one model study showed that the radiative forcing of elemental carbon was -0.27 W m^{-2} for an external mixture, 0.54 W m^{-2} for elemental carbon as a coated core and 0.78 W m^{-2} when it was internally well mixed.[14]

At present, there are few direct measurements of the optical properties of mixed aerosols with an insoluble component such as mineral dust or elemental carbon.[13-22] When mineral dust is mixed with biomass burning aerosol, it has been shown to reduce the solar radiation reaching the Earth's surface by a factor of two compared to mineral dust alone.[21] A study by Schnaiter et al., on the optical properties of soot aerosol showed that when soot was internally mixed with ammonium sulfate aerosol, there was minimal change in the absorption coefficient.[20, 22] However, when soot was mixed with α-pinene, a secondary organic aerosol precursor, the absorption was significantly enhanced.[20, 22] Others have found that coating soot with sulfuric acid or common dicarboxylic acids present in the atmosphere results in a profound enhancement in both absorption and scattering.[15, 17]

Due to a lack of experimental data, models often approximate the optical properties of mixed aerosols by assuming that all aerosol is externally mixed or by using "mixing rules" which assume homogeneous mixing between all constituents in the particle and that each constituent behaves independently even after mixing. Although mixing rules are helpful in predicting aerosol optical properties for simple systems, especially in the case of common electrolytes, this approach is inadequate for predicting the optical properties of more complex systems especially those including insoluble species.[13, 19]

Hygroscopicity

A particle's size and hence its optical properties are also greatly affected by its hygroscopicity, or ability to take up water. Particles containing soluble components like nitrates and sulfates are very hygroscopic and will readily take up available water. Hygroscopic particles will increase in size as they take up water with rising relative humidity (RH). This hygroscopic growth will affect the refractive indices of the particles, in turn further changing their optical properties. These interrelated effects are difficult to quantify since they can be non-linear and vary with aerosol composition. There is uncertainty associated with the response of the absorption coefficient to increasing RH based on experimental work although theoretical studies have shown that the response is much smaller than it is for scattering. Therefore, the single scattering albedo is expected to increase with increasing relative humidity. [23]

The hygroscopicity of insoluble particles like mineral dust and soot are much more complex and greatly depend on the mixing state of the particle. If soluble components are mixed with the particle, it can enhance water uptake onto the particle. Absorption and scattering are affected by the additional water taken up by the mixed particle in comparison to the single component particle. Mineral dust and soot also have the added complication of being irregular in shape and having varying degrees of porosity and density. This irregular shape can lead to compaction of the particle when exposed to water, changing the particle morphology and density and further affecting the optical properties. [16, 24-27]

The work presented here addresses the need for more direct, accurate optical measurements of atmospheric aerosols in order to decrease the uncertainty associated with their contribution to climate change. Specific focus is placed on the optical properties and hygroscopicity of pure mineral dust particles and their internal mixtures with other atmospherically relevant species. A two channel cavity ring down spectrometer, newly built at the University of New Hampshire, was used for these studies. Chapter 2 gives a brief background and description of this instrument and validation techniques. Chapters 3, 4 and 5 include the experimental design and results for the specific systems studied, including atmospheric implications. Chapter 6 will conclude with future directions.

CHAPTER 2

CAVITY RING DOWN SPECTROMETER

History and Background

Cavity ring down spectroscopy (CRD) is a relatively new technique developed in 1988 by O'Keefe and Deacon and was originally used to measure gas phase species.[28] To date, CRD has been used for a variety of optical measurements of both gas phase species and aerosols and has been reviewed extensively in the literature.[13, 18, 29-31] It was more recently developed as a technique to measure the extinction coefficient (α) of light by particles due to the need for improved accuracy and time resolution. CRD uses a cavity where a laser pulse can travel between two highly reflective mirrors at each end. This creates a long pathlength in a relatively short distance over which a laser pulse can decay, making it a highly sensitive instrument capable of measuring low values of extinction.[30]

Light decays within the cavity in two ways; either by absorption and scattering by particles and gases in between the mirrors or by transmission through the mirrors at each pass. Light intensity is detected by a photomultiplier tube (PMT) connected behind a mirror outside one end of the cavity. As the pulse circulates from mirror to mirror, the light intensity as seen by the detector rings down. The intensity of light within the cavity is determined as an exponential function of time:

$$I_t = I_0 exp\left(\frac{-t}{\tau}\right)$$

[2.1]

where I_t is the measured intensity of the light pulse, I_0 is the incident intensity of the laser light pulse, t is the time and τ is a decay time constant, known as the ring down time. Since the decay of the laser intensity is monitored, rather than the magnitude, variations in the laser intensity from pulse to pulse will not affect the analysis. This, along with the high sensitivity achieved by the long pathlengths (several kilometers), are the major advantages in using this type of spectroscopy.

With no aerosol sample or absorbing gases present in the cavity, the light intensity decays exponentially in time due solely to losses through the two end mirrors yielding a time constant τ_0, known as the sample free cavity ring down time. Particles and gases in the cavity will absorb and scatter light, and their extinction will decrease the time for equivalent light decay to reduce the ring down time to τ. The characteristic ring down
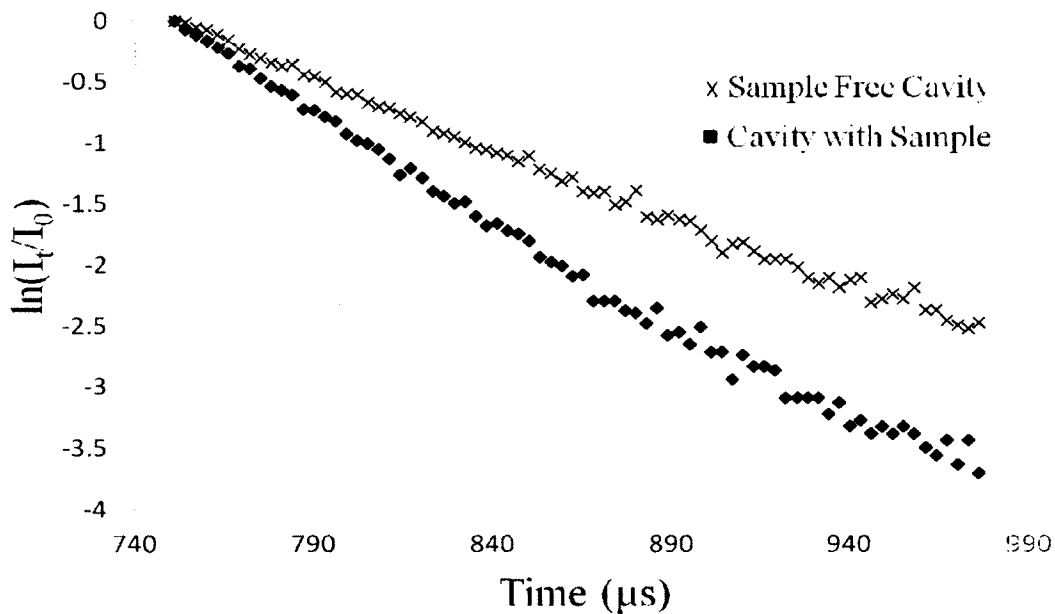
Figure 2.1: Graphically determining the characteristic ring down time, which is equal to the negative inverse slope of the linear fit to the data. As particles and gases are introduced into the cavity, the slope for the line decreases and therefore the ring down time is reduced.

time can be determined by taking the negative inverse slope of a plot of the natural log of the intensity of light at time t over the intensity of light at time 0 versus time as shown in Figure 2.1. The extinction coefficient for the particles, α_{ext}, is a measure of the fractional loss in intensity per unit path length and therefore has units of length^{-1} and is calculated according to equation 2.2:

$$\alpha_{ext} = \frac{R_L}{c}\left(\frac{1}{\tau} - \frac{1}{\tau_0}\right)$$
[2.2]

where R_L is the ratio of the cavity optical length to the sample length and c is the speed of light.

Instrument Design

The cavity ring down system consists of three main components: a laser, the optics and the sample cavity all mounted on a portable rack. The laser source is a solid state 20 Hz pulsed Nd:YAG (neodymium:yttrium-aluminum-garnet) laser (Big Sky Laser, now Quantel USA, Ultra). This laser has a high output power at 1064 nm (75 mJ) and operates by having a Nd:YAG rod next to a flashlamp which provides broadband, pulsed optical pumping. Generation of the second harmonic using a potassium titanyl phosphate crystal produces an output wavelength of 532 nm (45 mJ) which is used for experiments due to atmospheric relevancy. This wavelength is close to the center of the most intense portion of the solar spectrum and therefore is an obvious choice for studying the optical properties of aerosols in relationship to understanding climate change. In addition, the third harmonic at 355 nm (20 mJ) is also generated, but not used.

The optical layout and cavity setup are shown in Figure 2.2 a) and b) respectively. The two cavities have an optical length of 68.9 cm and a sample length of 62.1 cm. The

sample cavities consist of ½" stainless steel tubing mounted between two concave mirrors

1" in diameter with a 1 m radius of curvature and a reflectivity of >99.998% (Advanced

Thin Films). The mirrors are located at each end of the cavities. These are separated from

the sample flow and supplied with a constant flow of filtered nitrogen (0.006 L/min) to

prevent deposition of particulate matter onto the mirror surface. If particulate matter

were allowed to deposit the reflectivity would decrease causing the pathlength and
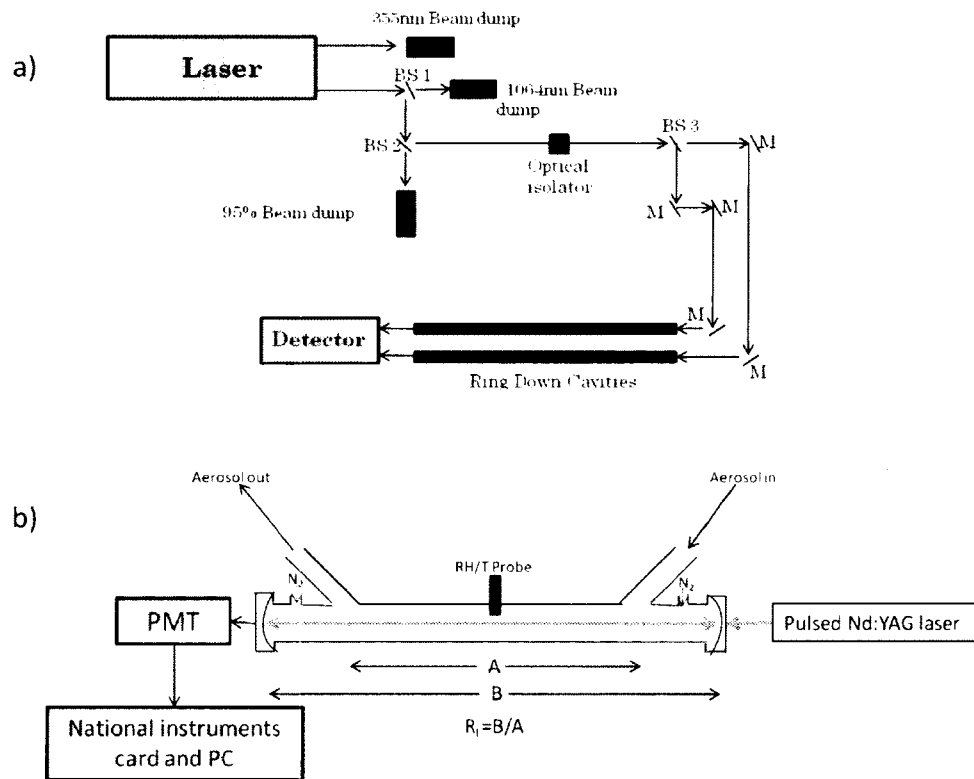
Figure 2.2: a) The optical layout of the cavity ring down spectrometer is shown. Laser light in the ultraviolet (355 nm) is immediately dumped. The other output is a combination of 1064 nm and 532 nm light. The first beam splitter (BS 1) is a long wave pass dichroic beam splitter that transmits the 1064 nm light to a beam dump and reflects 532 nm light at a 45° angle relative to the beam splitter towards the cavities. The 532 nm light then hits another beam splitter (BS 2) that transmits 95% of the light (which is dumped) and reflects 5% of the light. An optical isolator sits in the beam path which prevents back reflection from damaging the laser head. The next beam splitter (BS 3) transmits 50% of the light and reflects 50% of the light, splitting the beam in two. The remaining optics are highly reflective mirrors (M) and simply serve to align the beam into one of the two sample cavities. b) The cavity set up is shown. Our light source is a pulsed Nd:YAG laser which enters the optical cavity and is reflected between two mirrors. The decay of the laser pulse is captured by a PMT and sent to a computer for processsing. R_L, the ratio of the optical cavity length (B) to the sample length (A) and is used in calculating the extinction.

sensitivity to also decrease. The 532 nm light is coupled into the cavity through the back of a mirror and reflected between the two mirrors. The intensity is low, but this does not impact detection or sensitivity. The light intensity in a sample free cavity decays exponentially in time due to losses through the two end mirrors with a typical τ_0 value on the order of 90 μs. This yields an effective path length of about 27 km. The ring down signal of the decaying laser light is captured by a photomultiplier tube (PMT), (Hamamatusu H9433-03MOD), digitized using a National Instruments card (NI-USB-6259 BNC) and transferred to a personal computer to process the data using custom LabVIEW software.

The aerosol inlets and outlets are located near the end of the cavities at a 45° angle to the cavity and these locations define the sample length. Temperature and RH are monitored using Vaisala INTERCAP HMP50 probes (accuracy ±3%) located in the middle of both optical channels. Extinction is dependent on RH and therefore the RH measurements are important to include, especially since it will inform the influence of RH on direct aerosol radiative forcing. Using our two cavity system, we can investigate the influence of RH on extinction by changing the RH between the two cavities.

A schematic of the full set up used for experiments detailed in Chapters 3, 4 and 5 is shown in Figure 2.3. Particles are produced using a custom built, constant output atomizer. The atomized particles are directed through a diffusion dryer consisting of ½″ stainless steel tubing and 13x molecular sieves. After atomization and drying, the RH is <10% and the aerosol is directed to a differential mobility analyzer (DMA) that size selects particles based on their electrical mobility. The RH of the monodisperse dry
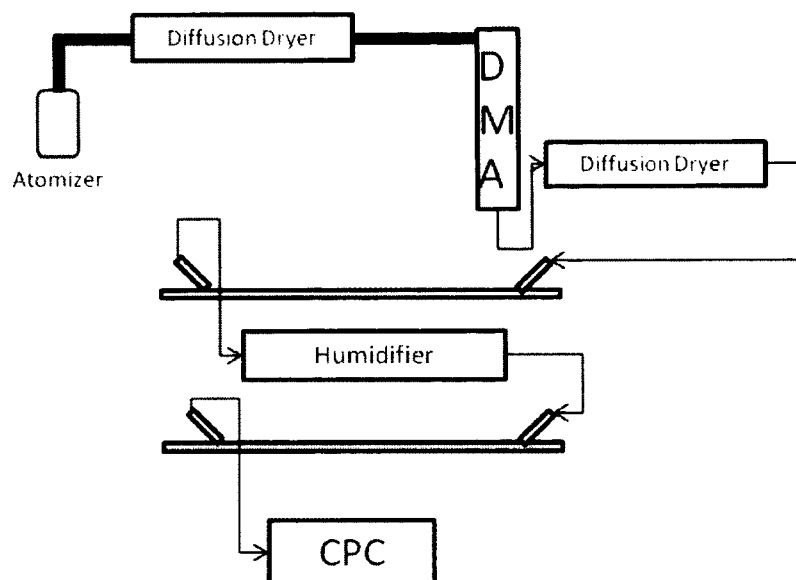
Figure 2.3: Atomized particles are first passed through a diffusion dryer before being directed to the DMA where a polydisperse population of aerosols is size selected. The particles are then dried to a RH<10% before entering the first optical cavity, where dry extinction is measured. After exiting the first cavity, the particles are humidified to a desired RH and enter the second optical cavity and the humidified extinction is measured before being counted by the CPC.

sample following the DMA is maintained by passing the aerosols through a second

diffusion dryer to remove any water vapor that was introduced via the sheath flow of the

DMA. The RH of the sheath flow in the DMA is dependent on the RH of the laboratory

air which can be high, especially during summer months. The dry aerosol sample enters

and exits the first cavity at a flow rate of 0.3 L/min, where the extinction of the sample,

$\alpha_{ext}(dry)$, is measured. After exiting the first cavity, the aerosol stream is humidified

using a custom built, temperature controlled humidifier made of Accurel tubing. The

particles then enter the second cavity where the extinction, $\alpha_{ext}(RH)$ is measured. The

extinction coefficients are converted to extinction cross sections (σ_{ext}) by dividing by the

particle number concentration which is measured by a condensation particle counter

(CPC). The dry and humidified extinction cross section values are then used to calculate

fRH_{ext}:

$$fRH_{ext}(RH, Dry) = \frac{\sigma_{RH}}{\sigma_{Dry}} \qquad [2.3]$$

which describes the RH dependence of light extinction. It is important to note that there is a slight difference in the number concentration of particles in the two cavities due to a small dilution by the purge flows. This dilution is accounted for numerically in the calculations.

Performance Tests

The measurement of extinction using the CRD is absolute and therefore does not require calibration assuming that the physical characteristics of the cavities (lengths and purge flows) are accurately known. However, performance tests were done to validate its use in measuring the optical properties of aerosols. The first validation done was using polystyrene latex (PSL) spheres from Duke Scientific with a reported size of 300±6 nm and refractive index of m(λ)=1.59+0i at 589 nm according to the manufacturer and a calculated m(λ)=1.57+0i at 532 nm.[32] Several drops of the spheres were diluted in a test tube with HPLC grade water and subsequently atomized with filtered nitrogen. A typical size distribution plot of the atomized PSL solution measured by the DMA and CPC is shown in Figure 2.4. The two smaller peaks between 100 nm and 300 nm are attributed to the surfactant added to the solution in order to stabilize the small particles and keep them from agglomerating.[33] Unsuccessful tests were done previously in the lab to try to remove this surfactant. The largest and broadest peak at small particle sizes (<100 nm) is due to the non-volatile impurities dissolved in the water used to dilute the sphere solution. The concentration of these particles can be reduced by using very pure water, but this impurity cannot be completely eliminated.[34] For all experiments particles were atomized

using particle free nitrogen as the background gas and were dried and directed into the

DMA for size selection. By size selecting the particles to be optically measured, any

contribution from the surfactant and water impurities is eliminated. The DMA was set to
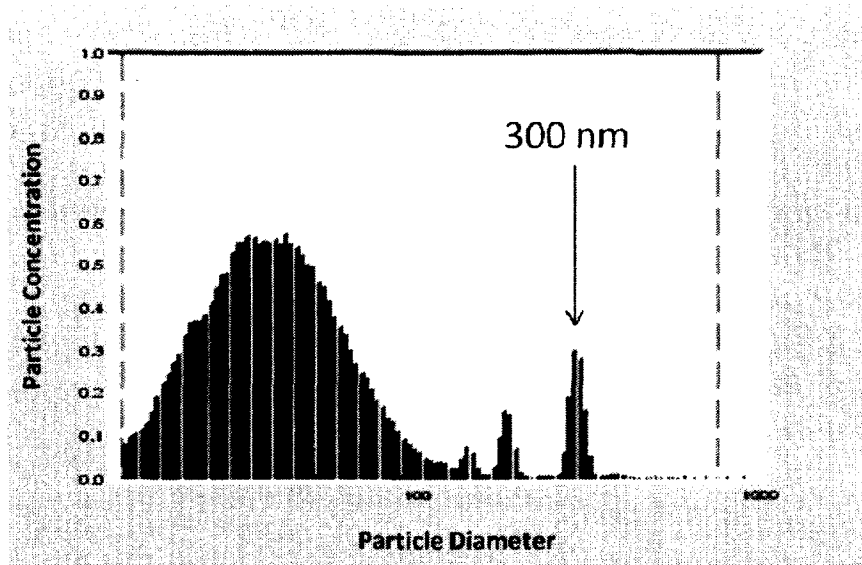
Figure 2.4: A scan of particle concentration (arbitrary units) versus particle diameter (nm, log scale) for 300 nm Duke Scientific PSL measured using a DMA for determining particle size and a CPC for particle counting.

zero causing particle free nitrogen to be sent through the cavities allowing for a

measurement of τ_0. The DMA was then set to size select 300 nm particles and the

monodisperse aerosol stream was directed through both cavities to measure τ. Finally, the

aerosol flow was terminated at the CPC to count particle number concentrations. Five

runs were completed, measuring τ_0 and τ in each case.

For PSL, the refractive index and sphere diameter are well defined variables and

can be entered into a Fortran Mie code program, along with the wavelength of light to

output a theoretical extinction cross section (σ_{MIE}) for the particles. Mie theory is an

analytical solution to Maxwell's equations and describes the interaction between particles

and radiation when the wavelength of light is on the same order of magnitude as the

particle size. It can be used to calculate the absorption, scattering and extinction cross sections by a particle when the appropriate inputs are known. The extinction cross section can then be used in equation 2.2, along with measured values of τ and τ_0 to calculate a theoretical particle concentration, N_{calc}:

$$\sigma_{MIE} * N_{calc} = \frac{R_L}{c}\left(\frac{1}{\tau} - \frac{1}{\tau_0}\right)$$

[2.4]

Since R_L and c are known constants, N_{calc} can be theoretically determined and compared to the number concentration of particles measured by the CPC. Since there is a ±10% error in particle counts measured by the CPC as reported by the manufacturer, any result within that error was considered to be acceptable. Table 2.1 shows the results of the described validation study. This type of validation was performed whenever the instrument was relocated or had to be realigned due to maintenance of the laser head.

Table 2.1: Results from a representative validation study of the CRD using 300 nm PSL. Each cavity was tested in 5 different trials and a % error of less than 10% was required for validation.

Cavity	τ_0 (μs)	τ (μs)	Measured Concentration (#/cm³)	Mie Calculated Concentration (#/cm³)	% Error
Cavity #1					
1	82.23	20.91	1012	972	4
2	82.53	20.71	1052	986	6
3	82.62	19.93	1094	1038	5
4	81.46	24.74	762	834	9
5	81.43	25.23	802	869	8
Cavity #2					
1	91.16	20.07	968	1059	9
2	90.59	19.48	1005	1099	9
3	90.65	18.90	1046	1142	8
4	89.44	24.74	738	797	7
5	89.70	25.23	721	777	7

In addition to validating our system using Mie theory, the ability of the system to determine accurate values of $fRH_{ext}(RH, Dry)$ was tested using ammonium sulfate. The

22

growth of ammonium sulfate as a function of RH has been extensively studied and is well defined.[35-39] The majority these studies report a growth factor (GF), the change in particle diameter or mass, as a function of RH. This type of analysis is usually performed using a humidity tandem differential mobility analyzer (HT-DMA) or electrodynamic balance to measure changes in particle size and mass, respectively. Garland et al., used a CRD system, similar to the one described here, to measure an fRH_{ext}(80%, Dry) for ammonium sulfate over the size range of 100-700 nm.[35] They compared their results to fRH_{ext}(80%, Dry) values calculated using GFs from Tang et al.[36] For 288 nm ammonium sulfate particles a range, based on error, in fRH_{ext}(80%, Dry) from 2.7 to 3.4 was reported from observed and calculated values.[35] In our CRD system we observe an fRH_{ext}(80%, Dry) of 2.86(0.11) for 288 nm ammonium sulfate, which agrees well with the previous study. The agreement between Mie theory predictions and measured extinction observed for both PSL and ammonium sulfate under dry and humid conditions confirms the absolute uncertainty in our CRD system.

CHAPTER 3

OPTICAL PROPERTIES AND ASSOCIATED HYGROSCOPICITY OF CLAY AEROSOLS

Introduction

Mineral dust aerosol is associated with windblown dust soil and has an estimated global source strength of 1,000-3,000 Tg yr^{-1}, accounting for 45% of the total aerosol mass load.[1, 40] Larger particles will sediment out quickly due to gravitational settling, but particles smaller than 10 μm have longer atmospheric lifetimes of about a week. During this time, mineral dust can be transported tens of thousands of kilometers, depositing particles in areas that are located far away from the source.[41, 42] For example, a large amount of Asian dust is subject to long range transport over the Pacific Ocean, showing up as background dust aerosol on the West Coast of the United States whereas African dust frequently gets deposited over the Caribbean.[43, 44]

Mineral dust is involved in many different atmospheric processes including deposition of micronutrients,[45, 46] providing surfaces for heterogeneous reactions[47-49] plus direct[50-52] and indirect radiative forcing.[53, 54] Each of these processes is complicated by the ability of mineral dust to take up water. For example, the more soluble a particle, the more likely it will be removed from the atmosphere via wet deposition. Further, if particle size and mass are affected by water uptake, it will influence the rate of gravitational settling.[24] Reactivity towards other species is also affected by aerosol

hygroscopicity. It has been shown that clay aerosols provide a sink for reactive gases and a substrate for chemical reaction, as a function of water content.[55-59] In particular, increased ambient relative humidity resulted in a greater concentration of short chain hydrocarbons on the surface of mineral dust particles, indicating water assisted uptake onto these particles.[59] Mashburn et al. showed a greater nitric acid content on montmorillonite particles with increased relative humidity as the particles were exposed to atmospherically relevant nitric acid concentrations.[55] In contrast, kaolinite samples showed decreased uptake of two different methyl siloxanes, in conjunction with an increase in surface absorbed water at elevated relative humidity.[58] These studies show that uptake of gas-phase species on dust surfaces can be either increased or decreased as a function of the water concentration on the surface and in air.

Understanding the hygroscopicity of atmospheric particles is also important in assessing their direct and indirect effects. Mineral dust particles contribute to radiative forcing, changing the energy balance of the atmosphere by scattering incoming short-wave radiation (negative forcing) and absorbing outgoing infrared terrestrial radiation (positive forcing).[50, 52, 54] The size of the particle and its complex refractive index are a function of water content and these two characteristics determine the extent of absorption and scattering of light by the particle. Due to the complicated chemical makeup and irregular shape of the species, along with high loading and spatial and temporal variability, mineral dust aerosols represent the largest uncertainty associated with climate change having a net negative forcing reported as -0.1 $\pm$ 0.5 W m^{-2}.[1] The Fourth Assessment Report of the Intergovernmental Panel on Climate Change reports "the level of scientific understanding" as very low for the radiative effects of mineral dust.[1]

Mineral dust particles can also impact the radiative balance of the atmosphere indirectly, by acting as cloud condensation nuclei (CCN) or ice nuclei (IN). Previously studies have shown that mineral dust can act as efficient nuclei for cloud droplet formation and cirrus cloud formation affecting cloud albedo and cloud lifetime.[26, 60, 61] The ability of the particle to act as an effective CCN or IN depends on its hygroscopicity. For mineral dust an increase in nucleation with increased relative humidity has been seen.[62, 63] Therefore, understanding water uptake and specifically the optical effect of water uptake is crucial for understanding mineral dust's direct and indirect impact on climate change. Mie theory is typically used to model the climate impact from the interaction of light with aerosols because it provides a basic estimate using spherically shaped particles and approximate values for the refractive index.[64] However, these calculations are not assumed to be valid for assessing the optical properties of mineral dust as the particles are irregular in shape and are composed of an inhomogeneous mix of minerals.[65, 66] A recent study investigated the agreement between Mie theory simulations for various shapes, including sphere and disk, and experimental extinction results for the major silicate resonance bands of mineral dust in the infrared region from 4000-10000 cm^{-1}. The results show a large deviation from spherical Mie theory for band position, band shape and peak intensity with the resonance peak red shifted 27-44 cm^{-1}.[65]

Generally, mineral dust is considered to be non-hygroscopic and therefore global climate models assume it to be fully insoluble. Recently, several studies of different clay components of mineral dust found that these particles are slightly hygroscopic and the extent of water uptake largely depends on the structure and chemical composition of the clay.[24, 26, 67-69] Measurements of the water uptake on mineral dust are highly uncertain and

difficult to quantify as their hygroscopicity is small in comparison to other aerosol species such as inorganic salts. In addition, water uptake by dust has been shown to affect the fRH(RH, Dry) of both extinction and absorption, with a pronounced effect for ambient African dust that has been transported long distances and is therefore well-aged.[70] This effect will have implications on the single scattering albedo, an important parameter in assessing the global radiation balance. To date, laboratory quantification of water uptake on mineral dust particles has been investigated using a humidified tandem differential mobility analyzer (HT-DMA) and a quartz crystal microbalance (QCM). Physical growth factors (GF) from a HT-DMA are a measure of hygroscopicity, where GF is defined as: [24-26, 69]

$$GF(RH, Dry) = \frac{D(RH)}{D(Dry)}$$ [3.1]

In these experiments the measured particle diameter (D), is based on its electrical mobility diameter which can have significant deviations from geometric size for aspherical particles. A QCM has been used to quantify the mass of water taken up by a clay sample.[67] Calculating the growth of the particle from its mass change provides an upper bound on particle growth as some water uptake may result from filling internal voids with water without causing the particle diameter to change.

In this study, we investigate water uptake on three clay minerals by quantifying optical growth upon humidification using cavity ring down spectroscopy (CRD). The three minerals considered, montmorillonite [(Na,Ca)(Al,Mg)$_6$(Si$_4$O$_{10}$)$_3$(OH)$_6$], kaolinite [Al$_2$Si$_2$O$_5$(OH)$_4$] and illite [(K,H$_3$O)(Al,Mg,Fe)$_2$(Si,Al)$_4$O$_{10}$(OH)$_2$], are common components of mineral dust from different source regions.[71] The relative abundance of

these clays can be used as a tracer to assess the origin of mineral dust aerosols. For example, the illite/kaolinite ratio seems to be the most sensitive indicator of Saharan dust even after long range transport.[72] Kaolinite is indicative of dust from low latitudes in west Africa whereas illite is more common in the northern regions toward the Mediterranean coast.[73] Montmorillonite is less commonly used as a tracer but is frequently associated with volcanic rock.[74]

Optical properties were determined by measuring the extinction cross section (σ_{ext}) of size selected clay aerosols as a function of relative humidity, $fRH_{ext}(RH, Dry)$, where fRH_{ext} is:

$$fRH_{ext}(RH, Dry) = \frac{\sigma_{ext}(RH)}{\sigma_{ext}(Dry)}.$$ [3.2]

CRD at 532 nm is used for these measurements and showed both decreases and increases in extinction with humidification depending on the clay and the humidity levels. Mie theory was used to convert the $fRH_{ext}(RH, Dry)$ into a calculated growth factor (GF_c) value at 68% RH for comparison with measured growth factors (GF_m) from the literature. Further, the electrical mobility size distributions of clay particles at 68% RH and dry conditions was measured and used to indicate size change for all clays in this study. Direct optical measurements are able to capture the effects of the irregular shapes and internal voids possible in clay particles, but are difficult to include in models. Our GF_c provides a lower limit and can be incorporated into climate models in conjunction with other results to reduce the uncertainty associated with the optical response to water uptake on clay aerosols.

Experimental Methods

Properties of Selected Clays and Aerosol Generation

The three clays investigated, illite (IMt-1), kaolinite (KGa-1b) and

montmorillonite (STx-1b), were purchased from the Source Clays Repository. These

clays have been previously well studied with other methods and their chemical

composition and structure are known. The structures of the three types of clay are useful

in understanding the different optical response upon humidification. Previous studies by

Cases et al. determined that all of the clays are composed primarily of layered aluminum

and silicon held together by interlayer Van der Waals forces, charge-countering cations,

or hydrogen bonds.[75] The layers are arranged with tetrahedrally coordinated silicon layers

and octahedrally coordinated aluminum layers.[75] The ability of these clays to swell upon

hydration is based on the type of interlayer interactions. In addition, they differ in the

number of hydroxyl groups on their surfaces which will influence the extent to which

they can hydrogen bond with water vapor.[62]

The layers of montmorillonite are composed of a 2:1 ratio of silicon to aluminum

held together by van der Waals forces and charge countering cations.[75] Montmorillonite

is classified as a "swelling clay" in which the extent of water uptake is largely dependent

on the availability of cations in between the structural sheets and their hydration

energies.[24, 67, 76] There are six hydroxyl groups on its surface, and it can therefore easily

hydrogen bond to water upon humidification. Illite has a similar structure to

montmorillonite with a 2:1 silicon to aluminum ratio in its layers, but it is considered a

"non-swelling" clay. The layers are held together by stronger electrostatic interactions

with interlayer cations such as potassium, calcium or magnesium. The degree of water

uptake can be affected by isomorphic substitution of these interlayer ions for cations of lower charge causing a charge imbalance.[75] There are only four hydroxyl groups on its surface leaving less sites for possible hydrogen bonding to water. The chemical structure of kaolinite is a 1:1 silicon to aluminum layered clay and is considered "non-swelling". Kaolinite has strong hydrogen bonding between the layers preventing cations and water molecules from entering the interlayer space forcing water to primarily absorb on the surface of the particle.[67] It only has two hydroxyl groups on its surface for hydrogen bonding to water.

To generate aerosols, illite was ground using a Wig-L-Bug prior to being atomized, while the kaolinite and montmorillonite powders were used as received. Suspensions of the clays (10 wt% clay) in HPLC grade water (J.T. Baker) were constantly mixed using a stir plate and atomized using a custom built constant output atomizer. The polydisperse aerosol was subsequently dried in a diffusion dryer with a residence time of ~12.5 s so that the RH of the aerosol stream was decreased to <10%.

After atomization and drying, the clay particles were directed through a differential mobility analyzer (DMA, TSI 3081L) to select a monodisperse size population for optical measurements. The electrical mobility size distribution for each clay type was determined at wet (68% RH) and dry conditions by following the DMA with a condensation particle counter (CPC, TSI 3775) to function as a scanning particle mobility sizer, SMPS (TSI, 3081L). Atomization produced a log normal distribution with a single mode for the diameter of montmorillonite, illite and kaolinite at 157, 209 and 346 nm respectively under dry (RH<10%) conditions. At elevated relative humidity, the diameter mode from the size distribution is approximately 10% lower in each case, where

differences seen between trials were considered. Due to the limitations of the current set up, only 68% RH was selected for these measurements.

For optical measurements, montmorillonite, illite and kaolinite aerosol populations were size selected for 200, 300 and 425 nm particles respectively. The particle size was chosen to be larger than the mode of the size distribution, which minimizes the contribution of multiply charged clay particles in the sample. The multiply charged particles result from the neutralizer of the DMA. A sufficient concentration of particles for optical measurements was still achieved. The DMA size selection has a reported uncertainty of ~10%[77] which is included in uncertainty calculations. The aerosol sizes selected for this study can be compared to ambient atmospheric mineral dust particles, which span a size range of 100-5000 nm.[78] We have chosen to focus on smaller particles because larger particles have lifetimes on the order of a few hours and tend to settle out quickly from the atmosphere. Smaller particles will reside in the atmosphere longer and can be transported long distances.[79]

Optical measurements are terminated at the CPC to count the population exiting the CRD and to determine the doublet concentrations by using the measured number concentration at the doublet size and the neutralizer charging distribution from the manufacturer for subsequent corrections. Since our measurements are reported as a function of particle size, the extinction contribution for particles with multiple charges are calculated and used to correct the extinction values of the size selected particles. Only doublets were used in corrections; the number of higher charged particles is expected to be small and would have a negligible effect on the extinction.[80] It is important to note that the CPC is the largest source of error with a reported uncertainty of 10% in particle

counts. This uncertainty is minimized by reporting the fRH$_{ext}$ as a ratio between

humidified extinction and dry extinction for the same sample.

Cavity Ring Down Spectrometer

CRD has been used for a variety of optical measurements of both aerosol and gas

phase species and has been reviewed extensively in the literature.[13, 18, 29-31] The system
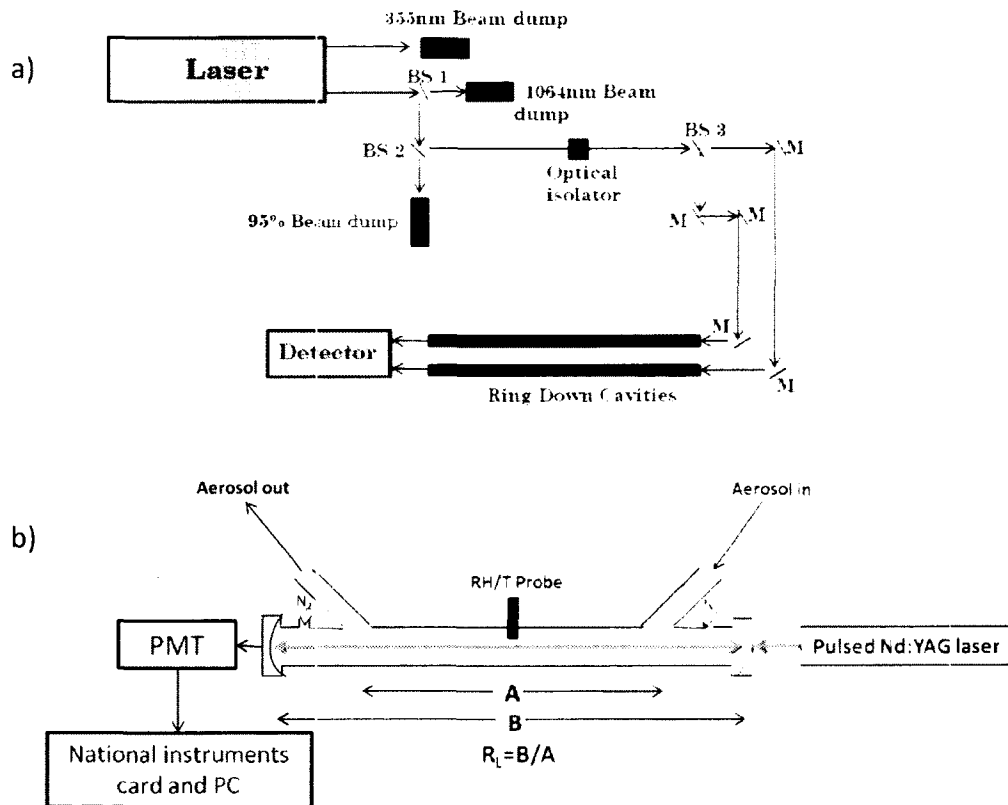
Figure 3.1: a) Optical layout of the cavity ring down spectrometer. Laser light in the ultraviolet (355 nm) is immediately dumped. The other output is a combination of 1064 nm and 532 nm light. The first beam splitter (BS 1) is a long wave pass dichroic beam splitter that transmits the 1064 nm light and reflects 532 nm light at a 45° angle relative to the beam splitter. The 532 nm light then hits another beam splitter (BS 2) that transmits 95% of the light (which is dumped) and reflects 5% of the light. An optical isolator sits in the beam path which prevents back reflection from damaging the laser head. The next beam splitter (BS 3) transmits 50% of the light and reflects 50% of the light, splitting the beam in two. The remaining optics are highly reflective mirrors (M) and simply serve to align the beam into one of the two sample cavities. b) Cavity set up: Our light source is a pulsed Nd:YAG laser which enters the optical cavity and is reflected between two mirrors. The decay of the laser pulse is captured by a PMT. R_L, the ratio of the optical cavity length (B) to the sample length (A) is used in calculating the extinction (equation 3.3).

used in the present work is newly constructed and similar to that fabricated by Baynard et al. and is briefly described here.[31] The optical layout and cavity setup is shown in Figure 3.1a) and b) respectively. The cavities have an optical length of 68.9 cm and a sample length of 57.8 cm. Two concave mirrors 1" in diameter with a 1 m radius of curvature and a reflectivity of >99.998% (Advanced Thin Films) are located at each end of the cavity. These are supplied with a constant flow of filtered nitrogen (0.02 L/min) to prevent deposition of particulate matter onto the mirror surface. The laser source is a solid state 20 Hz pulsed Nd:YAG laser (Big Sky Laser, now Quantel USA, Ultra). The second harmonic produces 532 nm light which is coupled into the cavity and reflected between the two mirrors. The light intensity decays exponentially in time due to losses through the two end mirrors with a time constant τ_0, known as the particle free cavity ring down time. Typical τ_0, values were on the order of 100 μs, which yields an effective path length of about 31 km. Particles in the cavity will absorb and scatter light, and their extinction will reduce the ring down time to τ. The extinction of the particles, α_{ext} (m^{-1}), is calculated according to equation 3.3:

$$\alpha_{ext} = \frac{R_L}{c}\left(\frac{1}{\tau} - \frac{1}{\tau_0}\right)$$

[3.3]

where R_L is the ratio of the cavity optical length to the sample length and c is the speed of light. The ring down signal is captured by a photomultiplier tube (Hamamatusu H9433-03MOD), digitized using a National Instruments card (NI-USB-6259 BNC) and transferred to a personal computer to process the data using custom LabVIEW software.

A schematic of the full experimental set up is shown in Figure 3.2. After atomization and drying the RH is <10% and the RH of the monodisperse dry sample following the DMA is maintained by passing the aerosols through a second diffusion
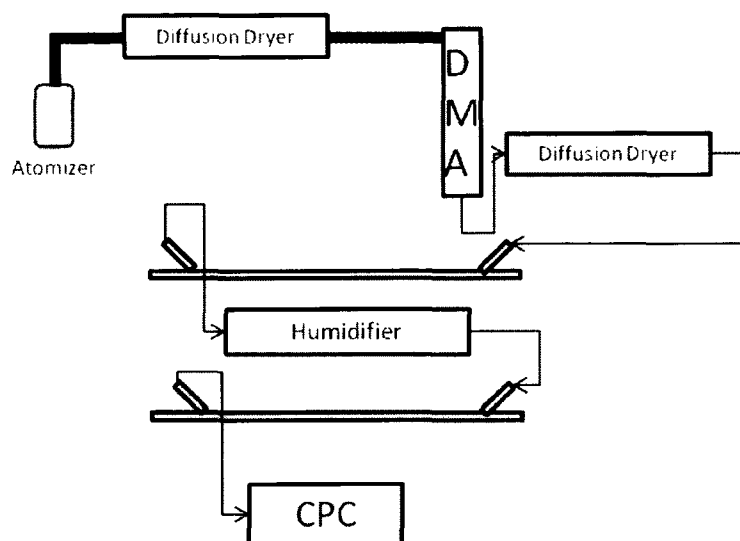
Figure 3.2: Atomized particles are first passed through a diffusion dryer before entering the DMA where a polydisperse population of aerosols is size selected. The particles are then dried to a RH<10% before entering the first optical cavity. After exiting the first cavity, the particles are humidified to a desired RH and enter the second optical cavity before being counted by the CPC.

dryer to remove any water vapor that was introduced via the sheath flow of the DMA. The dry aerosol sample enters and exits the first cavity at a flow rate of 0.3 L/min, where the extinction, α_{ext}(dry) is measured. After exiting the first cavity, the aerosol stream is humidified to 50%, 68% or 90% RH using a custom built temperature controlled humidifier. The particles then enter the second cavity where the extinction, α_{ext}(RH) is measured. Temperature and RH are monitored using Vaisala INTERCAP HMP50 probes (accuracy ±3%) in both optical channels. The extinction results are converted to extinction cross sections by dividing by the particle number concentration. The dry and humidified extinction cross section values are then used to calculate fRH_{ext}, which describes the dependence of light extinction on relative humidity by the aerosols. Errors

in fRH$_{ext}$ values are reported in Table 3.1 as the experimental standard deviation (1σ) of at least 18 trials at each RH for each clay type over 3 different experiments.

Growth Factors

GF$_c$ were calculated using optical measurements in combination with Mie theory. These closure based GF$_c$ use literature values for the refractive indices as an input for Mie theory to determine the effective optical diameter that corresponded to the dry and wet extinction cross section. The retrieved diameters were used to calculate a GF$_c$.[35]

Results and Discussion

The fRH$_{ext}$ of three clay components of mineral dust as measured by CRD at 50%, 68%, and 90% RH are shown in Figure 3.3 and Table 3.1. An fRH$_{ext}$ of 1 is
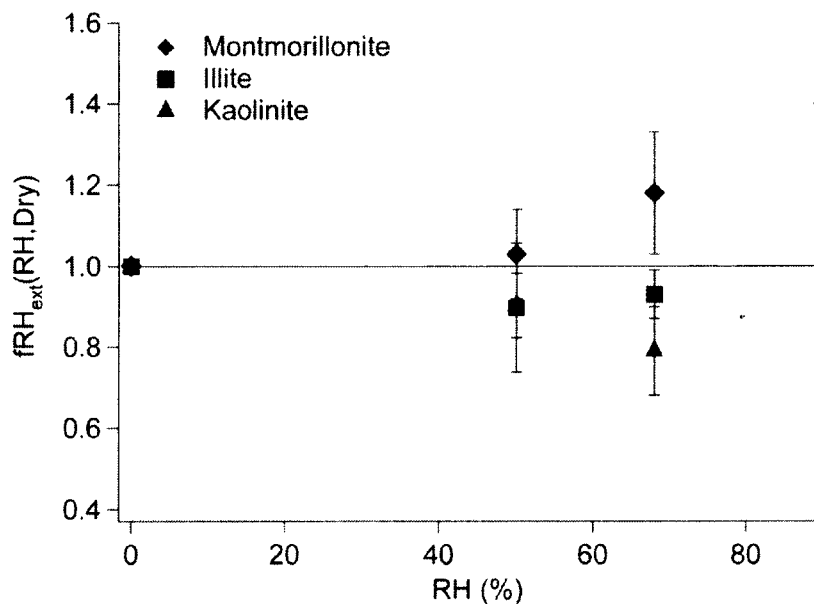
Figure 3.3: Measured fRH$_{ext}$ for montmorillonite (diamonds), Illite (squares) and kaolinite (triangles) at 50%, 68% and 90% relative humidity. The solid black line represents no change in extinction cross section upon humidification.

Table 3.1: fRH$_{ext}$ for all three clays at select relative humidities measured with cavity ring down spectroscopy. Errors in fRH$_{ext}$ values are reported as the experimental standard deviation (1σ) of at least 18 trials at each RH for each clay type over 3 different experiments.

Clay	fRH$_{ext}$ (50%)	fRH$_{ext}$ (68%)	fRH$_{ext}$ (90%)
Montmorillonite	1.03 (0.11)	1.18 (0.15)	1.4 (0.2)
Illite	0.90 (0.16)	0.93 (0.06)	1.06 (0.10)
Kaolinite	0.90 (0.08)	0.79 (0.11)	0.8 (0.17)

expected when there is no optical change in the particle upon humidification.

Montmorillonite showed a steady increase in extinction as a function of relative

humidity, with an fRH$_{ext}$ ranging from 1.03 at 50% RH to 1.4 at 90% RH. Illite showed a
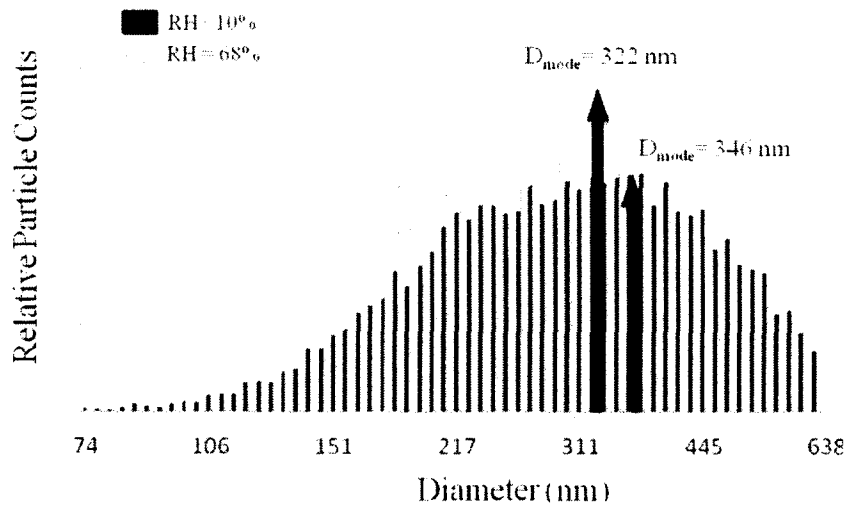
Figure 3.4: Size distributions of kaolinite clay under dry (RH<10%) and wet conditions (RH=68%) measured by the SMPS. A decrease in particle size upon humidification of approximately 10% is seen for this case and all other clays studied.

decrease in extinction upon humidification at 50% RH and 68% RH. At 90% RH, a

moderate increase in extinction was observed when compared to dry illite. Kaolinite

showed a decrease in extinction for all three relative humidity values studied. We also

monitored the aerosol electrical mobility diameter size distribution of wet and dry clay

particles and observed shrinkage of approximately 10% upon humidification for each

clay type as illustrated in Figure 3.4 for kaolinite. A decrease in extinction upon

humidification may be attributed to compaction of the particle leading to a decrease in

optical diameter, a shape transition to a more spherical humidified particle than its dry

counterpart, or a significant decrease in refractive index for the humidified particle.[24-26]

We will consider these explanations below.

A comparison between closure-based GF_c calculated from optical extinction

measured in this study and GF_m from the literature at 68% RH in all cases are shown in

Table 3.2 for all three clays investigated. The differences between the literature derived

GF_m values for specific clay types illustrates the general challenge associated with

growth factor measurements of clays. Each of these techniques has some disadvantages.

Table 3.2: Comparison of our GF_c with GF_m presented in the literature for clay minerals. All growth factors were measured at 68% RH. The HT-DMA study reported GF at comparable sizes and the QCM work reported mg H_2O per g of sample.

Clay	Calculated GF[a]	HT-DMA[b]	QCM[c]
Montmorillonite	1.03 (0.03)	~1	1.15
Illite	0.99 (0.02)	~1	1.17
Kaolinite	0.93 (0.05)	~1	1.07

[a]Calculated GF using the fRH$_{ext}$(68%, dry) from this study and refractive indices
  reported in the literature[81]
[b]Calculated from reported κ values measured by HT-DMA[24]
[c]Calculated using individual clay densities from literature and measurements
  using QCM[67]

The optical measurements in conjunction with Mie theory used to calculate a GF_c begins

with a high accuracy technique of CRD and accounts for the irregular shape and possible

internal voids of the clay particles. However, these calculated GF_c do not take into consideration the small decrease in refractive index for the clay particles that could accompany water uptake. Such a decrease leads to a larger calculated GF_c. Further, the GF_c calculated using Mie theory and optical measurements assumes that the particles are spherical. Recent work has shown that Mie theory underestimates extinction by clay particles, so sizes would have to be larger to reproduce the extinction intensity. [65] The impact of this on our calculations is minimized by reporting a ratio between two cases. These two complications mean that calculating the GF_c using Mie theory represents a lower bound for the growth factor of clays in comparison to HT-DMA and QCM measurements.

The fRH_{ext} for montmorillonite is the largest of all the clays at each relative humidity value studied. This can be explained by specific physical characteristics of montmorillonite which has a structure that is easily hydrated by water on the surface. Montmorillonite is also expected to have the greatest amount of swelling by incorporation of water between the layers after initial restructuring of the particle due to the weak Van der Waals forces holding the layers together. At 68% RH, montmorillonite had an fRH_{ext} of 1.18 which corresponds to a calculated GF_c of 1.03. The increase in GF_c is in contrast to a decrease of approximately 10% in the mode of the particle size distribution. Typically increases in optical results should be mirrored by increases in size as water is taken up. This apparent discrepancy could be attributed to enhanced absorption by a scattering (water) shell formed around an absorbing core.[6] Our hypothesis is supported by the steady increase in the optically determined fRH_{ext} with increased RH corresponding to the addition of subsequent water layers which are

expected to directly translate into enhanced absorption. The linearity of the montmorillonite trace from 50%-90% RH seen in Figure 3.3 could be indicative of the proportionality of the enhancement with increasing numbers of water monolayers.[82] At 90% RH, the fRH_{ext} of 1.4 could also be attributed to growth of the particle beyond its dry diameter in combination with an enhancement. The possibility of an increase in the mode of the particle size distribution could be confirmed with additional measurements at 90% RH; however this is beyond the current capabilities of our equipment.

Using Mie theory to model experimental extinction results, the optical fRH_{ext} (68%, Dry) values measured can be converted to a GF_c using the literature value for the refractive index of $1.523 + 0.0000382i$ for montmorillonite at 532 nm.[81] An fRH_{ext} (68%, Dry) of 1.18 corresponds to a calculated closure based GF_c of 1.03. This is assuming that the water associated with the particle, if any, has no influence on the refractive index. If this is not the case, the actual real portion of the refractive index of the humidified particle would be a composite, and it would decrease since the refractive index of water is 1.33. This potential decrease in refractive index would result in a higher calculated GF_c from the measured fRH_{ext}(68%, Dry). Recent studies have used other methods to quantify the water uptake onto the clay components of mineral dust.[24, 67] Herich et al. reported a GF_m for montmorillonite of approximately 1 using an HT-DMA technique, indicating no change of the electrical mobility diameter of the particle at 68% relative humidity.[24] Schuttlefield et al. measured water uptake on clays using a QCM at different relative humidities.[67] For a similar montmorillonite clay, an uptake of 225 mg of water/g of sample was measured at 68% RH.[67] This corresponds to GF_m of 1.15 using the literature value of 2.35 g/cm^3 for the density of montmorillonite.[83] This QCM based calculation

however, provides an upper limit of the growth factor due to the possibility that internal voids present in the clay particles could fill with water and increase the mass without causing particle growth as described previously.

Illite only reaches an fRH_{ext} (90%, Dry) of 1.06 in contrast to montmorillonite (1.4), probably due to its structure being less hygroscopic. The fRH_{ext} results for illite show the expected general trend, increasing extinction with increasing relative humidity after an initial decrease, although the changes are less significant than for montmorillonite. It is expected that decrease fRH_{ext} would translate to shrinkage of the particle. At 68% RH, the observed $fRH_{ext}<1$ which corresponds to a calculated GF_c of 0.99 can be compared to a 10% shrinkage seen when the mode of the size distributions are examined. These results are anticipated since a decrease in particle size should, based on physical structures, yield a decrease in extinction. It is also possible that water could be adding to the surface of the illite aerosols and an enhancement effect is being observed similar to montmorillonite. As more water is taken up (RH 90%), the fRH_{ext} increases to greater than one and this could also be due to hydration of interlayers causing the particle to grow beyond its dry diameter.

Using Mie theory, a GF_c can be calculated from the fRH_{ext} (68%, dry) using the literature value of $1.414 + 0.000773i$ for the refractive index of illite at 532 nm.[81] The calculated GF_c is 0.99. Similar to montmorillonite, Herich et al. found a GF_m of approximately 1 for illite at 68% RH and this is in good agreement with our results.[24] According to the QCM measurements by Schuttlefield et al., illite particles take up approximately 225 mg of water/g of sample.[67] This corresponds to a GF_m of 1.17

assuming the density of illite to be 2.75 g/cm^3 as reported in the literature.[83] Again, the QCM measurements provide an upper limit to describe the particle growth factors.

Kaolinite displays decreases at 50% and 68% RH for the fRH$_{ext}$ with no further significant change at 90% RH. The strong hydrogen bonding between the layers of kaolinite does not allow water to enter between the layers, so it primarily has to absorb on the surface of the particle. However, there are not many surface sites available and so after initial compaction, not much change is expected. As a result, this sample has a calculated GF$_c$ at 68% RH of 0.93 in good agreement with the approximately 10% shrinkage with humidification represented in the change of the mode of the particle size distributions measured at corresponding RH. At 68% RH, the particles have taken up the maximum amount of water possible onto the surface and between the layers, therefore further increasing the relative humidity, even as high as 90%, has little effect on the extinction. It is also possible that as these particles are exposed to water vapor, partial dissolution of the surface layer in addition to compaction of particles can occur. When dry, the clay particles have an irregular shape and rough edges.[67] The rough surface of the particle could smooth out during the redistribution and restructuring of the surface layer, which could help explain the decrease in extinction upon humidification. Specifically, it is known that particles with smooth surfaces scatter light less efficiently than particles with sharp edges.[15]

A closure based GF$_c$ of 0.93 for kaolinite was calculated at 68% RH using Mie theory and a refractive index of 1.493 + 0.0000477i.[81] Based on HT-DMA measurements, Herich et al. reported a GF$_m$ near 1, which is similar to the other two clays studied in that work but does not represent the shrinkage observed optically in this study.[24] The QCM

study by Schuttlefield et al. reported water uptake of approximately 88 mg water/g sample at 68% RH, which corresponds to a upper limiting GF_m of 1.07 assuming the density of kaolinite is 2.6 g/cm^3.[67,83] Again, it is clear that growth factor measurements of clays are variable by around 20% using different measurement techniques.

Conclusions and Atmospheric Implications

In this work, the fRH_{ext} was measured for three clay components of mineral dust using CRD at 50%, 68% and 90% RH in comparison to dry conditions (RH<10%). The optical behavior varied considerably between clay types indicating that different morphologies and chemical structures of the clays play an important role in water uptake. As mentioned previously, there are regional differences in the composition of mineral dust and the proportion of each clay type can be an indicator of source region.[72, 73] Therefore, it is reasonable to assume that aerosols from different regions will exhibit different optical properties as they encounter elevated RH in transport due to the differences in water uptake between the three clays. Since the fRH_{ext}(RH, Dry) differs from unity, neglecting the change in optical properties with variable relative humidity and neglecting the difference in water uptake between different clays in radiative forcing models will lead to incorrect predictions for the direct effect of mineral dust on climate. Typically the change in optical properties due to water uptake is inferred based on physically measured particle growth. However, based on the deviations between physical GF_m and optically based GF_c results noted in this work, the inclusion of direct optical property measurements for clays in climate models is advantageous for reducing uncertainties.

Closure based GF_c were calculated from optical measurements using Mie theory. These GF_c deviate from literature values highlighting the uncertainties in the techniques used to quantify water uptake and growth of mineral dust particles. Accurate measurements of water uptake for these particles are crucial for understanding their atmospheric lifetimes, their ability to act as CCN and IN and their reactivity in the atmosphere. Using fRH_{ext} measurements to calculate GF_c provides a lower limit for the physical growth factor and is an alternate method for assessing water uptake as compared to conventional measurements using an HT-DMA or a QCM. Converting the optical measurement to closure based GF_c using our method initially accounts for the effect of the irregular shape and possible voids of clay aerosols to provide advantages over other techniques. The bounding of the growth factor using our closure based calculations (lower bound) with QCM measurements (upper bound) may further reduce uncertainties associated with growth factor measurements.

Based on top of the atmosphere globally averaged direct aerosol radiative forcing (ΔF_R) calculations previously described by Chylek and Wong[84] and Garland et al.[35], we have performed calculations to estimate the impact of our results on radiative forcing in comparison to the assumption that clays do not take up water. ΔF_R is determined by equation 3.4:[84]

$$\Delta F_R = -\frac{S_0}{4} T^2_{atm}(1-N)(1-a)^2(2\beta\tau_{scat} - 4a\tau_{abs})$$ [3.4]

where S_0 is a solar constant, T_{atm} is the transmittance of the atmosphere above the aerosol layer, N is the fraction of the sky covered by clouds, a is the albedo of the underlying surface, β is the fraction of radiation scattered by the aerosol into the upper

hemisphere and τ_{scat} and τ_{abs} are the aerosol layer scattering and absorption optical

thickness respectively. Many of the parameters cancel in the ratio:

$$\frac{\Delta F_{R\text{ (measured)}}}{\Delta F_{R\text{ (assumed)}}} \qquad [3.5]$$

where measured refers to our results and assumed refers to the case where no water is

taken up by the clays. We calculated effective diameters and size changes from our work

which is necessary to determine β. Using literature values for the RI and Mie theory; we

separated scattering and absorption components for conversion to τ_{scat} and τ_{abs}. The

resulting radiative forcing ratio is dominated by a term equivalent to fRH because there

are only small changes in the β value between the measured and assumed cases. As a

result, the radiative forcing ratio as a function of RH is very similar to Figure 3.3. In this

case the fRH can be considered a proxy for the radiative forcing impact of including the

correct optical response of a given aerosol sample. For montmorillonite, there will be

greater cooling at the surface with measured values compared to the assumed case where

there is no interaction with water. The opposite will be true for kaolinite throughout the

RH range and for illite up to at least 68% RH.

As aerosols are emitted into the atmosphere, they can be transported over large

distances, experiencing changes in temperature, pressure and RH. For example, mineral

dust emanating from warm, arid regions of the Saharan desert are lofted up beyond the

marine boundary layer allowing for extended residence time and transport of mineral dust

over long distances.[85] At the source, the amount of water vapor in air is extremely low.

However, as it is transported over the Atlantic, the particles will experience fluctuations

in RH until reaching the warm, moist Caribbean, where they are usually deposited. It is

important to take these RH changes into account when considering mineral dust aerosol because as our data show, especially for montmorillonite and illite, the amount of water vapor available will affect particle size as well as its optical properties.

In the future, experiments based on work by others should be considered. For example, studies have measured the enhancement of the $fRH_{abs}(RH, Dry)$ to determine the change in single scattering albedo and therefore the global radiation balance.[70, 82] While the $fRH(RH, Dry)$ of scattering and absorption will be enhanced from particle growth due to water uptake, the $fRH(RH, Dry)$ of absorption can also be enhanced due to a lensing effect as previously described. This effect can be counteracted by a decrease in the imaginary portion of the refractive index due to the presence of water on the particle surface.[6, 70, 82] Therefore it is necessary to not only measure how water uptake affects extinction as reported here but also how scattering and absorption are affected individually, due to the changes in single scattering albedo.

It is also necessary to consider a size dependence to the RH response and the physical size changes at other RH values. Further, it would be useful to consider how the optical properties of these systems change as a function of wavelength as the solar spectrum is broad but we have only considered a central wavelength of 532 nm. Further experiments, especially considering mineral dust mixed with common aerosol components will improve understanding of realistic atmospheric conditions. For additional improvements in radiative forcing calculations, it is important to experimentally measure the fRH for extinction and absorption.

CHAPTER 4

DELIQUESCENCE BEHAVIOR OF INTERNALLY MIXED CLAY AND

SALT AEROSOLS BY OPTICAL EXTINCTION MEASUREMENTS

Introduction

Particulate matter contributes to radiative forcing, directly altering the energy

balance of the atmosphere by scattering incoming short-wave radiation (negative forcing)

and absorbing outgoing infrared terrestrial radiation (positive forcing).[50, 52, 54] Particles

can also act as cloud condensation nuclei (CCN) or ice nuclei (IN), indirectly impacting

the radiative balance of the atmosphere. The effect of the interaction of solar radiation

with particles on the Earth's climate system has been extensively studied yet is poorly

understood. The Fourth Assessment Report of the Intergovernmental Panel on Climate

Change reports "the level of scientific understanding" as "medium low" for the direct

radiative forcing of the Earth's atmosphere to "low" for the indirect radiative effect of

aerosols on clouds.[1] The uncertainty in aerosol forcing dominates the total uncertainty in

the radiative forcing of climate. This is due to limitations in the ability to accurately

quantify and model atmospheric loading and optical properties of aerosols under ambient

conditions. This uncertainty should be reduced by a factor of 3 to 10 in order to support

regulatory decisions related to climate change.[86]

Understanding the hygroscopicity of atmospheric particles is important in

assessing their direct and indirect effects. The particle size, complex refractive index and

shape are a function of water content and these three characteristics determine the extent of extinction, or the sum of absorption and scattering, of light by the particle. A positive water feedback loop exists in the Earth's atmosphere that is relatively well understood with respect to greenhouse gases. An increase in temperature will increase the water-holding capacity of the atmosphere, increasing the amount of water vapor and causing further warming due to the absorption capability of water.[1] The impact additional atmospheric water will have on aerosols is not fully characterized, but a set of opposing effects are known. In one case, absorbing aerosols take up water and their absorption is enhanced causing increased heating of the atmosphere.[6] Under the same conditions, more light will be reflected by scattering from aerosols due to an increase in size, thus enhancing their cooling effect. The relative magnitude of these opposing effects is not well understood.

Commonly, water uptake in models is directly associated with inorganic salts which comprise 25-50% of atmospheric fine aerosol mass and include compounds like ammonium sulfate [$(NH_4)_2SO_4$, which we will abbreviate AS] and sodium chloride (NaCl).[1] Their hygroscopic properties have been extensively studied, and they exhibit a phase transformation from a solid particle to a liquid droplet at a specific relative humidity (RH) referred to as the deliquescence relative humidity (DRH).[36, 87-90] At this relative humidity, the size, shape, chemical composition and refractive index of the particle transitioning to a droplet will change, impacting its radiative effects. Previous studies have modeled the effects of the physical state of AS particles on aerosol optical properties such as scattering efficiency, single scattering albedo and asymmetry parameter and found that the extent of their global radiative forcing is significantly

affected by the phase of the particle around its DRH.[91] This effect specifically arises from changes in particle size and the degree of light scattering due to water uptake and therefore emphasizes that radiative forcing by particles is dependent on water content as a function of RH.

Aerosols in the atmosphere exist as both external and internal mixtures of various components. Understanding the water uptake and deliquescence behavior of multicomponent aerosols is much more complicated than the individual components alone. Thermodynamically, the deliquescence transition is predicted to occur when the Gibbs free energy of the solid particle surrounded by water vapor is equal to that of the aqueous particle.[90, 92, 93] Typically, the Gibbs-Duhem equation is used to predict water uptake of mixtures based on the thermodynamic properties of the individual components.[90] This model accurately predicts the water uptake and deliquescence lowering of some mixed aerosols where the thermodynamic properties such as Henry's Law constants, equilibrium vapor pressures and solubilities are known.[37, 90, 94-96] Since insufficient thermodynamic data exists for many common aerosol components these predictions are not able to accurately assess the hygroscopicity of many mixed systems and more laboratory work is needed.[97, 98]

The majority of laboratory studies on the effect of water uptake on aerosol properties to date have focused on measuring a growth factor based on a change in particle diameter or particle mass as a function of RH.[37, 95, 99, 100] Optical properties are calculated using the measured growth factors in conjunction with Mie theory. There have been few direct studies on the optical properties of complex aerosol mixtures.[13, 15, 18, 35, 101] Recent studies have used models to approximate the effects using volume weighted

mixing rules, which assume minimal dependence on mixing state.[18, 35, 37-39, 90, 95] These studies of internal mixtures show good agreement between theory and experiment if each component in the mixture behaves independently in terms of water uptake. In this paper, we investigated the optical properties of AS and NaCl mixed with montmorillonite [$(Na,Ca)(Al,Mg)_6(Si_4O_{10})_3(OH)_6$], a common component of mineral dust originating from specific source regions like the Northern Sahara and southern United States.[71, 102] Our montmorillonite sample originated in Gonzales County in Texas. Mineral dust aerosol is associated with windblown dust soil and has an estimated global source strength of 1,000-5,000 Tg yr^{-1}, accounting for 45% of the total aerosol mass load.[1, 40, 103] Mineral dust is mixed with soluble species like AS and NaCl by coming in contact with seasalt particles containing such inorganic compounds during in cloud processing or through condensation of gas phase compounds onto the particle surface with up to 85% of transported dust being internally mixed with other material.[104-108] Generally, the effect of RH on the radiative properties of mineral dust is considered negligible as the particles are treated as non-hygroscopic.[109] More importantly, some measurements reported in the current literature suggest little change in the hygroscopic behavior or radiative properties of internal mixtures of mineral dust and soluble material.[91, 110-112] Recently, several studies of different clay components of mineral dust found that a number of these particles have a range of hygroscopicities and the extent of water uptake largely depends on the structure and chemical composition of the clay.[24, 26, 67-69, 113] Our group has recently shown that montmorillonite does take up water at high relative humidities and this has a significant effect on optical properties, although the magnitude of the enhancement in extinction is small compared to pure AS or NaCl.[113] Therefore, we

expect that montmorillonite will contribute to the change in optical properties of multicomponent aerosols.

To our knowledge, there have been no previous direct optical measurements on internal mixtures of inorganic salts and insoluble clays. Here, cavity ring down spectroscopy (CRD) at 532 nm is used to directly measure the extinction of montmorillonite particles mixed with either AS or NaCl to achieve various compositions. The sensitivity of the relative humidity dependence of extinction by these internal mixtures based on the fraction of salt present is examined. The CRD was used to determine the extinction cross section (σ_{ext}) of size selected clay aerosols as a function of relative humidity, $fRH_{ext}(RH, Dry)$, where fRH_{ext} is:

$$fRH_{ext}(RH, Dry) = \frac{\sigma_{ext}(RH)}{\sigma_{ext}(Dry)} .$$ [4.1]

Direct optical measurements of these mixtures have the ability to decrease the uncertainty associated with quantifying optical properties in climate models as compared to using growth factors and Mie theory. Further, our investigation gives insight into whether volume weighted mixing rules used in conjunction with the measured fRH_{ext} of the pure components is sufficient to approximate the optical changes in multicomponent aerosol systems composed of both soluble and largely insoluble species.

Experimental Methods

In this study, CRD was employed to measure extinction as a function of relative humidity and particle composition. CRD has been used for a variety of optical measurements of both aerosol and gas phase species and has been reviewed extensively

in the literature.[13, 18, 29-31] The system used in the present work is similar to that fabricated

by Baynard et al.[31] The optical layout and cavity setup is described in detail elsewhere.[113]

A schematic of the full experimental set up is shown in Figure 4.1. The clay

investigated, montmorillonite (STx-1b), was purchased from the Source Clays Repository

and used as received. This clay has been previously well studied with other methods and

its chemical composition and structure are known. The layers of montmorillonite are
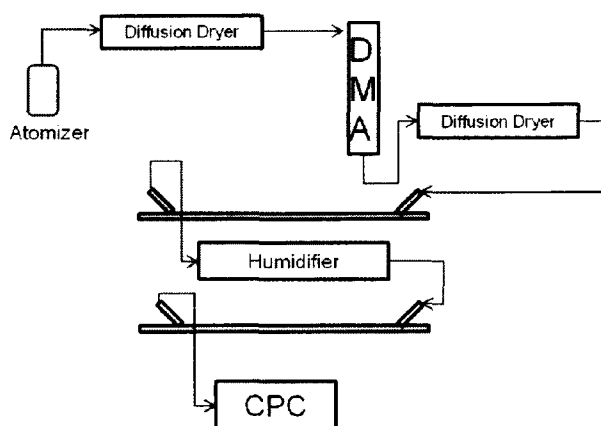
Figure 4.1: Atomized particles are first passed through a diffusion dryer before entering the differential mobility analyzer (DMA) where a polydisperse population of aerosols is size selected for 250 nm particles. The particles are then dried to a RH<10% before entering cavity. After exiting the first cavity, the particles are humidified to a desired RH and enter the second optical cavity before being counted by the condensation particle counter (CPC).

composed of a 2:1 ratio of silicon to aluminum held together by van der Waals forces and

charge countering cations.[75] Montmorillonite is classified as a "swelling clay" in which

the extent of water uptake is largely dependent on the availability of cations in between

the structural sheets and their hydration energies.[24, 67, 76] There are six hydroxyl groups on

its surface and therefore, it readily hydrogen bonds to absorbed water upon

humidification.[47]

To generate aerosols, a 10 wt% suspension of montmorillonite, a 1 wt% solution of AS (Sigma-Aldrich, ≥99.0%, ACS reagent grade), and a 1 wt% solution of NaCl (Fisher Chemicals, 99+%, ACS reagent grade) in HPLC grade water (J.T. Baker) were separately prepared for single component measurements. For mixed aerosol measurements, a suspension of 10 wt% montmorillonite with either AS or NaCl at 0.1-40 wt% was constantly mixed on a stir plate and atomized with pre-filtered nitrogen using a custom built constant output atomizer. The wet polydisperse aerosol was subsequently dried in a diffusion dryer with a residence time of ~12.5 s so the RH of the aerosol stream was decreased to <10%. We assume that the dry aerosol population exiting the dryer is internally mixed with the same composition as the atomized suspension. This assumption was tested by Freedman et al. using aerosol mass spectrometry (AMS) and Raman spectroscopy to determine the chemical composition and structure of similarly produced internally mixed aerosols consisting of ammonium sulfate and carboxylic acids with a range in solubilities.[18] Their AMS results confirmed that the concentration of the atomized solution is quite similar to that of the aerosols produced.[18] Raman spectroscopy was used to determine both the shape and composition of individual aerosol particles. Through this technique, they established that the particles were internally mixed as each individual particle showed a composite Raman spectrum of AS and dicarboxylic acid.[18] The assumption is further explored in this manuscript since the clays used were suspended in solution whereas the dicarboxylic acids used in Freedman et al. were all at least slightly soluble. Pure clay aerosols have been generated in sufficient concentration using this suspension method previously.[113, 114] The conversion of wt% of salt in the solutions to wt% of salt in aerosol samples can only be proven using microscopic or

spectroscopic techniques not currently available to us. The consequences of this assumption are discussed in the conclusions and atmospheric implications section. Salt concentrations were varied widely to ensure different mixtures even if atomized solutions were not perfectly representative of the aerosol sample.

After atomization and drying, the particles were directed through a differential mobility analyzer (DMA, TSI 3081L) to select a monodisperse size population for optical measurements. The DMA size selects particles based on an electrical mobility diameter with a reported uncertainty of 10% and therefore these are the diameters referred to throughout the manuscript.[77] Individual component and mixed montmorillonite/inorganic salt aerosol populations with diameters of 250 nm were size selected for optical investigation. The size chosen for this study can be compared to ambient atmospheric mineral dust particles, which span a size range of 100-5000 nm.[78] We have chosen to focus on smaller particles because larger particles have lifetimes on the order of a few hours and tend to settle out quickly from the atmosphere. Smaller particles in the size range selected will reside in the atmosphere longer and can be transported long distances.[79] The particle size was also chosen to be larger than the mode of the size distribution, which minimizes the contribution of multiply charged particles present in the sample. The multiply charged particles result from the neutralizer of the DMA. A sufficient concentration of particles for optical measurements was still achieved. Since our measurements are reported for a particular particle size, the extinction contribution for particles with multiple charges are calculated and used to correct the extinction values of the size selected particles. Only doublets were used in corrections; the number of

higher charged particles is expected to be small and would have a negligible effect on the extinction.[80]

The RH of the monodisperse sample following the DMA is maintained by passing the aerosols through a second diffusion dryer to remove any water vapor that was introduced via the sheath flow of the DMA. The dry aerosol sample enters and exits the first cavity of the CRD at a flow rate of 0.3 L/min, and the extinction, α_{ext}(dry) is measured according to the equation:

$$\alpha_{ext} = \frac{R_L}{c}\left(\frac{1}{\tau} - \frac{1}{\tau_0}\right) \qquad [4.2]$$

where R_L is the ratio of the cavity optical length to the sample length, c is the speed of light and τ and τ_0 are the ring down time with sample and the particle free ring down time, respectively.

After exiting the first cavity, the dry aerosol stream (RH<10%) passes through a custom built temperature controlled humidifier made with Accurel tubing. The relative humidity is ramped from 58% to 90% RH by slowly increasing the temperature of the humidifier from approximately 28° C to 35° C. The permeability of the Accurel tubing to water increases by raising the temperature. By changing the temperature in 0.5°- 1° C increments, the RH will slowly increase allowing for equilibrated measurements of the fRH$_{ext}$ throughout the RH range. Equilibration was achieved by allowing the RH and the ring down times to level off for several minutes before making an RH dependent measurement and then the temperature was increased to achieve a new RH. After humidification, the particles enter the second cavity where the extinction, α_{ext}(RH) is

measured at each RH. Temperature and RH are monitored in the center of each cavity using Vaisala INTERCAP HMP50 probes (accuracy ±3%) in both optical channels. The extinction results are converted to extinction cross sections (σ_{ext}) by dividing by the particle number concentration measured by a condensation particle counter (CPC, TSI 3775). The dry and humidified extinction cross section values are then used in equation 4.1 to calculate fRH_{ext}, which describes the relative humidity dependence of light extinction by the particles. Errors in fRH_{ext} values are reported as the experimental standard deviation (1σ) at specific RH values for each particle mixture over 3 different experiments. The CPC also determines the doublet concentration and correction using the measured number concentration at that size and the neutralizer charging distribution specified by the manufacturer for subsequent corrections. It is important to note that the CPC is the largest source of error with a reported uncertainty of 10% in particle counts. These uncertainties are minimized by reporting the fRH_{ext} as a ratio between humidified extinction and dry extinction for the same sample.

Results and Discussion

Single Component Aerosols

Single component aerosols were probed for comparison to other studies, as a reference for the aerosol mixtures and for calculations based on volume mixing rules. The fRH_{ext} of pure montmorillonite as a function of RH is shown in Figure 4.2. This figure along with Figures 4.3, 4.4, 4.5 and 4.6 all display a composite of individually measured fRH_{ext} following equilibration at each RH value. Results are reported for particles with a 250 nm diameter for montmorillonite and all other particles studied. An fRH_{ext} of 1 is expected when there is no optical change in the particle upon humidification.
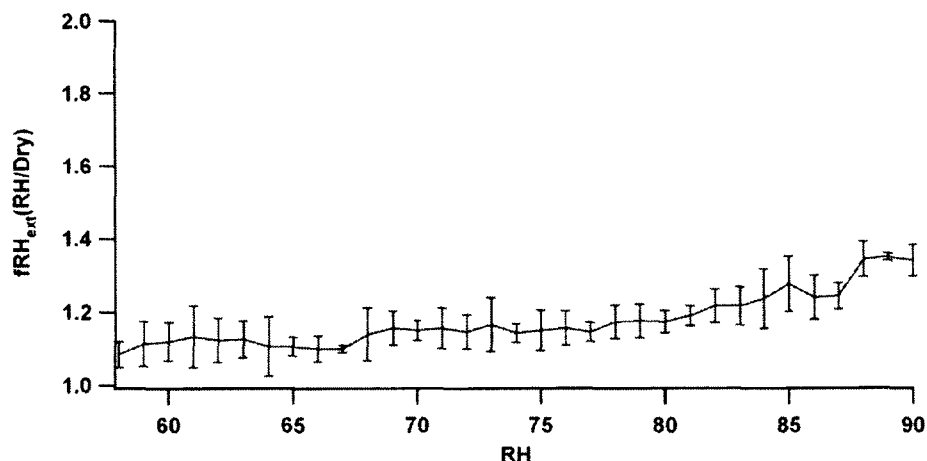
Figure 4.2: A composite of the individually measured fRH_{ext} as a function of RH for pure montmorillonite from 58-90% RH. Montmorillonite particles do not exhibit a DRH but do take up water gradually as RH is increased. The error in the RH measurement is ±3%.

Montmorillonite shows a steady increase in extinction as a function of relative humidity, with the fRH_{ext} reaching a maximum of 1.34±0.04 at 90% RH, the highest RH under study.[55] At 58% RH there is optical growth due to water associated with the particle, indicated by an fRH_{ext} > 1. These particles do not exhibit deliquescence, but do show a steady increase in extinction throughout the RH range studied. Although montmorillonite is largely insoluble, its ability to show an enhancement in extinction as a function of RH is known to occur as a result of swelling from incorporation of water between the layers or on the surface to increase particle size and hence extinction.[24, 67, 76, 113]

The heavy black traces in Figures 4.3 and 4.4 show the fRH_{ext} as a function of RH for pure AS and pure NaCl, respectively. Error bars for this data are included in Figures 4.5 and 4.6 and are omitted here for clarity. At low RH, AS does not take up water and there is no enhancement in extinction as shown by an fRH_{ext} = 1. An abrupt increase in
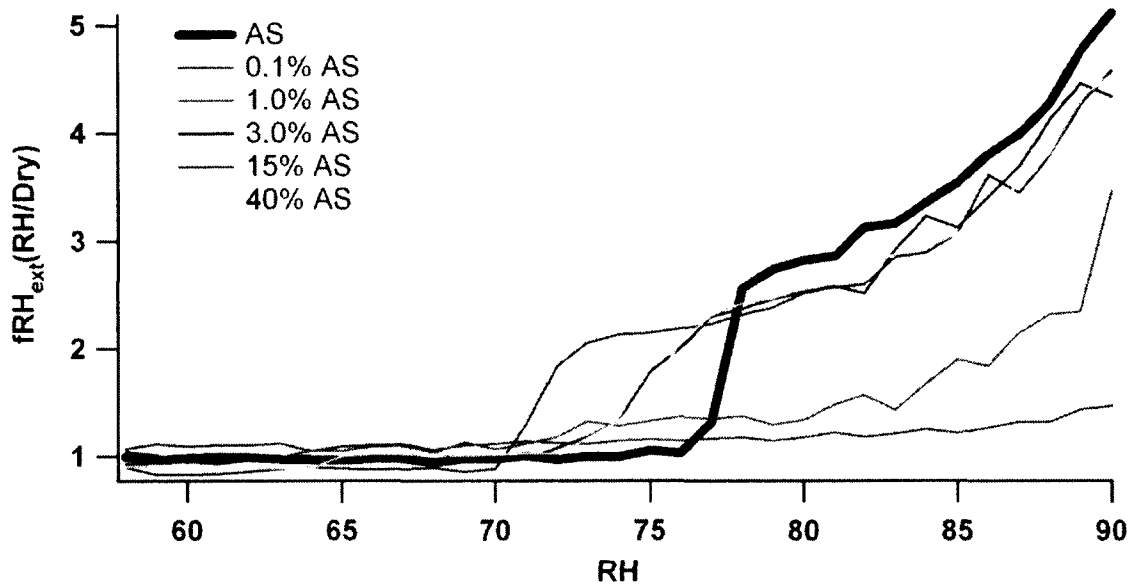
Figure 4.3: A composite of the individually measured fRH_{ext} as a function of RH for internal mixtures of 10 wt% montmorillonite with 0.1 wt% (red), 1.0 wt% (green), 3.0 wt% (blue), 15 wt% (purple) or 40 wt% (orange) AS. Results for pure AS are also shown in black. Particles have an initial diameter of 250 nm. Error bars are omitted for figure clarity but can be found in the panels of Figure 4.5.

fRH_{ext} at 77±3% RH shown in Figure 4.3 signifies the DRH for pure AS. This abrupt increase in extinction is due to an increase in particle size as the particle transitions from solid to liquid at that RH. Our results are consistent with other studies, which report the DRH of AS at 78-81% RH.[37, 95, 115-117] Since AS is soluble and very hygroscopic, the particles continue to take up water after deliquescence, increasing the extinction by the particles and hence the fRH_{ext} to 5.1±0.4 at 90% RH. The initial particle size stayed constant throughout the experiments and therefore we would not expect the fRH_{ext} as a function of RH to change with different salt concentrations (wt%). We only measured the fRH_{ext} of pure AS and NaCl at 1 wt% salt as the DRH is a physical property that does not vary with the concentration of the solution used to generate pure salt aerosols through atomization.
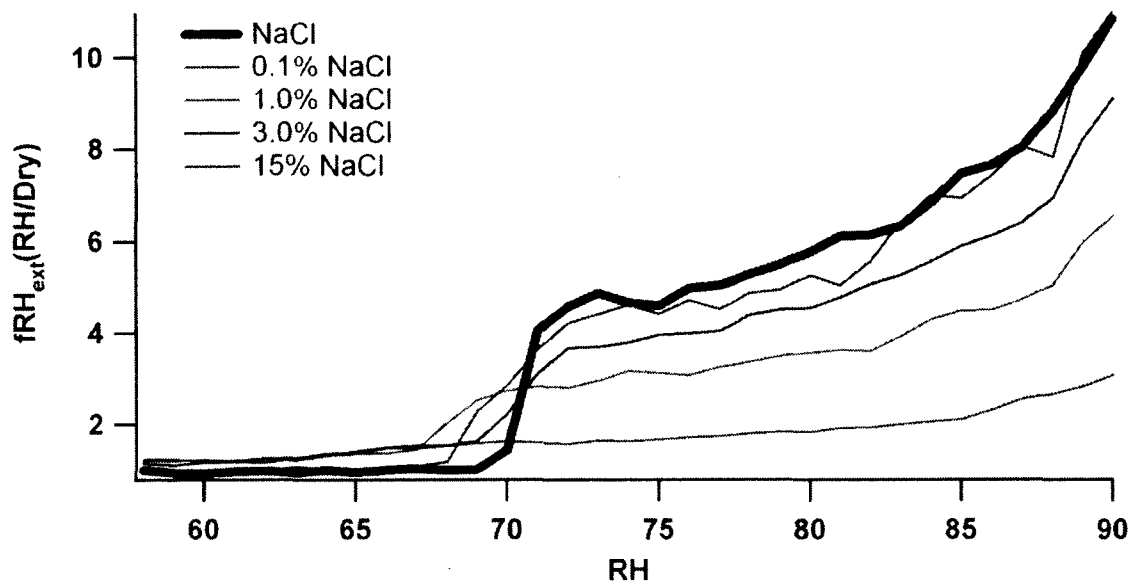
Figure 4.4: A composite of the individually measured fRH$_{ext}$ as a function of RH for internal mixtures of 10 wt% montmorillonite with 0.1 wt% (red), 1.0 wt% (green), 3.0 wt% (blue) or 15 wt% (purple) NaCl. Results for pure NaCl are also shown in black. Particles have an initial diameter of 250 nm. Error bars are omitted for figure clarity but can be found in the panels of Figure 4.6.

For pure NaCl, there is no enhancement in extinction until the RH reaches 70±3% and the particles deliquesce. This DRH is consistent with other studies which report the DRH of NaCl between 70-75% RH.[37, 95, 116, 117] NaCl shows an even greater enhancement in extinction, compared to AS, as the particles continue to take up water at high relative humidities reaching a maximum fRH$_{ext}$ of 11±2 at 90% RH. The measured enhancement in extinction of montmorillonite is significantly smaller than that of AS and NaCl at high RH due to the clay particles being insoluble and much less hygroscopic.

Internally Mixed Particles

Particles composed of internal mixtures of AS or NaCl and montmorillonite were produced at various salt/clay mass fractions in order to investigate the composition and RH dependence of extinction. Figures 4.3 and 4.4 show the change in fRH$_{ext}$ as a

function of RH for various mass fractions of AS and NaCl, respectively in comparison to single component salt aerosols. In all cases, the montmorillonite concentration stayed constant at 10 wt% whereas the salt mass fraction varied from 0.1-40 wt% for AS and from 0.1-15 wt% for NaCl. The lower solubility of NaCl prevented a measurement at 40 wt% NaCl. In the following, the mixed particles will be referred to by the wt% of the salt.

For 0.1 wt% AS, the particles showed no sharp deliquescence but rather continually take up water throughout the RH range behaving similarly to the pure montmorillonite particles as seen by comparing Figure 4.2 and 4.3. At low RH, water is associated with the particle due to the high relative proportion of the clay. At high RH the enhancement in fRH_{ext} is greater than montmorillonite alone. At 90% RH, montmorillonite has a maximum fRH_{ext} of 1.34±0.04 whereas this internal mixture reached an enhancement of 1.47±0.02. The higher extinction at 90% RH for 0.1 wt% AS indicates that the salt portion of the mixed particle has increased the hygroscopicity and enhanced the extinction at high RH even though the wt% of montmorillonite exceeds that of AS by two orders of magnitude. Insoluble/soluble internal mixtures can form different structures including an insoluble core surrounded by a soluble shell or particles with a soluble matrix and insoluble inclusions.[19, 118] Regardless of structure, the AS associated with the particle is more hygroscopic and will lead to an increase in the amount of water associated with the mixed aerosol in comparison to pure montmorillonite. At 1.0 wt% AS, there is a minor increase in fRH_{ext} at 72% RH, although it is unlikely it reflects a full phase transition. Therefore the gradual change in fRH_{ext} for 1.0 wt% AS may be interpreted similarly to the 0.1 wt% AS mixed and pure montmorillonite aerosols. For 1.0

wt% AS at 90% RH an enhancement in the extinction of 3.47±0.04 was observed as would be expected for the larger wt% AS.

As shown in Figure 4.4, the addition of montmorillonite has a similar effect on the optical properties of the mixtures with low salt fractions of NaCl as is seen with AS. Because of the mixture, the salt does not behave as a pure salt with a well defined DRH. For 0.1 wt% NaCl, the fRH_{ext} as a function of RH follows the same trend as pure montmorillonite. At 58% RH, water is associated with the particle and no DRH is observed even when the RH is increased to 90%. Water is continually taken up by the particles, with increasing extinction most likely due to increasing particle size. At 90% RH the fRH_{ext} reaches a maximum of 3.07±0.20 which is a larger enhancement then montmorillonite alone (1.34±0.04) or 0.1 wt% AS (1.47±0.02). At low relative salt compositions for the NaCl, like the AS case, montmorillonite enhances the extinction at low RH because water is associated with the clay as seen in the single component montmorillonite results. At high RH, salt incorporated in the particle increases the amount of water associated with the clay, enhancing extinction due to a probable increase in particle size beyond that seen with the clay alone. The higher fRH_{ext} observed in the pure NaCl cases is most likely due to the differences in density between the two salts. A direct correlation between particle density and hygroscopicity has been observed for mixed aerosol particles.[119] NaCl has a higher density (2.165 g/cm^3) compared with AS (1.769 g/cm^3) and therefore these results are expected.[83]

As the amount of AS in the particles is increased to 3.0, 15 and 40 wt%, the fRH_{ext} as a function of RH begins to have a shape similar to pure AS, showing little enhancement in extinction until an abrupt increase signifying the DRH of the pure salt.

However, the onset in DRH for these AS/montmorillonite mixtures occurs at a lower RH than pure AS. Similarly, the onset of deliquescence is observed at an RH lower than the DRH of pure NaCl for aerosols from 1.0, 3.0 and 15 wt% NaCl solutions. The decreases in DRH for the NaCl mixtures are not as pronounced as in the AS mixtures and are within the error of our RH probes. Deliquescence lowering is a well known phenomena occurring when there is physical contact between two or more deliquescent compounds and the thermodynamics of the process are explained in detail elsewhere.[90, 120, 121] Previous laboratory studies have shown DRH lowering for both AS and NaCl when mixed with another electrolyte or a weakly dissociating organic compound, but this is the first time to our knowledge that it has been observed in mixtures with an insoluble, non-deliquescent clay.[88, 90, 94, 122]

The decrease in DRH of mixed systems occurs at a thermodynamic global minimum that is at a lower RH than the DRH of either of the individual components. Our results demonstrate that DRH lowering can occur when montmorillonite is one of the components in the system, even though montmorillonite does not deliquesce and is insoluble. Of particular interest is that the extent to which the DRH decreases is independent of the relative proportions of the salt and montmorillonite in the sample. The DRH onset for the samples where DRH was lowered from 77±3% RH and 70±3% RH for pure AS and pure NaCl respectively, have a maximum variation in the DRH of 3% from 70-73% RH for AS and 2% from 67-69% RH for NaCl. Thus the variability in the lowered DRH values is within the uncertainty (±3%) of our RH measurements. Similar examples, where relative amounts of components had no influence on the extent of DRH lowering, have been reported in the literature.[123, 124]

The lowered DRH observed in the salt/clay mixtures studied here can be described thermodynamically by investigating changes in the Gibbs free energy of mixtures due to ion-molecule interactions.[93, 125] In mixtures where the contribution of salt to the particles is relatively high (i.e. 3.0, 15 and 40 wt% AS and 1.0, 3.0 and 15 wt% NaCl), montmorillonite has the ability to reduce the Coulomb attractive forces between the cation and anion in the salt. In addition, the montmorillonite will cause a disorder of the lattice structure of the pure salt component. Both of these factors will slightly increase the Gibbs free energy of the system in comparison to the pure components.[93, 125] The increase in energy will cause the particle to incorporate water at a lower RH than the DRH of the pure substances to allow return to a lower, more favorable overall Gibbs free energy of the system. Eventually, as the RH exceeds the DRH of the salt, complete dissolution of the salt will occur. At lower relative percentage of salt (0.1, 1.0 wt% AS and 0.1 wt% NaCl) the ion-molecule interactions are not as strong. The cation and anion interactions and the lattice structure of the salt are not affected by the montmorillonite to the point that it would cause a reduction in the DRH for these systems. In fact, the salt concentration is too low for a DRH to be observed and so the clay characteristics dominate.

The DRH of a mixture of two deliquescent compounds can be approximated by multiplying the water activities of each component in a saturated solution through the Ross equation:[126]

$$a_w = (a_w^\circ)_1 * (a_w^\circ)_2 \dots \qquad [4.3]$$

This equation can be written in terms of DRH, assuming that a_w° is directly related to DRH by ignoring any kinetic effects:

$$\frac{DRH_{mixture}}{100} = \frac{DRH_1}{100} * \frac{DRH_2}{100} \cdots \qquad [4.4]$$

This approximation has been successful in predicting the DRH of different mixtures where the water activities or individual DRH values are well known.[120, 124] However, since montmorillonite is not water soluble and therefore does not have a water activity in a saturated solution, this approach is not helpful when trying to describe the influence of clay on the water uptake and consequently the optical properties of AS and NaCl.

Another approach widely used in predicting the optical response to an increase in RH is volume weighted mixing rules based on the Zdanovskii-Stokes-Robinson (ZSR) model.[127] This technique has been shown to be valid in assessing water uptake for inorganic salts mixed with organics.[18, 35, 37-39, 90, 95, 100, 128] We used the measured fRH_{ext} data for the pure components to predict the fRH_{ext} of mixtures using the ZSR equation as follows:

$$fRH_{ext}(RH) = [\epsilon_0 * fRH_{ext,mont}^3 + (1 - \epsilon_0) * fRH_{ext,salt}^3]^{1/3} \qquad [4.5]$$

where ϵ_0 is the volume fraction of montmorillonite in the dry particle and $fRH_{ext,mont}$ and $fRH_{ext,salt}$ are the fRH_{ext} for pure montmorillonite and pure salt at a given RH, respectively.

Figures 4.5 and 4.6 display comparisons of the measured and predicted enhancement in fRH_{ext} as a function of RH for AS and NaCl internally mixed aerosols, respectively.
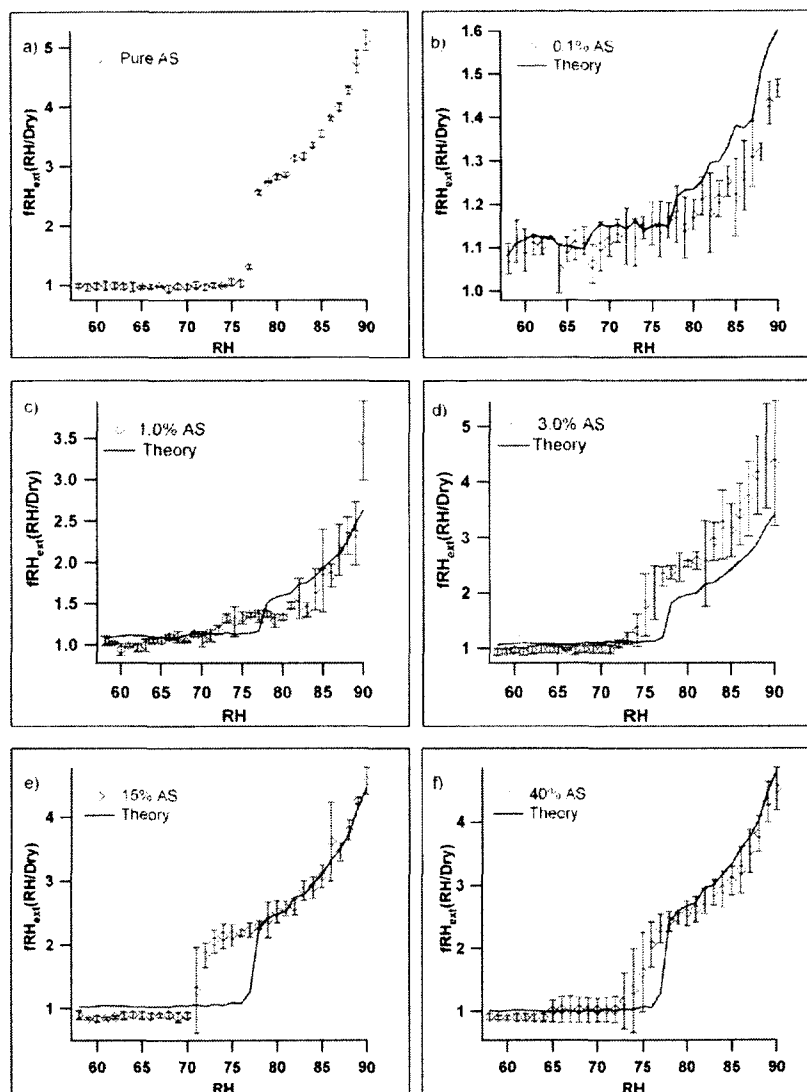
Figure 4.5: A composite of the individually measured fRH_{ext} as a function of RH for pure ammonium sulfate and internal mixtures of montmorillonite and ammonium sulfate (diamonds). The solid lines represent the theoretical prediction based on single component measurements and the ZSR model. Initial particle diameter is 250 nm and reported error is 1σ.

Since experiments were run using different mass fractions of the salt, these values were converted to volume fractions using the density of each component in the dry particle as shown in Table 4.1. For AS at RH $\leq71\%$ and for NaCl at RH$\leq63\%$, both prior to deliquescence, the ZSR approximation accurately predicts the optical response for all
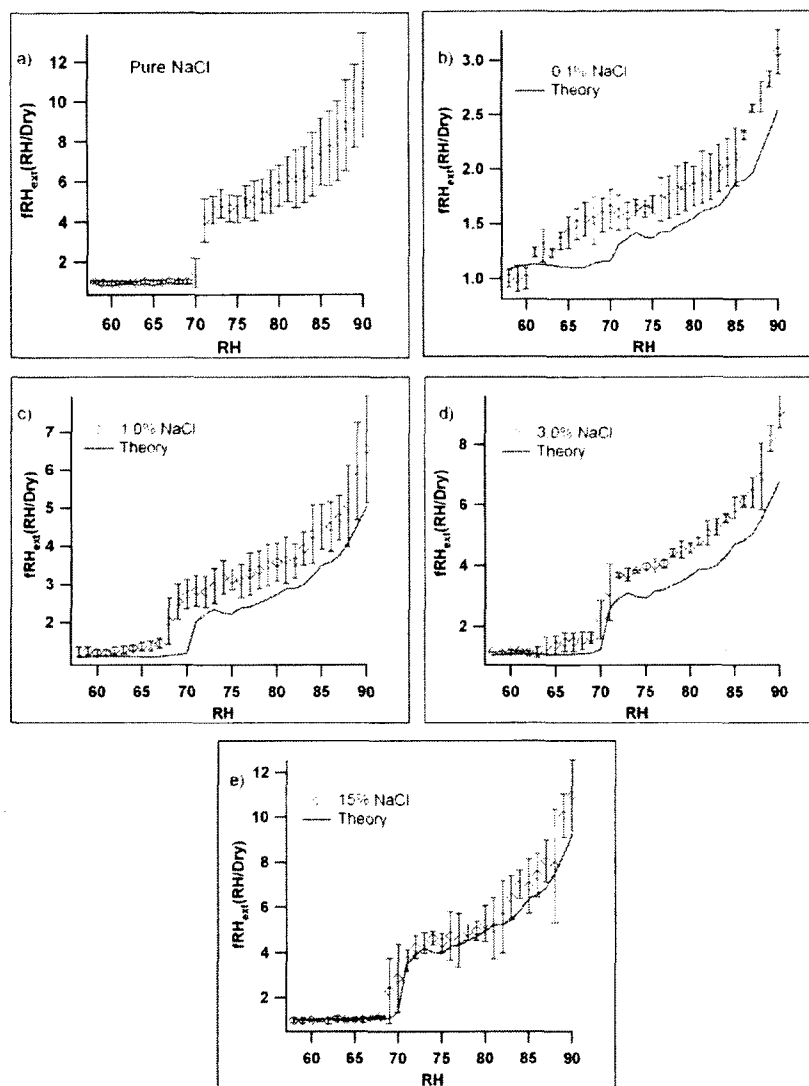
Figure 4.6: A composite of the individually measured fRH$_{ext}$ as a function of RH for pure sodium chloride and internal mixtures of montmorillonite and sodium chloride (diamonds). The solid lines represent the theoretical prediction based on single component measurements and the ZSR model. Initial particle diameter is 250 nm and reported error is 1σ.

salt/clay mixtures to within 10%. Any enhancement in extinction at these humidities is most likely dominated by the presence of montmorillonite which is non deliquescent but will cause water to be associated with the particle at a RH lower than the DRH of the salt. The simple ZSR approximation used here proves to be sufficient in capturing this enhancement at RH below deliquescence.

Table 4.1: Comparison of the weight percent (wt%) and volume percent (vol%) of ammonium sulfate and sodium chloride calculated using densities.

	wt% salt[a]	vol% salt[a]
Ammonium Sulfate	0.1	1.3
1.769 g/cm³	1.0	12
	3.0	28
	15	66
	40	84
Sodium Chloride	0.1	1.1
2.165 g/cm³	1.0	9.8
	3.0	25
	15	62

This model approximation fails to reproduce the more complicated effect of montmorillonite on AS and NaCl in the region around the DRH. It does not account for changes in the Gibbs free energy of the system caused by molecular disturbances in the attractive forces between the ions and the lattice structure. The largest error occurs for internally mixed AS and NaCl particles within ±6% of their pure component DRH. This deviation from theory occurs at all compositions where DRH lowering is observed. In some cases the error exceeds 100%. For example, at 76% RH for 15 wt% AS in Figure 4.5(e), the measured fRH_{ext}=2.19±0.05 corresponds to a predicted fRH_{ext}=1.09. This large discrepancy between the measured and theoretical values is significant since theory would predict there to be essentially no enhancement in extinction for these particles at 76% RH but experiment shows that extinction more than doubles at this RH. Our results indicate that there would be obvious consequences in using ZSR theory to predict the extent of radiative forcing for these internally mixed aerosol particles between 72% and 80% RH. The NaCl/clay mixed particles also show large discrepancies around the DRH, with the biggest errors increasing from 20% at 64% RH [for 1 wt% NaCl, Figure 4.6(c)] to 130% at 70% RH with an experimental fRH_{ext}=2.73±0.38 and a theoretical

fRH$_{ext}$=1.19. Once again, based on theory, little enhancement in extinction is expected to occur whereas experiment shows more than a doubling in the extinction of light by the particles. For internally mixed NaCl particles in this RH region (64<RH<70), the simple ZSR approximation is not valid for assessing the enhancement in extinction for these mixtures.

The ZSR approximation is generally useful in predicting fRH$_{ext}$ for particles internally mixed with AS or NaCl when they are fully deliquesced and optical growth is a consequence of gradual water uptake by the particle. This approximation is slightly better for internally mixed AS particles. The only compositions that exceed a 10% error between the measured and predicted fRH$_{ext}$ is 3 wt% AS and a single measurement at 90% RH for 1% AS. In the 3 wt% AS case, theory underestimates the enhancement by approximately 35% from 80%<RH<90%. This is similar to what is seen in the NaCl/clay mixed particles. Theory underestimates fRH$_{ext}$ between 20-40% for 0.1, 1.0 and 3.0 wt% NaCl. The difference in accuracy between the two salts could be due to the large differences in the volume weighted fractions calculated at each mass fraction as shown in Table 4.1. Due to differences in density between the two salts, the volume percentages of AS are higher than NaCl. ZSR predicts fRH$_{ext}$ based on the volume fraction of each salt in the particle which could explain the better agreement between theoretical and measured values for AS at high RH.

Conclusions and Atmospheric Implications

In this work, the fRH$_{ext}$ was measured for internal mixtures of montmorillonite with AS or NaCl at various compositions over a RH range of 58-90%. The different physical properties and chemical structures of the two salts played an important role in

the variability in the humidity dependence for the optical properties of their mixtures.
Contrary to previous studies on insoluble mineral dust, we have shown that
montmorillonite does affect the hygroscopic properties of salt particles.[90, 91, 110] The onset
of deliquescence for 3.0, 15 and 40 wt% AS and 1.0, 3.0 and 15 wt% NaCl, was lowered
in comparison to the salt alone. These observations have important implications for the
atmosphere, suggesting that the transformation of a mixed salt/montmorillonite particle
from solid to predominantly liquid can occur at a lower RH then is expected by the pure
salt due to perturbations in the ion-molecule interactions and lattice structure that result
from the presence of montmorillonite. We have also shown that this effect cannot be
predicted by simple mixing rules based on the fRH_{ext} of the pure components, mainly due
to errors in replicating the lowered DRH. If the lowered DRH is not accounted for when
assessing the optical properties of the mixed particles, the predicted extinction has the
potential to be underestimated especially within 6% of the pure salt DRH. In addition,
water may be present on the mixed particle prior to deliquescence due to the presence of
the montmorillonite which takes up water even at low RH. This will change the physical
and chemical properties of the mixed particle. In particular, the rates of heterogeneous
chemical reactions have been shown to be influenced by particle phase and water
content.[55, 57, 129-134] The reaction probability for the hydrolysis of N_2O_5 decreases an order
of magnitude from 0.02-0.06 to <0.003 for liquid and solid ammonium sulfate particles,
respectively. Therefore, our results indicate a broadened range of RH in which such
liquid phase reactions can take place. [56, 135, 136]

Pure, unmixed aerosols are uncommon in the atmosphere and most aerosols,
including mineral dust, will exist as a mixture with other components. Our results also

show that the amount of light scattered and absorbed by a salt particle and hence the size and phase is dependent on whether or not it is internally mixed with montmorillonite. Based on the data for the individual pure components, we used the ZSR approximation as a predictor for optical growth of the mixed particles and found that in some cases using this estimate for fRH_{ext} ratios at high (above 85%) and low (below 60%) RH is an adequate first approximation. However, in the RH=65-80% range where typical ambient RH of the atmosphere falls, the effects of montmorillonite on the optical properties of the salts are the most complex and this approximation was shown to be inadequate. Specifically, the complex ion-molecule interactions inferred from our experiments change the overall energy of the mixed systems around the DRH and are not accurately captured for most ambient humidity conditions using a simple volume weighted mixing rule.

Disagreement between theoretical and measured values using the ZSR equation could be attributed to the assumption that the aerosol samples had the same composition as the atomized suspension. For example, if the concentration of NaCl in the particle in Figure 4.6(d) was greater than the 3 wt% in the atomized solution, there would be better agreement between measured and theoretical values. For this case, the particles would have to contain approximately 45 wt% NaCl, more than 40 wt% greater than assumed, to agree within 10% of the fRH_{ext} values predicted by ZSR theory at high RH. However, this is one extreme case, and the agreement in the rest of the model comparisons suggests that our assumption is correct. If the reported wt% salt in the particle is inaccurate, adjustments still would not predict the DRH lowering using ZSR theory. This is the first time DRH lowering has been observed due to addition of mineral dust to aerosols and it

is important to consider the challenges of predicting the phase of mixed aerosol in this

range of atmospherically relevant humidities.

CHAPTER 5

EXTINCTION AND HYGROSCOPICITY OF CLAY AEROSOLS MIXED

WITH REPRESENTATIVE DICARBOXYLIC ACIDS: A PROXY FOR

ATMOSPHERIC PROCESSING

Introduction

Mineral dust particles are associated with windblown dust soil and have an

estimated global source strength of 1,000-5,000 Tg yr^{-1}, accounting for 45% of the total

aerosol mass load.[1, 40, 103] Mineral dust is involved in many different atmospheric

processes including deposition of micronutrients[45, 46], providing surfaces for

heterogeneous reactions[47-49] plus direct[50-52] and indirect radiative forcing.[53, 54] They

change the energy balance of the atmosphere by scattering incoming short-wave radiation

(negative forcing) and absorbing outgoing infrared terrestrial radiation (positive

forcing).[50, 52, 54] Due to the complicated chemical makeup and irregular shape of the

species, along with high loading and spatial and temporal variability, mineral dust

aerosols represent the largest uncertainty associated with climate change having a net

negative forcing reported as -0.1 ± 0.5 W m^{-2}.[1] The Fourth Assessment Report of the

Intergovernmental Panel on Climate Change reports "the level of scientific

understanding" as very low for the radiative effects of mineral dust.[1]

Particle size, complex refractive index and shape largely determine the extent of

extinction, or the sum of absorption and scattering, of light by the particle. Each of these

characteristics can be affected by mixing with other species and water uptake as a particle is transported through the atmosphere. Atmospheric particles are often observed as a mixture of organic and inorganic material including salts, insoluble soot and mineral dust. The organic portion contributes 30-50% of fine particulate mass depending on location.[3, 137-139] The organic fraction has been the subject of many recent studies due to its ability to affect light extinction, hygroscopicity, phase transitions, solubilities and chemical reactivities of mixed particles; although the majority of these studies focus on particles consisting of organics mixed with inorganic salts such as ammonium sulfate and sodium chloride.[37-39, 59, 93, 95, 96, 99, 128, 140, 141]

Field studies have identified several different types of organic components, including short chain dicarboxylic acids, on the surface of mineral dust particles with up to 80% of transported dust being internally mixed with other material.[59, 70, 104, 105, 108] However, the optical and hygroscopic properties of mineral dust[24, 25, 65-68, 113] and organic particles[142, 143] are typically studied independently, with few experiments regarding their radiative effects when mixed. In addition, studies of mixed dust aerosols have only indirectly investigated the changes in optical properties of mixed particles, typically using an electrodynamic balance or humidified tandem differential mobility analyzer (HT-DMA) to measure a change in particle mass or diameter, respectively, as a function of relative humidity (RH). There is a lack of direct spectroscopic data on the optical properties of these mixtures.

In addition to the radiative effects of processing by coating or mixing organic species with mineral dust, the amount of scattering and absorption is further complicated by the water content, the hygroscopicity and phase of a particle. When exposed to

increasing RH, some inorganic and organic species undergo a phase transition from solid to liquid droplet at a specific RH known as the deliquescence relative humidity (DRH). Although mineral dust does not explicitly exhibit deliquescence, several recent studies of different clay components of mineral dust found that these particles have a range of hygroscopicities dependant on the structure and chemical composition of the clay.[24, 26, 67-69, 113]

The effects of aerosols on climate are usually modeled using Mie theory, providing an estimate based on spherically shaped particles and approximate values for the refractive index.[64, 144] However, these calculations tend to overestimate the scattering of mineral dust particles because of irregular shape and inhomogeneous composition.[64-66] A recent study investigated the agreement between Mie theory simulations for various shapes, including sphere and disk, and experimentally obtained extinction for the major silicate resonance bands of mineral dust in the infrared region from 800-1600 cm^{-1}. Results showed a large deviation from spherical Mie theory for band position, band shape and peak intensity.[65]

To better quantify the effects of mineral dust on climate, a detailed quantitative connection between optical properties and mixing state is required. However, there are a limited number of laboratory studies on the optical properties of mineral dust and no laboratory studies, to our knowledge, of the optical properties of mineral dust internally mixed with atmospherically relevant dicarboxylic acids that would be representative of a processed aerosol. In this study, we used cavity ring down spectroscopy (CRD) to directly measure the optical properties of montmorillonite, a common clay component of mineral dust, internally mixed with succinic, glutaric and malonic acid, which are all

abundantly found in the atmosphere. Our technique investigates how simulated atmospheric processing represented by mineral dust mixed with these organic species affects the optical properties in comparison to freshly emitted, single component montmorillonite particles. Fresh and mixed processed mineral dust particles are analyzed under both dry and humidified conditions to detect any additional enhancement in extinction due to water uptake on the mixed processed particles. In the following, we will show that the difference in extinction between freshly emitted, single component and mixed processed mineral dust is dependent on particle size and the type of dicarboxylic acid associated with the particle.

Experimental

A CRD was employed to measure extinction of laboratory generated mixed processed mineral dust in comparison to freshly emitted mineral dust aerosols and dicarboxylic acid particles. The details of the experimental setup used to generate and measure the optical properties of mineral dust containing aerosols have been described in detail previously.[113, 145] Figure 5.1 summarizes the CRD system employed including additional instrumentation for particle generation, sizing and counting. Briefly, single component aerosols are generated via atomization of a 10 wt% suspension of montmorillonite (The Clay Minerals Society, Source Clays Repository, STx-1b) as a mineral dust proxy or a 1 wt% solution of the dicarboxylic acids, succinic acid (Mallinckrodt, 99+% ACS reagent grade), glutaric acid (Acros Organics, 99+% ACS reagent grade) or malonic acid (Acros Organics, 99+% reagent grade), in HPLC grade water (J.T. Baker). For mixed processed aerosol measurements, a suspension of 10 wt% montmorillonite with each individual dicarboxylic acid at 1.0 wt% in water was
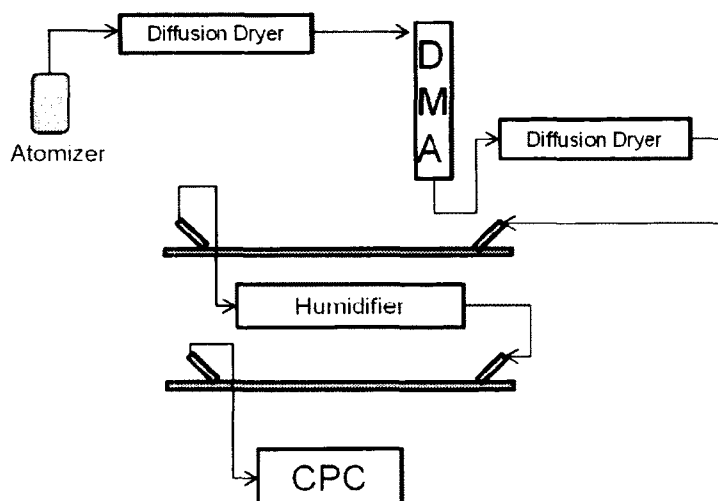
Figure 5.1: Experimental setup used to measure the extinction of light by mineral dust and internal mixtures of mineral dust and dicarboxylic acids.

constantly mixed and atomized with pre-filtered nitrogen using a custom built constant output atomizer. For glutaric and malonic acid samples, the wet polydisperse aerosol was subsequently dried in a diffusion dryer with a residence time of ~12.5 s. An additional dryer was used for succinic acid to ensure maximum removal of water from the particle, increasing the residence time in the dryers to ~25 s. In both cases, the RH of the aerosol stream was decreased to <10%.

We assume that the dry aerosol population is physically and chemically homogeneous and internally mixed with the same composition as the atomized suspension. This assumption was validated by Freedman et al. using aerosol mass spectrometry (AMS) and Raman spectroscopy to determine the chemical composition and structure of similarly produced internally mixed aerosols consisting of ammonium sulfate and a number of different carboxylic acids with a range in solubilities.[18]   After atomization and drying, the particles were directed through a differential mobility analyzer (DMA, TSI 3081L) to select a monodisperse size population for optical

measurements. The DMA size selects particles based on an electrical mobility diameter with a reported uncertainty of 10% and therefore these are the diameters referred to throughout the chapter.[77] Individual component and mixed processed aerosol populations with diameters ranging from 250 nm to 600 nm were selected. These sizes were chosen in comparison to ambient atmospheric mineral dust particles, which span a size range of 100-5000 nm.[78] A focus on smaller particles is relevant because larger particles have shorter lifetimes and quickly settle from the atmosphere, while smaller particles can be transported long distances.[79] The particle sizes are larger than the mode of the size distribution, minimizing the contribution of multiply charged particles and thus the required optical correction for the sample. The multiply charged particles result from the neutralizer of the DMA and can complicate optical measurements. Since our measurements are reported for a particular particle size, the extinction contribution for particles with multiple charges are calculated and used to correct the extinction values of the size selected particles. Only doublets were used in corrections; the number of higher charged particles is expected to be small and would have a negligible effect on the extinction.[80]

The RH of the monodisperse sample following the DMA is maintained by passing the aerosols through a second diffusion dryer. The dry aerosol sample enters and exits the first cavity of the CRD at a flow rate of 0.3 L/min, and the extinction, $\alpha_{ext}(Dry)$ is measured according to the equation:

$$\alpha_{ext} = \frac{R_L}{c}\left(\frac{1}{\tau} - \frac{1}{\tau_0}\right)$$

[5.1]

where R_L is the ratio of the cavity optical length to the sample length, c is the speed of light and τ and τ_0 are the ring down time with sample and particle free, respectively.

The dry aerosol stream (RH<10%) passes through a custom built temperature controlled humidifier made with permeable Accurel tubing (Microdyn Technologies, Inc). The RH is ramped from 58% to 90% RH by slowly increasing the temperature of the humidifier from approximately 28° C to 35° C. Changing the temperature in 0.5°- 1° C increments, allows for equilibrated measurements of the fRH_{ext} throughout the RH range so that the DRH can be observed. For mixed processed aerosol components, the elevated RH is kept constant at 80% RH. After humidification, the particles enter the second cavity where the extinction, $\alpha_{ext}(RH)$ is measured. Temperature and RH are monitored using Vaisala INTERCAP HMP50 probes (accuracy ±3%) in both optical channels. The extinction results are converted to extinction cross sections (σ_{ext}) by dividing by the particle number concentration (N) measured by a condensation particle counter (CPC, TSI 3775):

$$\sigma_{ext} = \frac{\alpha_{ext}}{N}.$$ [5.2]

The dry and humidified extinction cross section values are then used to calculate fRH_{ext} for single component measurements:

$$fRH_{ext}(RH, Dry) = \frac{\sigma_{ext}(RH)}{\sigma_{ext}(Dry)}$$ [5.3]

which describes the relative humidity dependence of light extinction by the particles. For mixed processed aerosols, enhancement factors (EF) were calculated using the equation:

$$EF = \frac{\sigma_{ext,processed}}{\sigma_{ext,fresh}}$$ [5.4]

77
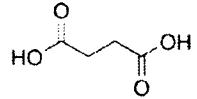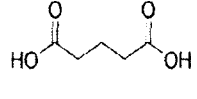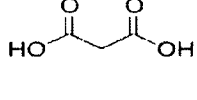
as described by Zhang et al.[15] In this equation, $\sigma_{ext,processed}$ is represented by the extinction cross section of the mixed processed mineral dust and $\sigma_{ext,fresh}$ is represented by the extinction cross section of the single component mineral dust. EFs were measured under dry (RH<10%) and humidified (RH=80%) conditions. Errors in both values are reported as the experimental standard deviation (1σ) for each particle mixture over 3 different experiments.

Results and Discussion

Succinic Acid

The fRH$_{ext}$ calculated using equation 5.3 at 80% RH for single component succinic acid, malonic acid, glutaric acid and montmorillonite at 250 nm, 350 nm, 450 nm and 600 nm are reported in Table 5.1. An fRH$_{ext}$<1 indicates that total extinction by the particle decreased upon humidification, while particles experiencing an increase in extinction have an fRH$_{ext}$>1 and those particles showing no change upon humidification have an fRH$_{ext}$=1. Succinic acid has an fRH$_{ext}$=1.11(0.05) for 250 nm particles at 80% RH, similar to what is seen in other studies reported in the literature, and reaches a maximum fRH$_{ext}$=4.1 at 90% RH, the highest RH studied.[39, 100, 142, 143] Our observed DRH is lower (DRH=81%) than what is reported for bulk solution or electrodynamic balance measurements as shown in Table 5.1. This discrepancy can be attributed to the hygroscopic state of the particles during the experiment. Although the RH of the first cavity was below 10% and the crystallization RH of succinic acid is 53.2-53.4%, it is possible that some water could still be associated with the particles, thus allowing water uptake at RH below the DRH.[35, 142] Contrary to our technique, the bulk studies reported in

Table 5.1: fRH$_{ext}$ values and selected properties for the dicarboxylic acids and montmorillonite.

Compound		fRH$_{ext}$(80%, dry)	DRH	RI	Solubility[a] (g/100g H$_2$O at 25°C)	Structure
Succinic Acid	250 nm	1.11 (0.05)				
	350 nm	1.06 (0.03)	81[c], NONE[d], 98.8[e], 97.6[f], 99[h], 98-100[i]	1.450[j]	8.8	
	450 nm	1.05 (0.03)				
	600 nm	1.02 (0.03)				
Glutaric Acid	250 nm	1.42 (0.11)				
	350 nm	1.6 (0.3)	NONE[c], 83.5-85[d], 88.0-88.5[e], 88.9[f], 92[h], 89-99[i]	1.419[j]	116	
	450 nm	1.82 (0.03)				
	600 nm	1.91 (0.11)				
Malonic Acid [b]	250 nm	2.60 (0.20)				
	350 nm	2.09 (0.06)	NONE[c], NONE[d], 65.2[e], 71.9[f], 74.3[g], 70[h], 74-91[i]	----	161	
	450 nm	2.10 (0.09)				
	600 nm	2.10 (0.07)				
Montmorillonite	250 nm	1.17 (0.03)				
	350 nm	1.05 (0.06)	NONE[k]	1.523 + 3.82x10^{-5}i[l]	Insoluble	[(Na,Ca)(Al,Mg)$_6$(Si$_4$O$_{10}$)$_3$(OH)$_6$]
	450 nm	0.92 (0.03)				
	600 nm	0.954 (0.018)				

[a] Saxena and Hildman[140]

[b] There is no data available for the refractive index of malonic acid

[c] This study;CRD

[d] Peng et al. electrodynamic balance[142]

[e] Peng et al. bulk solution measurements[142]

[f] Wise et al. bulk solution measurements[39]

[g] Cziczo et al. absorption cell measurements[116]

[h] Ming et al. model predictions[141]

[i] Saxena et al. UNIFAC predictions[146]

[j] CRC[53]

[k] Attwood and Greenslade CRD[113]

[l] Egan and Hildeman[51]

Table 5.1 cannot measure water absorption prior to full deliquescence and therefore

would not show any water uptake prior to the succinic acid DRH.[39] The residence time in

our dryer is fairly long (~25 s for succinic acid); but for other techniques longer times are

utilized (e.g. several minutes for an electrodynamic balance). The relatively short

residence time here could have prevented full crystallization of the particles.[38, 95, 142] Our

results are still relevant especially since atmospheric results will depend on the cycle of

RH experienced by the particle.

The enhancement in extinction of mineral dust particles that were mixed with

succinic acid, as a proxy for processed aerosol, is shown in Figure 5.2. EFs are reported

for particles with diameters of 250 nm, 350 nm, 450 nm and 600 nm at dry (RH<10%)

and elevated RH (RH=80%). The EFs describe the change in extinction by mixed

processed mineral dust in comparison to freshly emitted single component

Figure 5.2: Enhancement factors for succinic acid as a function of size. Values are reported for <10% RH and 80% RH representing dry and wet conditions, respectively. For comparision, the fRH$_{ext}$(80%,Dry) for succinic acid and montmorillonite are given in Table 5.1.

montmorillonite particles at 80% RH. The largest enhancement is seen for 250 nm particles, where extinction is increased by approximately 1.3 after mixing with succinic acid. However, no significant difference exists between mixed processed particles at low and high RH and this indicates that any enhancement in extinction due to the processing of mineral dust and is due to mixing and not the water uptake. This is to be expected since succinic acid has a high DRH and does not take up water at 80% RH. As a result, the addition of succinc acid should not contribute any additional water uptake in comparison to the mineral dust particles alone. In addition, the fRH_{ext} at 80% RH for succinic acid ranges from 1.02 (0.03) to 1.11 (0.05) depending on particle size, which is similar to the range in fRH_{ext} for montmorillonite, 0.954 (0.018) to 1.17 (0.03), for the same particle sizes. The enhancement is also not due to an increase in refractive index because the refractive index of succinic acid is slightly lower than montmorillonite. A decrease in the refractive index predicted for the mixed processed particle would lead to a decrease in the total extinction.

The enhancement in extinction seen particularly for the 250 nm and 600 nm mixed processed particles is most likely due to an increase in absorption by the mineral dust particle caused by a transparent succinic acid shell or a change in particle density or morphology. The enhancement in extinction is more pronounced at 250 nm because single component montmorillonite particles experience the least amount of compaction at that size, indicated by the greatest fRH_{ext} as seen in Table 5.1.

Glutaric Acid

Glutaric acid has an fRH_{ext}=1.42 (0.11) for 250 nm particles at 80% RH. A DRH spanning from 83.5-99% RH has been reported in the literature.[39, 141, 142, 146] However, no

apparent DRH was observed with this study. Instead, glutaric acid had a continually

changing fRH which indicates the gradual water uptake as a function of RH, in

agreement with previous studies that noted the ability of glutaric acid to absorb water at

all RHs. [146-148] The continuous change in extinction indicates that the particles never

fully crystallized during the experiment, despite the low RH of the aerosol stream (<10%)

and the crystallization RH=54.4%.[95]

The change in extinction of mineral dust aerosol after mixing with glutaric acid is

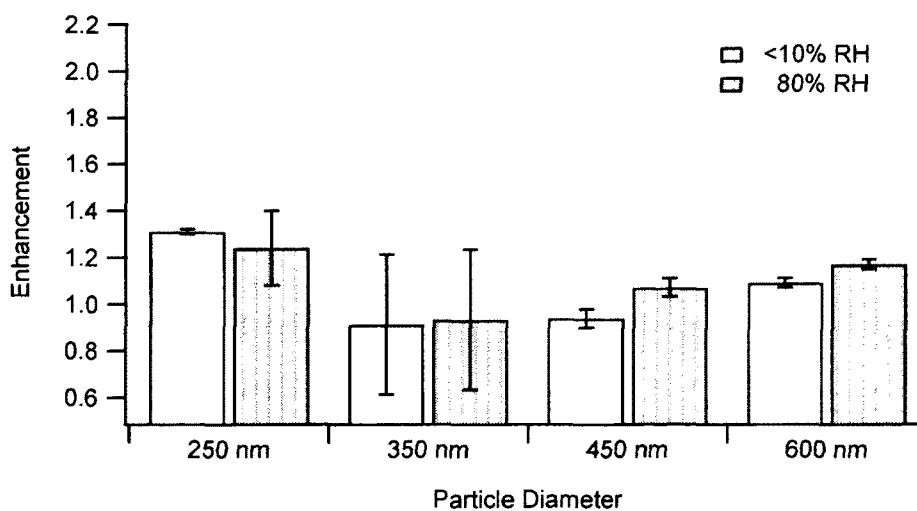depicted in Figure 5.3. No significant difference in the enhancement at high or low
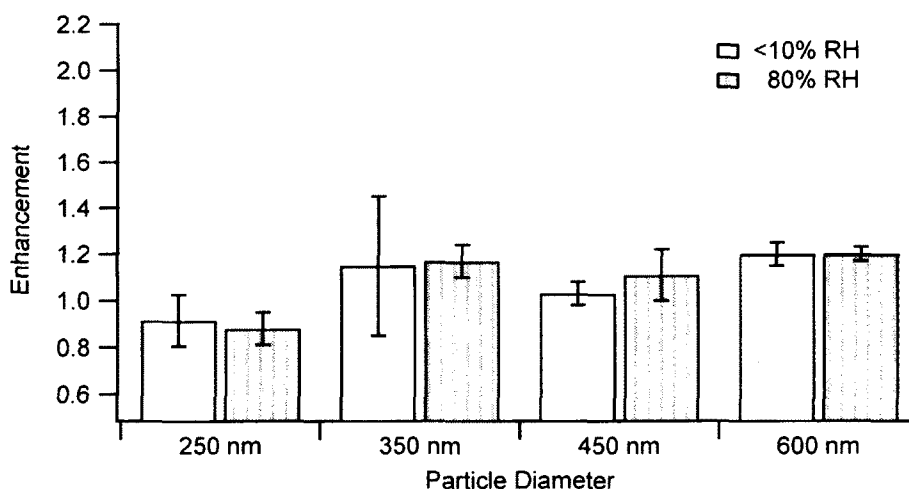
Figure 5.3: Enhancement factors for glutaric acid as a function of size. Values are reported for <10% RH and 80% RH representing dry and wet conditions, respectively. For comparison, the fRH$_{ext}$(80%, Dry) for glutaric acid and montmorillonite are given in Table 5.1.

relative humidity is observed, similar to the succinic acid results, indicating that any

enhancement observed in the mixed processed particle is not due to an increase in water

uptake as a result of the addition of organic acid to the particle. At 250 nm, mineral dust

particles mixed with glutaric acid have an EF<1 indicating that the processing in this case

decreases extinction by the particle. This can occur due to evaporation of glutaric acid

between the dry and humidified cavities or by compaction of the particle, reducing its

size and hence the amount of light scattered and absorbed. The semivolatile nature of glutaric acid has been reported previously in both field and laboratory experiments.[143, 149] The reduction in fRH$_{ext}$ due to particle compaction is particularly interesting because at that size, the least amount of compaction is expected based on the fRH$_{ext}$ value of pure montmorillonite. Further, a compaction upon coating is not observed for succinic acid. This observation is discussed in more detail below. A modest enhancement is seen for 350 nm, 450 nm and 600 nm mixed processed particles although the extent of the enhancement does not seem to be size dependent. Like succinic acid, glutaric acid has a slightly smaller refractive index than montmorillonite and therefore a change in the refractive index of the mixed particle cannot account for the observed enhancement.

Malonic Acid

Malonic acid has an fRH$_{ext}$=2.6(0.2) at 80% RH indicating that it takes up a significant amount of water by this RH. This is more than double what is observed for the other two dicarboxylic acids and is in agreement with other studies which report an fRH$_{ext}$ ranging from 1.81-3.19.[35, 39, 142, 143] Like glutaric acid, no DRH was observed, and malonic acid took up water continually throughout the RH range. A similar observation was reported by Peng et al.[142] using an electrodynamic balance and Prenni et al.[38] using an HT-DMA technique, whereas other studies show a DRH for malonic acid ranging from 65.2-91% RH.[39, 116, 141, 146] As noted with the other dicarboxylic acids, a possible explanation for the discrepancies between the studies likely results from the difficulty in obtaining completely dry particles. In all cases, a significant amount of water is associated with single component malonic acid particles at 80% RH, thus explaining the large difference in the enhancement factors for dry and wet particles of mineral dust

processed with malonic acid shown in Figure 5.4. At high RH, the enhancement in extinction can be attributed to the uptake of additional water by the malonic acid present in the mixed processed particles in comparison to mineral dust alone. The organic portion will increase the overall hygroscopicity of the mixed processed particle, allowing for greater water uptake, increased particle size and enhanced extinction.
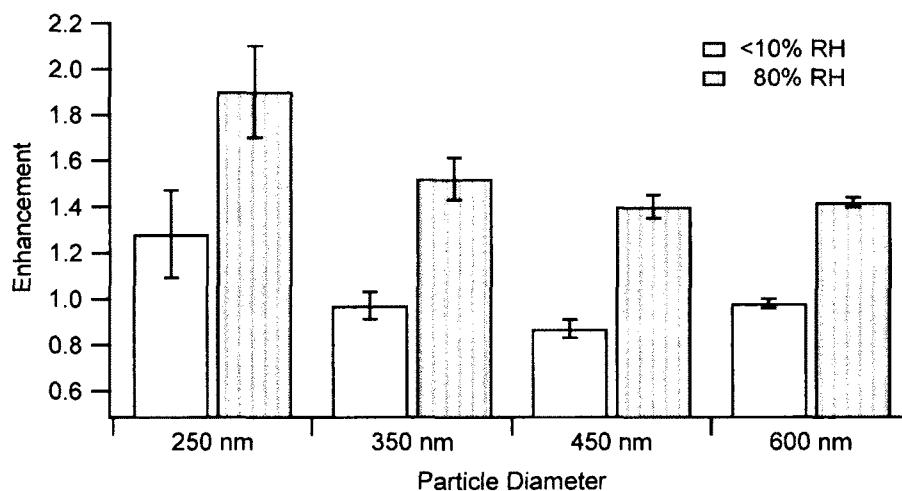
Figure 5.4: Enhancement factors for malonic acid as a function of size. Values are reported for <10% RH and 80% RH representing dry and wet conditions, respectively. For comparison, the fRH_{ext}(80%,Dry) for malonic acid and montmorillonite are given in Table 5.1.

At elevated RH, a maximum enhancement of 1.9 (0.2) is experienced by 250 nm mixed processed particles and seems to decrease with size. It is possible that this size dependence is caused by a greater degree of compaction by the montmorillonite at larger sizes as shown in pure component montmorillonite as a decrease in the fRH_{ext}. In addition, pure malonic acid has a decrease in fRH_{ext} with size reinforcing the observed trend. When the particles are dry, there is no enhancement in extinction except for 250 nm mixed processed particles with an enhancement factor of 1.28 (0.19). This enhancement could be attributed to an increase in absorption due to the transparent malonic acid shell, or a change in density or morphology of the particle upon processing.

It is important to note that for 350 nm and 450 nm mixed processed particles a slight decrease in extinction is observed, similar to what is seen for 250 nm mixed montmorillonite and glutaric acid particles and this can be explained by looking at the physical properties of the dicarboxylic acids as discussed below.

Characteristics of Dicarboxylic Acids Contributing to the Extinction Observations

Aside from the enhancement due to water uptake observed when mineral dust is mixed with malonic acid and measured high RH, the increase in extinction is observed in extinction in these mixed processed particles may be attributed to an increase in absorption caused by the formation of a transparent dicarboxylic acid shell or a change in particle density or morphology. Transparent shells formed by non absorbing compounds have been shown to increase absorption in spherical or irregular shaped soot particles, by focusing the radiation on the core.[16, 20, 150, 151] Although the extent of absorption by freshly emitted mineral dust is expected to be less than is typically seen in soot aerosols, an enhancement in absorption with the addition of a transparent dicarboxylic acid shell would lead to enhanced extinction.

Increased scattering and absorption by the processed mineral dust can also be attributed to a restructuring of the particle to yield a more compact form with a spherical shape, thus increasing the particle density. We have previously observed compaction of mineral dust particles upon exposure to water vapor.[113] This type of compaction is also commonly seen in soot particles when the irregular, fractal nature of the freshly emitted soot particles is replaced with a more spherical morphology as a result of internal mixing.[15-17, 20, 150] In these studies, soot particles coated with a non-absorbing material showed increased scattering and absorption as described above. In addition to the

compaction seen in the these studies, Xue et al. showed that after the coating was removed, both scattering and absorption of the processed particles remained higher than the initial values for the freshly emitted soot particles.[15] The restructuring of the particle caused an increase in particle density and a change in particle morphology enhancing the scattering and absorption by the particle. The enhancement in extinction seen by processed mineral dust particles in this study could be caused by a similar effect.

There are noticeable differences in the extinction effects for mineral dust mixing with the different dicarboxylic acids. For example, mineral dust mixed with glutaric acid at 250 nm and malonic acid at 350 nm and 450 nm exhibit a decrease in extinction, indicated by an EF<1. This is contrary to what is seen for succinic acid, where coating the mineral dust causes either an enhancement or no significant change in extinction. Structurally the three dicarboxylic acids only differ by the number of CH_2 groups, with glutaric acid and malonic acids having an odd number of carbon atoms (5 and 3 carbons, respectively) and succinic acid having an even (4) number of carbon atoms. This small difference proves to be important as the physical properties of C3-C9 dicarboxylic acids are very different and exhibit alternating trends for even versus odd numbers of carbon atoms.[152-154] For odd numbers of carbons, the additional carbon creates a twisted conformation in the crystal lattice, causing a strained torsional conformation. This conformation leads to lower melting points, higher vapor pressures and lower sublimation enthalpies for glutaric and malonic acids.[153, 154] This less stable conformation leads to excess energy as compared to their even number counterparts. The additional energy leads to stronger interactions with the montmorillonite surfaces and causes the particles to

collapse and compact, even under dry conditions.[152] This phenomenon has been previously observed in soot particles exposed to succinic (even) and glutaric (odd) acids.[152] In the succinic acid case, no restructuring or change in particle diameter was observed. However, when soot is exposed to glutaric acid, restructuring occurs, shrinking the diameter by 10-40% of its initial value.[152]

Comparison of Experimental fRH$_{ext}$ with Calculations Based on Simple Mixing Rules

Predictions of the optical growth of mixed processed mineral dust aerosol have been made using, a simple linear mixing rule as described by Cruz and Pandis.[37] Here, we use the Zdanovskii, Stokes and Robinson (ZSR) method applied to optical growth assuming that each component in the mixture behaves independently. The experimentally measured fRH$_{ext}$ data for the pure components is used to predict the fRH$_{ext}$ of mixtures using the ZSR equation as follows:

$$fRH_{ext}(RH) = [\epsilon_0 * fRH_{ext,mont}^3 + (1 - \epsilon_0) * fRH_{ext,DCA}^3]^{\frac{1}{3}} \qquad [5.5]$$

where ϵ_0 is the volume fraction of montmorillonite in the dry particle and fRH$_{ext,mont}$ and fRH$_{ext,DCA}$ are the fRH$_{ext}$ for pure montmorillonite and pure dicarboxylic acid at a given RH, respectively.

Figure 5.5 displays comparisons of the experimentally measured and predicted fRH$_{ext}$ for each of the mixed processed aerosols. Since aerosols were generated based on the wt% of the components, these values were converted to volume fractions using the density of each component in the dry particle. In all cases the fRH$_{ext}$ modeled by equation 5.5 are in good agreement with the measured values. The error does not exceed 15% except for montmorillonite particles mixed with glutaric acid at high RH. Therefore, the

ZSR equation is useful in estimating the fRH$_{ext}$ for processed mineral dust since there is little inconsistency between the predicted and measured values.
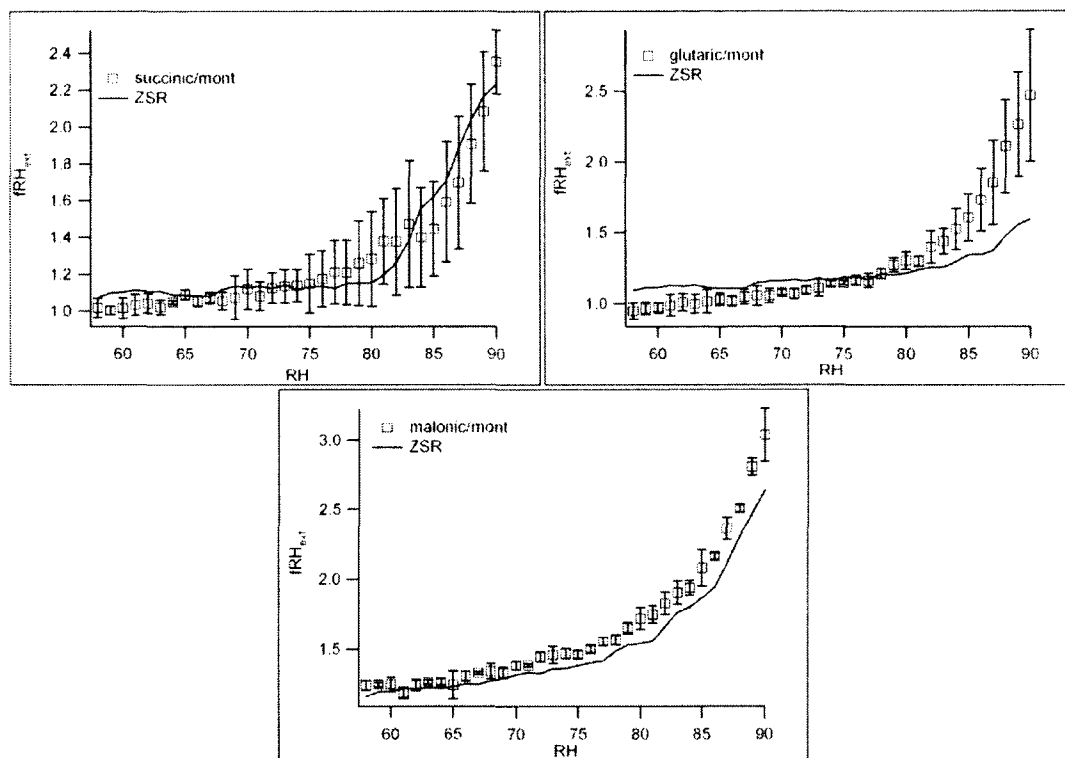
Figure 5.5: Experimentally measured and predicted optical growth of 250 nm internally mixed dicarboxylic and montmorillonite particles. Error bars are reported as the experimental standard deviation (1σ) for each particle mixture over 3 different experiments.

Conclusions and Atmospheric Implications

We have investigated the effect of processing on the optical properties of montmorillonite, a clay component of mineral dust aerosol. Mineral dust particles were mixed with succinic, glutaric and malonic acid, three dicarboxylic acids commonly found in atmospheric particles. Once internally mixed, the processed particles were subjected to low and high RH during optical interrogation by CRD to quantify changes in extinction relative to freshly emitted pure mineral dust particles.

Mineral dust particles mixed with all three dicarboxylic acids showed changes in extinction, depending on size. For succinic acid, the enhancement was greatest for small particles and no significant difference was seen between the dry and elevated RH conditions, indicating that water uptake is not significant upon addition of the DCA. The enhancement seems to have a size dependence most likely to due to compaction of the mineral dust particle upon coating. Mineral dust showed a significant decrease in extinction upon coating with glutaric acid at 250 nm, most likely due to restructuring of the particle to a smaller diameter. At larger sizes, the mixed processed mineral dust and glutaric acid mixtures showed a slight enhancement in extinction, most likely due to enhanced absorption by the transparent glutaric acid shell or a change in particle density and morphology. Mineral dust mixed with malonic acid, the carboxylic acid with the greatest uptake in water at low RH, showed a strong enhancement in extinction at high RH due to significant water uptake and increased particle size. In all cases, the physical and chemical characteristics of the coating material had a significant effect on the optical properties of the mixed particle. These results have important implications for the atmosphere since they suggest that the type of dicarboxylic acid coating on a mineral dust particle will determine the degree of enhancement in extinction for that particle. Further, the EFs observed in the mixed processed mineral dust are likely due to changes in both the scattering and absorption by the particle and the relative magnitude of each will determine the degree of radiative forcing in the atmosphere. Our results also provide evidence that the ZSR equation, using simple linear mixing rules, is an accurate representation of these systems if the optical properties of the individual components are known.

CHAPTER 6

CONCLUDING REMARKS

Summary

A newly built CRD was used to measure the optical properties of single component mineral dust particles and their mixtures with salts or dicarboxylic acids under a range of conditions. The particles and conditions were chosen based on atmospheric relevancy and to our knowledge there have been no other direct optical measurements at 532 nm of these types of particles reported in the literature. The newly built CRD was tested and evaluated for similar cases before the original work was completed. As a result of this testing, it was determined that the new CRD is capable of making accurate, highly sensitive measurements of extinction by laboratory generated aerosols, similar to instruments used by others.[31, 35, 155]

The initial studies on mineral dust measured the fRH$_{ext}$ for three clays: montmorillonite, illite and kaolinite. These species served as proxies for mineral dust as they comprise a large fraction of the smallest sized ambient mineral dust particles. Optical extinction was measured using the CRD at 50%, 68% and 90% RH and compared to dry conditions (RH<10%) to obtain fRH$_{ext}$. The optical behavior varied considerably between clay types indicating that the different morphologies and chemical structures of these clays play an important role in water uptake.

Other measurement technologies determine the change in optical properties due to water uptake by inferring that change based on physically measured particle growth. However, based on the deviations between physical growth factors, mass based growth factors and optically based growth factor described in this work, the inclusion of direct optical property measurements for clays based on species specific loading would be advantageous for reducing uncertainties in climate models. We concluded that our calculated optically derived growth factor provides a lower limit for the physical growth factor and is an alternate method for assessing water uptake as compared to measurements using an HT-DMA or a QCM. The bounding of the growth factor using our closure based calculations (lower bound) with those calculated using QCM measurements (upper bound) may further reduce uncertainties associated with growth factor measurements.

Since aerosols can only exist as a single species close to the source but mix as they age in the atmosphere, the second study looked at internal mixtures of montmorillonite clay and two common atmospheric salts, ammonium sulfate and sodium chloride. The fRH_{ext} for the single components and internal mixtures were measured over a RH range of 58-90%. Montmorillonite affects the hygroscopic properties of salt particles and for the first time, a lowering in the onset of deliquescence for many of the soluble/insoluble mixtures studied was observed. This effect cannot be predicted by simple mixing rules based on the fRH_{ext} of the pure components, due to errors in replicating the lowered DRH. If the decrease in DRH is not accounted for when assessing the optical properties of the mixed particles, the predicted extinction has the potential to be dramatically underestimated especially within 6% of the pure salt DRH.

In the third study, the effect of processing on the optical properties of montmorillonite by mixing with organic compounds was investigated. Montmorillonite particles were internally mixed with succinic, glutaric and malonic acid, three dicarboxylic acids commonly found in atmospheric particles, and subjected to low and high RH. Particle sizes between 250 nm and 600 nm in diameter were selected for optical interrogation. The addition of each of the three dicarboxylic acids to montmorillonite yielded changes in extinction, somewhat dependent on size. In most cases, the physical and chemical characteristics of the added dicarboxylic acid had a significant effect on the optical properties of the mixed particle. These results have important implications for the atmosphere since they suggest that the type of dicarboxylic acid mixed with a mineral dust particle can influence the degree of enhancement, if any, in extinction for that particle in comparison to the pure clay aerosols. This is also likely to depend on the composition of the mineral dust, as well as the distribution of their particle sizes in the ambient environment. Our results also provide evidence that the ZSR equation, using simple linear mixing rules, is an accurate representation of these systems if the optical properties of the individual components are known.

Considerations for Future Work

The studies described above demonstrate the ability of the CRD to provide sensitive, accurate measurements of total extinction of laboratory generated aerosols as a function of relative humidity. Yet, there are additional measurements that can be done in the future to complement the CRD technique and further improve climate models, ultimately decreasing the uncertainty associated with aerosols and climate change.

As mentioned previously, the composition of our internally mixed aerosols is approximated by the composition of the atomized suspension. The internal structure of these mixed particles is also unknown but could give insight into physical and chemical properties such as water uptake. A combination of microscopy and spectroscopy of the mixed particles could elucidate the chemical composition and structure and thus eliminate the need for an approximation. For example, transmission electron microscopy (TEM) and scanning electron microscopy (SEM) are commonly used to probe particle structure and can be paired with electron dispersion spectroscopy (EDS) to give information on elemental composition. Raman spectroscopy also can provide detailed information about the chemical composition of single particles by looking at the position and intensity of Raman active vibrational modes. Possible correlations of chemical and structural composition with extinction data from the CRD could be powerful in future predictions of optical properties.

The addition of a humidified tandem differential mobility analyzer (HT-DMA), to measure the change in particle diameter as a function of RH, would help to explain the results of our CRD measurements. Simultaneous growth factor and fRH_{ext} measurements, especially on mixed particles not previously studied, will help determine if changes in the optical properties are correlated with particle size as a function of increasing RH. In addition, this type of measurement could be used to produce numerical comparisons between growth factors calculated using the optical growth measured by the CRD and growth factors physically measured by the HT-DMA.

It would also be advantageous to have a complementary measurement of either scattering or absorption of the aerosol samples to determine single scattering albedo. As

previously mentioned, single scattering albedo is the ratio of aerosol scattering to total aerosol extinction (scattering + absorption), and this quantity decreases from 1 (purely scattering) as aerosol absorption increases. Since mineral dust can have an absorbing component and an estimated radiative forcing ranging from +0.4 to -0.6 W m^2, the calculation of the single scattering albedo would help to determine if mineral dust has a net cooling or heating effect on the climate. Scattering is typically measured using an integrating nephelometer which measures scattering intensity over different angles relative to the aerosol sample.[156] Aerosol absorption is difficult to quantify by the difference method (extinction − scattering = absorption) since its relative magnitude is typically much smaller than both extinction and scattering. Some common examples of direct absorption measurements include optically based filter measurements using a particle soot absorption photometer (PSAP) or aethelometer. Alternatively, *in situ* measurements are possible using photoacoustic absorption spectroscopy that measures sound waves produced by an aerosol sample after heat is released from absorbed light. The robust extinction measurements provided by the CRD offers accurate and direct measurements of aerosol optical properties and could potentially be used to evaluate the uncertainties associated with measuring scattering and absorption using other techniques.

LIST OF REFERENCES

1.   Solomon, S.; Qin, D.; Manning, M.; Chen, Z.; Marquis, M.; Averyt, K. B.; Tignor, M.; Miller, H. L. Climate Change 2007. *The Physical Science Basis: Working Group I Contribution to the Fourth Assessment Report of the Intergovernmental Panel on Climate Change.*

2.   Löndahl, J.; Swietlicki, E.; Lindgren, E.; Loft, S., Aerosol exposure versus aerosol cooling of climate: what is the optimal emission reduction strategy for human health? *Atmos. Chem. Phys.* 10, (19), 9441-9449.

3.   Seinfeld, J. H., Pandis, S.N., *Atmospheric Chemistry and Physics: From Air Pollution to Climate Change 2nd edition.* 2 ed.; John Wiley & sons, INC: Hoboken, 2006.

4.   Crutzen, P. J.; Andreae, M. O., Biomass Burning in the Tropics: Impact on Atmospheric Chemistry and Biogeochemical Cycles. *Science* **1990,** 250, (4988), 1669-1678.

5.   Finlayson-Pitts, B. J.; James N. Pitts, J., *Chemistry of the Upper and Lower Atmosphere.* Academic Press: Boston, 2000.

6.   Fuller, K. A.; Malm, W. C.; Kreidenweis, S. M., Effects of Mixing on Extinction by Carbonaceous Particles. *J. Geophys. Res.* **1999,** 104 (D13), 15941-15954.

7.   Hinds, W. C., *Aerosol Technology: Properties, Behavior, and Measurement of Airborne particles.* Second ed.; John Wiley and Sons, INC.: New York, 1999.

8.   Römpp, A.; Winterhalter, R.; Moortgat, G. K., Oxodicarboxylic acids in atmospheric aerosol particles. *Atmos. Environ.* **2006,** 40, (35), 6846-6862.

9.   Kanakidou, M.; Seinfeld, J. H.; Pandis, S. N.; Barnes, I.; Dentener, F. J.; Facchini, M. C.; Van Dingenen, R.; Ervens, B.; Nenes, A.; Nielsen, C. J.; Swietlicki, E.; Putaud, J. P.; Balkanski, Y.; Fuzzi, S.; Horth, J.; Moortgat, G. K.; Winterhalter, R.; Myhre, C. E. L.; Tsigaridis, K.; Vignati, E.; Stephanou, E. G.; Wilson, J., Organic aerosol and global climate modelling: a review. *Atmos. Chem. Phys.* **2005,** 5, 1053-1123.

10.   Haywood, J. M.; Shine, K. P., The effect of anthropogenic sulfate and soot aerosol on the clear sky planetary radiation budget. *Geophys. Res. Lett.* **1995,** 22, (5), 603-606.

11.   Hansen, J.; Sato, M.; Ruedy, R., Radiative forcing and climate response. *J. Geophys. Res.* **1997,** 102, (D6), 6831-6864.

12.   Lesins, G.; Chylek, P.; Lohmann, U., A study of internal and external mixing scenarios and its effect on aerosol optical properties and direct radiative forcing. *J. Geophys. Res.* **2002,** 107, (D10), 4094, DOI:10.1029/2001JD000973.

13.   Lang-Yona, N.; Abo-Riziq, A.; Erlick, C.; Segre, E.; Trainic, M.; Rudich, Y., Interaction of Internally Mixed Aerosols with Light. *Phys. Chem. Chem. Phys.* **2010,** 12, (1), 21-31.

14.   Jacobson, M. Z., A physically-based treatment of elemental carbon optics: Implications for global direct forcing of aerosols. *Geophys. Res. Lett.* **2000,** 27, (2), 217-220.

15.   Xue, H.; Khalizov, A. F.; Wang, L.; Zheng, J.; Zhang, R., Effects of Dicarboxylic Acid Coating on the Optical Properties of Soot. *Phys. Chem. Chem. Phys.* **2009,** 11, (36), 7869-7875.

16.   Khalizov, A. F.; Zhang, R.; Zhang, D.; Xue, H.; Pagels, J.; McMurry, P. H., Formation of highly hygroscopic soot aerosols upon internal mixing with sulfuric acid vapor. *J. Geophys. Res.* **2009,** 114, (D5), D05208.

17.   Zhang, R. Y.; Khalizov, A. F.; Pagels, J.; Zhang, D.; Xue, H. X.; McMurry, P. H., Variability in morphology, hygroscopicity, and optical properties of soot aerosols during atmospheric processing. *Proc. Natl. Acad. Sci. U. S. A.* **2008,** 105, (30), 10291-10296.

18.   Freedman, M. A.; Hasenkopf, C. A.; Beaver, M. R.; Tolbert, M. A., Optical Properties of Internally Mixed Aerosol Particles Composed of Dicarboxylic Acids and Ammonium Sulfate. *J. Phys. Chem. A* **2009,** 113, (48), 13584-13592.

19.   Abo Riziq, A.; Erlick, C.; Dinar, E.; Rudich, Y., Optical properties of absorbing and non-absorbing aerosols retrieved by cavity ring down (CRD) spectroscopy. *Atmos. Chem. Phys.* **2007,** 7, (6), 1523-1536.

20.   Schnaiter, M.; Linke, C.; Möhler, O.; Naumann, K. H.; Saathoff, H.; Wagner, R.; Schurath, U.; Wehner, B., Absorption amplification of black carbon internally mixed with secondary organic aerosol. *J. Geophys. Res.* **2005,** 110, D19204, DOI:10.1029/2005JD006046.

21.   Derimian, Y.; Léon, J. F.; Dubovik, O.; Chiapello, I.; Tanré, D.; Sinyuk, A.; Auriol, F.; Podvin, T.; Brogniez, G.; Holben, B. N., Radiative properties of aerosol mixture observed during the dry season 2006 over M'Bour, Senegal (African Monsoon Multidisciplinary Analysis campaign). *J. Geophys. Res.* **2008,** 113, (D23), D00C09.

22.   Schnaiter, M.; Horvath, H.; Möhler, O.; Naumann, K. H.; Saathoff, H.; Schöck, O. W., UV-VIS-NIR spectral optical properties of soot and soot-containing aerosols. *J. Aerosol Sci.* **2003,** 34, (10), 1421-1444.

23.   Yu, H.; Kaufman, Y. J.; Chin, M.; Feingold, G.; Remer, L. A.; Anderson, T. L.; Balkanski, Y.; Bellouin, N.; Boucher, O.; Christopher, S.; DeCola, P.; Kahn, R.; Koch, D.; Loeb, N.; Reddy, M. S.; Schulz, M.; Takemura, T.; Zhou, M., A review of measurement-based assessments of the aerosol direct radiative effect and forcing. *Atmos. Chem. Phys.* **2006,** 6, (3), 613-666.

24.   Herich, H.; Tritscher, T.; Wiacek, A.; Gysel, M.; Weingartner, E.; Lohmann, U.; Baltensperger, U.; Cziczo, D. J., Water Uptake of Clay and Desert Dust Aerosol Particles at Sub- and Supersaturated Water Vapor Conditions. *Phys. Chem. Chem. Phys.* **2009,** 11, (36), 7804-7809.

25.   Vlasenko, A.; Sjogren, S.; Weingartner, E.; Gaggeler, H. W.; Ammann, M., Generation of Submicron Arizona Test Dust Aerosol: Chemical and Hygroscopic Properties. *Aerosol Sci. Technol.* **2005,** 39, (5), 452-460.

26.   Koehler, K. A.; Kreidenweis, S. M.; DeMott, P. J.; Petters, M. D.; Prenni, A. J.; Carrico, C. M., Hygroscopicity and Cloud Droplet Activation of Mineral Dust Aerosol. *Geophys. Res. Lett.* **2009,** 36, L08805, DOI:10.1029/2009GL037348.

27.   Kuznetsov, B. V.; Rakhmanova, T. A.; Popovicheva, O. B.; Shonija, N. K., Water adsorption and energetic properties of spark discharge soot: Specific features of hydrophilicity. *J. Aerosol Sci.* **2003,** 34, (10), 1465-1479.

28.   O'Keefe, A.; Deacon, D. A. G., Cavity Ring-Down Optical Spectrometer for Absorption Measurements Using Pulsed Laser Sources. *Rev. Sci. Instrum.* **1988,** 59.

29.   Atkinson, D. B., Solving Chemical Problems of Environmental Importance Using Cavity Ring-down Spectroscopy. *Analyst* **2003,** 128, (2), 117-125.

30.   Smith, J. D.; Atkinson, D. B., A Portable Pulsed Cavity Ring-down Transmissometer for Measurement of the Optical Extinction of the Atmospheric Aerosol. *Analyst* **2001,** 126, (8), 1216-1220.

31.   Baynard, T.; Lovejoy, E. R.; Pettersson, A.; Brown, S. S.; Lack, D.; Osthoff, H.; Massoli, P.; Ciciora, S.; Dube, W. P.; Ravishankara, A. R., Design and Application of a Pulsed Cavity Ring-Down Aerosol Extinction Spectrometer for Field Measurements. *Aerosol Sci. Technol.* **2007,** 41, (4), 447-462.

32.   Boundy, R. H., *Styrene. Its Polymers, Copolymers and Derivatives.* Reinhold Publishing Corp: New York, 1952.

33.   Corporation, D. S., An Evaluation of a Scanning Mobility Particle Sizer With NIST Traceable Particle Size Standards. In 2004.

34.   Whitby, K. T.; Liu, B. Y. H., Polystyrene aerosols--electrical charge and residue size distribution. *Atmos. Environ.* **1968,** 2, (2), 103-116.

35.   Garland, R. M.; Ravishankara, A. R.; Lovejoy, E. R.; Tolbert, M. A.; Baynard, T., Parameterization for the Relative Humidity Dependence of Light Extinction: Organic-ammonium Sulfate Aerosol. *J. Geophys. Res.* **2007,** 112 (D19), (D19), D19303, DOI:10.1029/2006JD008179.

36.   Tang, I. N.; Tridico, A. C.; Fung, K. H., Thermodynamic and optical properties of sea salt aerosols. *J. Geophys. Res.* **1997,** 102 (D19), 23269-23275.

37.   Cruz, C. N.; Pandis, S. N., Deliquescence and Hygroscopic Growth of Mixed Inorganic and Organic Atmospheric Aerosol. *Environ. Sci. Technol.* **2000,** 34, (20), 4313-4319.

38.   Prenni, A. J.; DeMott, P. J.; Kreidenweis, S. M., Water uptake of internally mixed particles containing ammonium sulfate and dicarboxylic acids. *Atmos. Environ.* **2003,** 37, (30), 4243-4251.

39.   Wise, M. E.; Surratt, J. D.; Curtis, D. B.; Shilling, J. E.; Tolbert, M. A., Hygroscopic growth of ammonium sulfate/dicarboxylic acids. *J. Geophys. Res.* **2003,** 108 (D20), (D20), DOI:10.1029/2003JD003775.

40.   Caquineau, S.; Gaudichet, A.; Gomes, L.; Legrand, M., Mineralogy of Saharan Dust Transported Over Northwestern Tropical Atlantic Ocean in Relation to Source Regions. *J. Geophys. Res.* **2002,** 107, (D15), D154251, DOI:10.1029/2000JD000247.

41.   Grousset, F. E.; Ginoux, P.; Bory, A.; Biscaye, P. E., Case Study of a Chinese Dust Plume Reaching the French Alps. *Geophys. Res. Lett.* **2003,** 30, 1277, DOI:10.1029/2002GL016833.

42.   Biscaye, P. E.; Grousset, F. E.; Revel, M.; Van der Gaast, S.; Zielinski, G. A.; Vaars, A.; Kukla, G., Asian Provenance of Glacial Dust (stage 2) in the Greenland Ice Sheet Project 2 Ice Core, Summit, Greenland. *J. Geophys. Res.* **1997,** 102 (C12), 765-781.

43.   Perry, K. D.; Cliff, S. S.; Jimenez-Cruz, M. P., Evidence for Hygroscopic Mineral Dust Particles from the Intercontinental Transport and Chemical Transformation Experiment. *J. Geophys. Res.* **2004,** 109, (D23), D23S28.

44.   Evan, A. T.; Mukhopadhyay, S., African Dust over the Northern Tropical Atlantic: 1955-2008. *J. Appl. Meteorol. Climatol.* **2010,** 49, (11), 2213-2229.

45.   Duce, R. A.; Tindale, N. W., Atmospheric Transport of Iron and its Deposition in the Ocean. *Limnol. Oceanogr.* **1991,** 36, (8), 1715-1726.

46.   Uematsu, M.; Wang, Z.; Uno, I., Atmospheric Input of Mineral Dust to the Western North Pacific Region Based on Direct Measurements and a Regional Chemical Transport Model. *Geophys. Res. Lett.* **2003,** 30, (6), 1342, DOI:10.1029/2002GL016645.

47.   Cwiertny, D. M.; Young, M. A.; Grassian, V. H., Chemistry and Photochemistry of Mineral Dust Aerosol. *Annu. Rev. Phys. Chem.* **2008,** 59, (1), 27-51.

48.   Bauer, S. E.; Balkanski, Y.; Schulz, M.; Hauglustaine, D. A.; Dentener, F., Global Modeling of Heterogeneous Chemistry on Mineral Aerosol Surfaces: Influence on Tropospheric Ozone Chemistry and Comparison to Observations. *J. Geophys. Res.* **2004,** 109, (D02), D02304, DOI:10.1029/2003jd003868.

49.   McNaughton, C. S.; Clarke, A. D.; Kapustin, V.; Shinozuka, Y.; Howell, S. G.; Anderson, B. E.; Winstead, E.; Dibb, J.; Scheuer, E.; Cohen, R. C.; Wooldridge, P.; Perring, A.; Huey, L. G.; Kim, S.; Jimenez, J. L.; Dunlea, E. J.; DeCarlo, P. F.; Wennberg, P. O.; Crounse, J. D.; Weinheimer, A. J.; Flocke, F., Observations of Heterogeneous Reactions Between Asian Pollution and Mineral Dust Over the Eastern North Pacific During INTEX-B. *Atmos. Chem. Phys.* **2009,** 9, (21), 8283-8308.

50.   Carlson, T. N.; Benjamin, S. G., Radiative Heating Rates for Saharan Dust. *J. Atmos. Sci.* **1980,** 37, (1), 193-213.

51.   Sokolik, I. N.; Toon, O. B., Direct Radiative Forcing by Anthropogenic Airborne Mineral Aerosols. *Nature* **1996,** 381, (6584), 681-683.

52.   Miller, R. L.; Tegen, I., Climate Response to Soil Dust Aerosols. *J. Climate* **1998,** 11, (12), 3247-3267.

53.   Sassen, K., Indirect Climate Forcing over the Western US from Asian Dust Storms. *Geophys. Res. Lett.* **2002,** 29 (10), (10), 1465, DOI:10.1029/2001GL014051.

54.   Lohmann, U.; Diehl, K., Sensitivity Studies of the Importance of Dust Ice Nuclei for the Indirect Aerosol Effect on Stratiform Mixed-Phase Clouds. *J. Atmos. Sci.* **2006,** 63, (3), 968-982.

55.   Mashburn, C. D.; Frinak, E. K.; Tolbert, M. A., Heterogeneous Uptake of Nitric Acid on Na-montmorillonite Clay as a Function of Relative Humidity. *J. Geophys. Res.* **2006,** 111, D15213, DOI:10.1029/2005JD006525.

56.   Hallquist, M.; Stewart, D. J.; Stephenson, S. K.; Cox, R. A., Hydrolysis of N_2O_5 on Sub-micron Sulfate Aerosols. *Phys. Chem. Chem. Phys.* **2003,** 5, (16), 3453-3463.

57.   Vlasenko, A.; Sjogren, S.; Weingartner, E.; Stemmler, K.; Gaggeler, H. W.; Ammann, M., Effect of Humidity on Nitric Acid Uptake to Mineral Dust Aerosol Particles. *Atmos. Chem. Phys.* **2006,** 6, 2147-2160.

58.   Navea, J. G.; Xu, S.; Stanier, C. O.; Young, M. A.; Grassian, V. H., Heterogeneous Uptake of Octamethylcyclotetrasiloxane (D4) and Decamethylcyclopentasiloxane (D5) onto Mineral Dust Aerosol Under Variable RH Conditions. *Atmos. Environ.* **2009,** 43, (26), 4060-4069.

59.   Falkovich, A. H.; Schkolnik, G.; Ganor, E.; Rudich, Y., Adsorption of Organic Compounds Pertinent to Urban Environments onto Mineral Dust Particles. *J. Geophys. Res.* **2004,** 109, D02208.

60.   DeMott, P. J.; Sassen, K.; Poellot, M. R.; Baumgardner, D.; Rogers, D. C.; Brooks, S. D.; Prenni, A. J.; Kreidenweis, S. M., African Dust Aerosols as Atmospheric Ice Nuclei. *Geophys. Res. Lett.* **2003,** 30, 1732, DOI:10.1029/2003GL017410.

61.   Hung, H.-M.; Malinowski, A.; Martin, S. T., Kinetics of Heterogeneous Ice Nucleation on the Surfaces of Mineral Dust Cores Inserted into Aqueous Ammonium Sulfate Particles. *J. Phys. Chem. A* **2003,** 107, (9), 1296-1306.

62.   Salam, A.; Lohmann, U.; Crenna, B.; Lesins, G.; Klages, P.; Rogers, D.; Irani, R.; MacGillivray, A.; Coffin, M., Ice Nucleation Studies of Mineral Dust Particles with a New Continuous Flow Diffusion Chamber. *Aerosol Sci. Technol.* **2006,** 40, (2), 134-143.

63.   Kumar, P.; Sokolik, I. N.; Nenes, A., Measurements of Cloud Condensation Nuclei Activity and Droplet Activation Kinetics of Fresh Unprocessed Regional Dust Samples and Minerals. *Atmos. Chem. Phys. Discuss.* **2010,** 10, (12), 31039-31081.

64.   Bohren, C. F.; Huffman, D. R., *Absorption and Scattering of Light by Small Particles.* Wiley-VCH Verlag GmbH & Co.: Weinheim, 2004.

65.   Hudson, P. K.; Gibson, E. R.; Young, M. A.; Kleiber, P. D.; Grassian, V. H., Coupled Infrared Extinction and Size Distribution Measurements for Several Clay Components of Mineral Dust Aerosol. *J. Geophys. Res.* **2008,** 113, D01201.

66.   Curtis, D. B.; Meland, B.; Aycibin, M.; Arnold, N. P.; Grassian, V. H.; Young, M. A.; Kleiber, P. D., A Laboratory Investigation of Light Scattering from Representative Components of Mineral Dust Aerosol at a Wavelength of 550 nm. *J. Geophys. Res.* **2008,** 113, D08210.

67.   Schuttlefield, J. D.; Cox, D.; Grassian, V. H., An Investigation of Water Uptake on Clays Minerals Using ATR-FTIR Spectroscopy Coupled with Quartz Crystal Microbalance Measurements. *J. Geophys. Res. Atmos.* **2007,** 112, (D21), D21303, DOI:10.1029/2007JD008973.

68.   Seisel, S.; Pashkova, A.; Lian, Y.; Zellner, R., Water Uptake on Mineral Dust and Soot: A Fundamental View of the Hydrophilicity of Atmospheric Particles. *Faraday Discuss.* **2005,** 130, 437-451.

69.   Gustafsson, R. J.; Orlov, A.; Badger, C. L.; Griffiths, P. T.; Cox, R. A.; Lambert, R. M., A Comprehensive Evaluation of Water Uptake on Atmospherically Relevant Mineral Surfaces: DRIFT Spectroscopy, Thermogravimetric Analysis and Aerosol Growth Measurements. *Atmos. Chem. Phys.* **2005,** 5, (12), 3415-3421.

70.   Lack, D. A.; Quinn, P. K.; Massoli, P.; Bates, T. S.; Coffman, D.; Covert, D. S.; Sierau, B.; Tucker, S.; Baynard, T.; Lovejoy, E.; Murphy, D. M.; Ravishankara, A. R., Relative humidity dependence of light absorption by mineral dust after long-range atmospheric transport from the Sahara. *Geophys. Res. Lett.* **2009,** 36, L24805, DOI:10.1029/2009GL041002.

71.   Usher, C. R.; Michel, A. E.; Grassian, V. H., Reactions on Mineral Dust. *Chem. Rev.* **2003,** 103, (12), 4883-4940.

72.   Caquineau, S.; Gaudichet, A.; Gomes, L.; Magonthier, M.; Claude; Chatenet, B., Saharan Dust: Clay Ratio as a Relevant Tracer to Assess the Origin of Soil-derived Aerosols. *Geophys. Res. Lett.* **1998,** 25, (7), 983-986.

73.   Prospero, J. M., Long-range Transport of Mineral Dust in the Global Atmosphere: Impact of African dust on the Environment of the Southeastern United States. *Proc. Natl. Acad. Sci. U. S. A.* **1999,** 96, (7), 3396-3403.

74.   Sudo, T.; Shimoda, S., Clays and Clay Minerals of Japan. In *Developments in Sedimentology*, Elsevier North-Holland, Inc: New York, 1978.

75.   Cases, J. M.; Berend, I.; Besson, G.; Francois, M.; Uriot, J. P.; Thomas, F.; Poirier, J. E., Mechanism of Adsorption and Desorption of Water Vapor by Homoionic Montmorillonite. 1. The Sodium-Exchanged Form. *Langmuir* **1992,** 8, (11), 2730-2739.

76.   Hensen, E. J. M.; Smit, B., Why Clays Swell. *J. Phys. Chem. B* **2002,** 106, (49), 12664-12667.

77.   McMurry, P. H., A Review of Atmospheric Aerosol Measurements. *Atmos. Environ.* **2000,** 34, (12-14), 1959-1999.

78.   Duce, R. A., Sources, Distributions, and Fluxes of Mineral Aerosols and their Relationship to Climate. In *Dahlem Workshop on Aerosol Forcing of Climate*, Charlson, R. J.; Heintzenberg, J., Eds. John Wiley: Chichester, U.K., 1995; pp 43-72.

79.   Tegen, I.; Fung, I., Modeling of Mineral Dust in the Atmosphere: Sources, Transport, and Optical Thickness. *J. Geophys. Res.* **1994,** 99 (D11), 22897-22914.

80.   Wiedensohler, A., An Approximation of the Bipolar Charge Distribution for Particles in the Submicron Size Range. *J. Aerosol Sci.* **1988,** 19, (3), 387-389.

81.   Egan, W. G.; Hilgeman, T. W., *Optical Properties of Inhomogeneous Materials: Applications to Geology, Astronomy, Chemistry, and Engineering* Academic Press: New York :, 1979.

82.   Nessler, R.; Weingartner, E.; Baltensperger, U., Effect of Humidity on Aerosol Light Absorption and its Implications for Extinction and the Single Scattering Albedo Illustrated for a Site in the Lower Free Troposphere. *J. Aerosol Sci.* **2005,** 36, (8), 958-972.

83.   Lide, D., *CRC Handbook of Chemistry and Physics, 88th Edition* CRC: Boca Raton, FL, 2007.

84.   Chylek, P.; Wong, J., Effect of Absorbing Aerosols on Global Radiation Budget. *Geophys. Res. Lett.* **1995,** 22, (8), 929-931.

85.   Petit, R. H.; Legrand, M.; Jankowiak, I.; Molinié, J.; Asselin de Beauville, C.; Marion, G.; Mansot, J. L., Transport of Saharan Dust over the Caribbean Islands: Study of an Event. *J. Geophys. Res.* **2005,** 110, (D18), D18S09.

86.   Schwartz, S. E., Uncertainty Requirements in Radiative Forcing of Climate Change. *J. Air Waste Manage.* **2004,** 54, 1351-1359.

87.   Tang, I. N.; Munkelwitz, H. R., Aerosol growth studies--III ammonium bisulfate aerosols in a moist atmosphere. *J. Aerosol Sci.* **1977,** 8, (5), 321-330.

88.   Tang, I. N., Phase transformation and growth of aerosol particles composed of mixed salts. *J. Aerosol Sci.* **1976,** 7, (5), 361-371.

89.   Ansari, A. S.; Pandis, S. N., Prediction of multicomponent inorganic atmospheric aerosol behavior. *Atmos. Environ.* **1999,** 33, (5), 745-757.

90.   Wexler, A. S.; Seinfeld, J. H., Second-generation inorganic aerosol model. *Atmos. Environ., Part A* **1991,** 25, (12), 2731-2748.

91.   Martin, S. T.; Hung, H. M.; Park, R. J.; Jacob, D. J.; Spurr, R. J. D.; Chance, K. V.; Chin, M., Effects of the physical state of tropospheric ammonium-sulfate-nitrate particles on global aerosol direct radiative forcing. *Atmos. Chem. Phys.* **2004**, 4, (1), 183-214.

92.   Mifflin, A. L.; Smith, M. L.; Martin, S. T., Morphology hypothesized to influence aerosol particle deliquescence. *Phys. Chem. Chem. Phys.* **2009**, 11, (43), 10095-10107.

93.   Miñambres, L.; Méndez, E.; Sánchez, M. N.; Castaño, F.; Basterretxea, F. J., Water uptake properties of internally mixed sodium halide and succinic acid particles. *Atmos. Environ.* **2011**, 45, (32), 5896-5902.

94.   Ge, Z.; Wexler, A. S.; Johnston, M. V., Deliquescence Behavior of Multicomponent Aerosols. *J. Phys. Chem. A* **1998**, 102, (1), 173-180.

95.   Choi, M. Y.; Chan, C. K., The Effects of Organic Species on the Hygroscopic Behaviors of Inorganic Aerosols. *Environ. Sci. Technol.* **2002**, 36, (11), 2422-2428.

96.   Brooks, S. D.; Wise, M. E.; Cushing, M.; Tolbert, M. A., Deliquescence behavior of organic/ammonium sulfate aerosol. *Geophys. Res. Lett.* **2002**, 29, (19), 1917, DOI:10.1029/2002GL014733.

97.   Malm, W. C.; Kreidenweis, S. M., The effects of models of aerosol hygroscopicity on the apportionment of extinction. *Atmos. Environ.* **1997**, 31, (13), 1965-1976.

98.   Saxena, P.; Peterson, T. W., Thermodynamics of multicomponent electrolytic aerosols. *J. Colloid Interface Sci.* **1981**, 79, (2), 496-510.

99.   Hansson, H. C.; Rood, M. J.; Koloutsou-Vakakis, S.; Hämeri, K.; Orsini, D.; Wiedensohler, A., NaCl Aerosol Particle Hygroscopicity Dependence on Mixing with Organic Compounds. *J. Atmos. Chem.* **1998**, 31, (3), 321-346.

100.   Svenningsson, B.; Rissler, J.; Swietlicki, E.; Mircea, M.; Bilde, M.; Facchini, M. C.; Decesari, S.; Fuzzi, S.; Zhou, J.; Mønster, J.; Rosenørn, T., Hygroscopic growth and critical supersaturations for mixed aerosol particles of inorganic and organic compounds of atmospheric relevance. *Atmos. Chem. Phys.* **2006**, 6, (7), 1937-1952.

101.   Abo Riziq, A.; Trainic, M.; Erlick, C.; Segre, E.; Rudich, Y., Extinction efficiencies of coated absorbing aerosols measured by cavity ring down aerosol spectrometry. *Atmos. Chem. Phys.* **2008**, 8, (6), 1823-1833.

102.   Neiheisel, J.; Weaver, C. E., Transport and deposition of clay minerals, southeastern United States. *J. Sediment. Res.* **1967**, 37, (4), 1084-1116.

103.   Heintzenberg, J., The SAMUM-1 experiment over Southern Morocco: overview and introduction. *Tellus B* **2009**, 61, (1), 2-11.

104.	Zhang, D.; Iwasaka, Y.; Shi, G.; Zang, J.; Matsuki, A.; Trochkine, D., Mixture state and size of Asian dust particles collected at southwestern Japan in spring 2000. *J. Geophys. Res.* **2003,** 108, (D24), 4760, DOI: 10.1029/2003JD003869.

105.	Andreae, M. O.; Charlson, R. J.; Bruynseels, F.; Storms, H.; Van Grieken, R.; Maenhaut, W., Internal Mixture of Sea Salt, Silicates, and Excess Sulfate in Marine Aerosols. *Science* **1986,** 232, (4758), 1620-1623.

106.	Levin, Z.; Ganor, E.; Gladstein, V., The Effects of Desert Particles Coated with Sulfate on Rain Formation in the Eastern Mediterranean. *J. Appl. Meteorol.* **1996,** 35, (9), 1511-1523.

107.	Levin, Z.; Teller, A.; Ganor, E.; Yin, Y., On the interactions of mineral dust, sea-salt particles, and clouds: A measurement and modeling study from the Mediterranean Israeli Dust Experiment campaign. *J. Geophys. Res.* **2005,** 110, (D20), D20202, DOI:10.1029/2005JD005810.

108.	Trochkine, D.; Iwasaka, Y.; Matsuki, A.; Yamada, M.; Kim, Y. S.; Nagatani, T.; Zhang, D.; Shi, G. Y.; Shen, Z., Mineral aerosol particles collected in Dunhuang, China, and their comparison with chemically modified particles collected over Japan. *J. Geophys. Res.* **2003,** 108, (D23), 8642, DOI:10.1029/2002JD003268.

109.	Bates, T. S.; Anderson, T. L.; Baynard, T.; Bond, T.; Boucher, O.; Carmichael, G.; Clarke, A.; Erlick, C.; Guo, H.; Horowitz, L.; Howell, S.; Kulkarni, S.; Maring, H.; McComiskey, A.; Middlebrook, A.; Noone, K.; O'Dowd, C. D.; Ogren, J.; Penner, J.; Quinn, P. K.; Ravishankara, A. R.; Savoie, D. L.; Schwartz, S. E.; Shinozuka, Y.; Tang, Y.; Weber, R. J.; Wu, Y., Aerosol direct radiative effects over the northwest Atlantic, northwest Pacific, and North Indian Oceans: estimates based on in-situ chemical and optical measurements and chemical transport modeling. *Atmos. Chem. Phys.* **2006,** 6, (6), 1657-1732.

110.	Carrico, C. M.; Kus, P.; Rood, M. J.; Quinn, P. K.; Bates, T. S., Mixtures of pollution, dust, sea salt, and volcanic aerosol during ACE-Asia: Radiative properties as a function of relative humidity. *J. Geophys. Res.* **2003,** 108 (D23), 8650, DOI:10.1029/2003JD003405.

111.	Semeniuk, T. A.; Wise, M. E.; Martin, S. T.; Russell, L. M.; Buseck, P. R., Water uptake characteristics of individual atmospheric particles having coatings. *Atmos. Environ.* **2007,** 41, (29), 6225-6235.

112.	Bauer, S. E.; Mishchenko, M. I.; Lacis, A. A.; Zhang, S.; Perlwitz, J.; Metzger, S. M., Do sulfate and nitrate coatings on mineral dust have important effects on radiative properties and climate modeling? *J. Geophys. Res.* **2007,** 112, (D6).

113.	Attwood, A. R.; Greenslade, M. E., Optical Properties and Associated Hygroscopicity of Clay Aerosols. *Aerosol Sci. Technol.* **2011,** 45, (11), 1350-1359.

114.	Gibson, E. R.; Gierlus, K. M.; Hudson, P. K.; Grassian, V. H., Generation of Internally Mixed Insoluble and Soluble Aerosol Particles to Investigate the Impact of Atmospheric Aging and Heterogeneous Processing on the CCN Activity of Mineral Dust Aerosol. *Aerosol Sci. Technol.* **2007,** 41, (10), 914-924.

115. Onasch, T. B.; Siefert, R. L.; Brooks, S. D.; Prenni, A. J.; Murray, B.; Wilson, M. A.; Tolbert, M. A., Infrared spectroscopic study of the deliquescence and efflorescence of ammonium sulfate aerosol as a function of temperature. *J. Geophys. Res.* **1999,** 104 (D17), 21317-21326.

116. Cziczo, D. J.; Nowak, J. B.; Hu, J. H.; Abbatt, J. P. D., Infrared spectroscopy of model tropospheric aerosols as a function of relative humidity: Observation of deliquescence and crystallization. *J. Geophys. Res.* **1997,** 102, (D15), 18843-18850.

117. Schuttlefield, J.; Al-Hosney, H.; Zachariah, A.; Grassian, V. H., Attenuated total reflection Fourier transform infrared spectroscopy to investigate water uptake and phase transitions in atmospherically relevant particles. *Appl. Spectrosc.* **2007,** 61, (3), 283-292.

118. Erlick, C., Effective refractive indices of water and sulfate drops containing absorbing inclusions. *J. Atmos. Sci.* **2006,** 63, (2), 754-763.

119. Zelenyuk, A.; Imre, D.; Han, J.-H.; Oatis, S., Simultaneous Measurements of Individual Ambient Particle Size, Composition, Effective Density, and Hygroscopicity. *Anal. Chem.* **2008,** 80, (5), 1401-1407.

120. Mauer, L. J.; Taylor, L. S., Water-Solids Interactions: Deliquescence. *Annu. Rev. Food Sci. Technol.* 1, (1), 41-63.

121. Salameh, A. K.; Taylor, L. S., Role of Deliquescence Lowering in Enhancing Chemical Reactivity in Physical Mixtures. *J. Phys. Chem. B* **2006,** 110, (20), 10190-10196.

122. Clegg, S. L.; Seinfeld, J. H.; Brimblecombe, P., Thermodynamic modelling of aqueous aerosols containing electrolytes and dissolved organic compounds. *J. Aerosol Sci.* **2001,** 32, (6), 713-738.

123. Salameh, A. K.; Taylor, L. S., Deliquescence-Induced Caking in Binary Powder Blends. *Pharm. Dev. Technol.* **2006,** 11, (4), 453-464.

124. Salameh, A. K.; Taylor, L. S., Deliquescence in Binary Mixtures. *Pharm. Res.* **2005,** 22, (2), 318-324.

125. Miñambres, L.; Sánchez, M. N.; Castaño, F.; Basterretxea, F. J., Hygroscopic Properties of Internally Mixed Particles of Ammonium Sulfate and Succinic Acid Studied by Infrared Spectroscopy. *J. Phys. Chem. A* **2010,** 114, (20), 6124-6130.

126. Ross, K. D., Estimation of Water Activity in Intermediate Moisture Foods. *Food Technol.* **1975,** 29, (3), 24-34.

127. Stokes, R. H.; Robinson, R. A., Interactions in Aqueous Nonelectrolyte Solutions. I. Solute-solvent Equilibria. *J. Phys. Chem.* **1966,** 70, (7), 2126-2131.

128. Chan, M. N.; Lee, A. K. Y.; Chan, C. K., Responses of Ammonium Sulfate Particles Coated with Glutaric Acid to Cyclic Changes in Relative Humidity: Hygroscopicity and Raman Characterization. *Environ. Sci. Technol.* **2006,** 40, (22), 6983-6989.

129.	Preszler Prince, A.; Grassian, V. H.; Kleiber, P.; Young, M. A., Heterogeneous conversion of calcite aerosol by nitric acid. *Phys. Chem. Chem. Phys.* **2007,** 9, (5), 622-634.

130.	Mogili, P. K.; Kleiber, P. D.; Young, M. A.; Grassian, V. H., Heterogeneous Uptake of Ozone on Reactive Components of Mineral Dust Aerosol: An Environmental Aerosol Reaction Chamber Study. *J. Phys. Chem. A* **2006,** 110, (51), 13799-13807.

131.	Mogili, P. K.; Kleiber, P. D.; Young, M. A.; Grassian, V. H., N_2O_5 hydrolysis on the components of mineral dust and sea salt aerosol: Comparison study in an environmental aerosol reaction chamber. *Atmos. Environ.* **2006,** 40, (38), 7401-7408.

132.	Hao, N.; Zhou, B.; Chen, D.; Chen, L., Observations of nitrous acid and its relative humidity dependence in Shanghai. *J. Environ. Sci.* **2006,** 18, (5), 910-915.

133.	Santschi, C.; Rossi, M. J., Uptake of CO_2, SO_2, HNO_3 and HCl on Calcite ($CaCO_3$) at 300 K:Mechanism and the Role of Adsorbed Water *J. Phys. Chem. A* **2006,** 110, (21), 6789-6802.

134.	Stutz, J.; Alicke, B.; Ackermann, R.; Geyer, A.; Wang, S.; White, A. B.; Williams, E. J.; Spicer, C. W.; Fast, J. D., Relative humidity dependence of HONO chemistry in urban areas. *J. Geophys. Res.* **2004,** 109 (D3), (D3), D03307, DOI:10.1029/2003JD004135.

135.	Hu, J. H.; Abbatt, J. P. D., Reaction Probabilities for N_2O_5 Hydrolysis on Sulfuric Acid and Ammonium Sulfate Aerosols at Room Temperature. *J. Phys. Chem. A* **1997,** 101, (5), 871-878.

136.	Mozurkewich, M.; Calvert, J. G., Reaction Probability of N_2O_5 on Aqueous Aerosols. *J. Geophys. Res. Atmos.* **1988,** 93, (D12), 15889-15896.

137.	Duce, R. A.; Mohnen, V. A.; Zimmerman, P. R.; Grosjean, D.; Cautreels, W.; Chatfield, R.; Jaenicke, R.; Ogren, J. A.; Pellizzari, E. D.; Wallace, G. T., Organic material in the global troposphere. *Rev. Geophys.* **1983,** 21, (4), 921-952.

138.	Chow, J. C.; Watson, J. G.; Fujita, E. M.; Lu, Z.; Lawson, D. R.; Ashbaugh, L. L., Temporal and spatial variations of $PM_{2.5}$ and PM_{10} aerosol in the Southern California air quality study. *Atmos. Environ.* **1994,** 28, (12), 2061-2080.

139.	Molnár, A.; Mészáros, E.; Hansson, H. C.; Karlsson, H.; Gelencsér, A.; Kiss, G. Y.; Krivácsy, Z., The importance of organic and elemental carbon in the fine atmospheric aerosol particles. *Atmos. Environ.* **1999,** 33, (17), 2745-2750.

140.	Saxena, P.; Hildemann, L. M.; McMurry, P. H.; Seinfeld, J. H., Organics alter hygroscopic behavior of atmospheric particles. *J. Geophys. Res.* **1995,** 100, (D9), 18755-18770.

141.	Ming, Y.; Russell, L. M., Thermodynamic equilibrium of organic-electrolyte mixtures in aerosol particles. *AIChE J.* **2002,** 48, (6), 1331-1348.

142.   Peng, C.; Chan, M. N.; Chan, C. K., The Hygroscopic Properties of Dicarboxylic and Multifunctional Acids: Measurements and UNIFAC Predictions. *Environ. Sci. Technol.* **2001,** 35, (22), 4495-4501.

143.   Prenni, A. J.; DeMott, P. J.; Kreidenweis, S. M.; Sherman, D. E.; Russell, L. M.; Ming, Y., The Effects of Low Molecular Weight Dicarboxylic Acids on Cloud Formation. *J. Phys. Chem. A* **2001,** 105, (50), 11240-11248.

144.   Kiehl, J. T.; Briegleb, B. P., The Relative Roles of Sulfate Aerosols and Greenhouse Gases in Climate Forcing. *Science* **1993,** 260, (5106), 311-314.

145.   Attwood, A. R.; Greenslade, M. E., Deliquescence Behavior of Internally Mixed Clay and Salt Aerosols by Optical Exticntion Measurements *Accepted in J. Phys. Chem. A* **2012**.

146.   Saxena, P.; Hildemann, L. M., Water Absorption by Organics: Survey of Laboratory Evidence and Evaluation of UNIFAC for Estimating Water Activity. *Environ. Sci. Technol.* **1997,** 31, (11), 3318-3324.

147.   Dougle, P. G.; Veefkind, J. P.; ten Brink, H. M., Crystallisation of mixtures of ammonium nitrate, ammonium sulphate and soot. *J. Aerosol Sci.* **1998,** 29, (3), 375-386.

148.   Sorooshian, A.; Hersey, S.; Brechtel, F. J.; Corless, A.; Flagan, R. C.; Seinfeld, J. H., Rapid, Size-Resolved Aerosol Hygroscopic Growth Measurements: Differential Aerosol Sizing and Hygroscopicity Spectrometer Probe (DASH-SP). *Aerosol Sci. Technol.* **2008,** 42, (6), 445-464.

149.   Limbeck, A.; Puxbaum, H.; Otter, L.; Scholes, M. C., Semivolatile behavior of dicarboxylic acids and other polar organic species at a rural background site (Nylsvley, RSA). *Atmos. Environ.* **2001,** 35, (10), 1853-1862.

150.   Mikhailov, E. F.; Vlasenko, S. S.; Krämer, L.; Niessner, R., Interaction of soot aerosol particles with water droplets: influence of surface hydrophilicity. *J. Aerosol Sci.* **2001,** 32, (6), 697-711.

151.   Bond, T. C.; Habib, G.; Bergstrom, R. W., Limitations in the enhancement of visible light absorption due to mixing state. *J. Geophys. Res.* **2006,** 111, (D20), D20211.

152.   Xue, H.; Khalizov, A. F.; Wang, L.; Zheng, J.; Zhang, R., Effects of Coating of Dicarboxylic Acids on the Mass-Mobility Relationship of Soot Particles. *Environ. Sci. Technol.* **2009,** 43, (8), 2787-2792.

153.   Bilde, M.; Svenningsson, B.; Mønster, J.; Rosenørn, T., Even–Odd Alternation of Evaporation Rates and Vapor Pressures of C3–C9 Dicarboxylic Acid Aerosols. *Environ. Sci. Technol.* **2003,** 37, (7), 1371-1378.

154.   Thalladi, V. R.; Nüsse, M.; Boese, R., The Melting Point Alternation in α,ω-Alkanedicarboxylic Acids. *J. Am. Chem. Soc.* **2000,** 122, (38), 9227-9236.

155.   Pettersson, A.; Lovejoy, E. R.; Brock, C. A.; Brown, S. S.; Ravishankara, A. R., Measurement of aerosol optical extinction at 532 nm with pulsed cavity ring down spectroscopy. *J. Aerosol Sci.* **2004,** 35, (8), 995-1011.

156.   Anderson, T. L.; Covert, D. S.; Marshall, S. F.; Laucks, M. L.; Charlson, R. J.; Waggoner, A. P.; Ogren, J. A.; caldow, R.; Holm, R. L.; Quant, F. R.; Sem, G. J.; Wiedensohler, A.; Ahlquist, N. A.; Bates, T. S., Performance characteristics of a high-sensitivity, three-wavelength, total scatter/backscatter nephelometer. *J. Atmos. Oceanic Tech.* **1996,** 13, 967-986.